CHAPTER 10

DISPERSION OF THE STRUCTURAL RELAXATION AND THE VITRIFICATION OF LIQUIDS

KIA L. NGAI

Naval Research Laboratory, Washington, DC 20375, USA

RICCARDO CASALINI

Naval Research Laboratory, Washington, DC 20375, USA; and Chemistry Department, George Mason University, Fairfax, Virginia 20030, USA

SIMONE CAPACCIOLI

Dipartimento di Fisica and INFM, Università di Pisa, I-56127, Pisa, Italy; and CNR-INFM Center "SOFT: Complex Dynamics in Structured Systems," Università di Roma "La Sapienza," I-00185 Roma, Italy

MARIAN PALUCH

Institute of Physics, Silesian University, 40-007 Katowice, Poland

C. M. ROLAND

Naval Research Laboratory, Washington, DC 20375, USA

Fractals, Diffusion, and Relaxation in Disordered Complex Systems: A Special Volume of Advances in Chemical Physics, Volume 133, Part B, edited by William T. Coffey and Yuri P. Kalmykov. Series editor Stuart A Rice.

CONTENTS

I. INTRODUCTION

The glass transition, which refers to the dramatic slowing down of kinetic processes, such as viscous flow and molecular reorientations, is a general phenomenon found in organic, inorganic, metallic, polymeric, colloidal, and biomolecular materials. On decreasing temperature T or increasing pressure P, the structural relaxation time τ_α of supercooled liquids, or analogously the local segmental relaxation time of polymers, becomes increasingly large. Eventually the molecules cannot attain their dynamic equilibrium configurations and vitrification commences. The science and technology of glass formation has a long history, with the first recorded recipe for glass appearing a few millennia ago in Babylon

(in present-day Iraq), while modern glasses are formed from many different starting materials, including not only inorganic glasses but also organic glasses, metallic glasses, and many plastics. The use of glass is widespread, and the glass-making industry contributes significantly to the world economy.

In spite of the long history and technological significance of glass, a universally accepted, fundamental understanding of the dynamics of materials undergoing vitrification is still lacking. There is not even a consensus concerning the factors governing the dramatic slowing down of the structural relaxation and related kinetic processes, such as viscous flow and molecular reorientations. This situation is highly unusual—most problems in the physical and materials sciences have been solved within a few decades—and is a testament to the complexity of the structural relaxation process in the precursor supercooled liquid. Development of a microscopic and quantitatively accurate theory of the glass transition, applicable to real materals, has become even more challenging with the improvement of experimental techniques and the introduction of new ones; these have led to the discovery of an increasing number of general properties of the dynamics of glass-forming materials spanning the range from picoseconds to years [1,2]. Some of these general properties are discussed in sections to follow in this chapter. Acceptance of a theory or model of the glass transition requires more than offering a description of selected properties. A theory is viable only if it can explain, or at least be consistent with, *all* the known general properties. The most obvious dynamic property, being the immediate cause of vitrification, is the divergence of τ_α with decreasing temperature at constant pressure. This temperature dependence can be represented in the vicinity of the glass transition by the Vogel–Fulcher–Tammann–Hesse (VFTH) equation [3–5] or the equivalent Williams–Landel–Ferry (WLF) equation [6]. The factor governing the divergence of τ_α was identified as unoccupied volume in the free volume model [6,7], and configurational entropy in the Adam and Gibbs [8] entropy model. An increase of pressure, similar to a temperature decrease, reduces both the free volume and configurational entropy and slows down structural relaxation. The free volume model has been extended to include the effect of hydrostatic pressure [6,7,9], and an extension of the Adam–Gibbs model for elevated pressures has been proposed [10–16]. Offshoots of these two classic approaches to describing vitrification have been proposed and are generally more sophisticated, without deviating from the basic idea that free volume or entropy is the factor controlling $\tau_\alpha(T,P)$. However, such models do not address other general properties of the dynamics of glass-formers—for example, the dispersion of the structural relaxation times τ_α. The dispersion is ignored or at best considered as an afterthought. If derived, the dispersion is obtained separately from τ_α, entailing other factors or assumptions. These are the common traits of not only the free volume and configurational entropy models, but practically all known theories and models of the glass transition, notwithstanding any differences in the underlying physics.

Accordingly, since the dispersion and τ_α are obtained independently as separate and unrelated predictions, in such models the dispersion (or the time/frequency dependence) of the structural relaxation bears no relation to the structural relaxation time. This means it cannot govern the dynamic properties. As have been shown before [2], and will be further discussed in this chapter, several general properties of the dynamics are well known to be governed by or correlated with the dispersion. Therefore, neglect of the dispersion means a model of the glass transition cannot be consistent with the important and general properties of the phenomenon. The present situation makes clear the need to develop a theory that connects in a fundamental way the dispersion of relaxation times to τ_α and the various experimental properties.

This chapter is organized as follows:

1. At the outset, we emphasize the fundamental importance of the dispersion of the structural relaxation by presenting a recently discovered experimental fact for many glass-formers—that is, that the dispersion of the structural relaxation remains unchanged for widely different combinations of temperature and pressure, provided that the most probable structural relaxation time τ_α is constant. Certainly τ_α can be constant for different combinations of temperature and pressure because of their compensating effects on the molecular mobility, even though the specific or free volume, entropy or configurational entropy, and static structure factor may change. However, if the dispersion of the structural relaxation is derived independently of τ_α, it is not expected to be constant for these same combinations of T and P because the two quantities do not necessarily have the same dependence on volume, entropy, and so on. This apparently general property implies that the dispersion of the structural relaxation is defined by τ_α, or at least τ_α and the dispersion have to be coupled predictions of any viable theoretical interpretation. If the dispersion of the structural relaxation is derived independently of τ_α, as in conventional theories, it is unlikely that τ_α would uniquely define the dispersion. This observation and the conclusions drawn from it have important consequences for the study of the glass transition.

2. The dispersion is shown to govern or correlate with various dynamic properties, further indicating that the dispersion plays a fundamental role in the glass transition. In the case of amorphous polymers, the dispersion of the structural relaxation (i.e., of the local segmental relaxation) even influences the relation of the relaxation to mechanisms at longer times and larger length-scales and the viscoelastic spectrum as a whole.

3. Although vitrification is related directly to structural relaxation, processes that occur at earlier times may underly structural relaxation and thus ultimately the glass transition itself. The following scenario is presented for the evolution of the dynamics as a function of time. At short times, molecules are mutually caged and cannot relax by reorientation or translation. The cage starts to decay

(loss of near-neighbor order) at intermediate times by independent (primitive) relaxation, associated with a relaxation time τ_0 identifiable with the relaxation time τ_{JG} of a special class of secondary relaxation which we call the Johari–Goldstein (JG) β-relaxation [17–18,19,20]. The primitive relaxation is the initiator of the ensuing many-molecule relaxation dynamics, which evolve in time to become increasingly "cooperative," merging eventually into structural relaxation. There is a strong correlation between the ratio $\tau_\alpha/\tau_{\rm JG}$ and the dispersion of the structural relaxation at any fixed τ_α. This correlation suggests that the dispersion originates from the primitive or JG relaxation, through the evolution of the many-molecule relaxation dynamics. This is another indication that the dispersion of the structural relaxation is a fundamental quantity, which along with τ_α is a consequence of the many-molecule relaxation dynamics.

4. Experimental data are presented to show that the JG relaxation mimics the structural relaxation in its volume–pressure and entropy–temperature dependences, as well as changes in physical aging. These features indicate that the dependences of molecular mobility on volume–pressure and entropy–temperature have entered into the faster JG relaxation long before structural relaxation, suggesting that the JG relaxation must be considered in any complete theory of the glass transition.

5. A model having predictions that are consistent with the aforementioned experimental facts is the Coupling Model (CM) [21–26]. Complex many-body relaxation is necessitated by intermolecular interactions and constraints. The effects of the latter on structural relaxation are the main thrust of the model. The dispersion of structural relaxation times is a consequence of this cooperative dynamics, a conclusion that follows from the presence of fast and slow molecules (or chain segments) interchanging their roles at times on the order of the structural relaxation time τ_α [27–29]. The dispersion of the structural relaxation can usually be described by the Kohlrausch–William–Watts (KWW) [30,31] stretched exponential function,

$$\phi(t) = \exp[-(t/\tau_\alpha)^{\beta_{KWW}}] \tag{1}$$

The fractional exponent β_{KWW} can be rewritten as $(1-n)$, where n is the coupling parameter of the CM. The breadth of the dispersion is reflected in the magnitude of n and increases with the strength of the intermolecular constraints. The dispersion and the structural relaxation time are simultaneous consequences of the many-molecule dynamics, and hence they are related to each other. The intermolecularly cooperative dynamics are built upon the local independent (primitive) relaxation, and thus a relation between the primitive relaxation time τ_0 and τ_α is expected to exist. The CM does not solve the many-body relaxation problem but uses a physical principle to derive a relation between τ_α and τ_0 that involves the dispersion parameter, n. This defining relation of the CM

has many applications. Although τ_0 is not predicted, nor are its T and P dependences described by the model, it can be calculated from the parameters, τ_α and n, of the measured structural relaxation. The primitive relaxations have properties similar to the Johari–Goldstein (JG) secondary relaxation (but they are not identical if the JG relaxation is interpreted in the conventional sense and not in the CM way) and good correspondence between their relaxation times, τ_0 and τ_{JG}, is found for many glass-formers [32–44]. From $\tau_0 \approx \tau_{JG}$ and the aforementioned properties of τ_{JG}, we can infer that τ_0 also has properties that mimic τ_α. Moreover, from $\tau_0 \approx \tau_{JG}$ and the CM relation (to be given later), both the dispersion of the structural relaxation and τ_{JG} are shown to be invariant to changes of temperature and pressure while τ_α is constant, in accord with experimental findings. Furthermore, we show that the difficult problem of tackling the structural relaxation time τ_α and its properties, which involves complex many-body interactions, is made easy through the CM by starting from the tractable independent (primitive) relaxation time τ_0.

The intermolecular interactions/constraints of a glass-former can be changed by various means including (a) confinement in nanometer space, location at a free surface, and at interfaces with another material, (b) mixture with another glass-former, and (c) increase in the number of covalent bonds by polymerization or chemical cross-links. Some of these modifications of a glass-former introduce factors that influence the dispersion, other than intermolecular interactions/constraints. An example is concentration fluctuation in a mixture. Therefore, in some cases, it is more appropriate to consider the change in the coupling parameter of the CM instead of the dispersion. We discuss the changes of dynamics with various modifications of the material and explain the changes by the CM.

II. INVARIANCE OF THE α-DISPERSION TO DIFFERENT COMBINATIONS OF T AND P AT CONSTANT τ_α

Studies of molecular dynamics have focused on the effect of temperature due largely to experimental convenience. Isobaric measurements of relaxation times and viscosities are carried out routinely as a function of temperature. From these experiments it is well established that the shape of the α-dispersion (i.e., the KWW stretch exponent β_{KWW}), when compared at T_g or some other reference value of τ_α, varies among different glass-formers [45,46]. Many experimental studies have shown also that for a given material, very often the distribution of relaxation times systematically broadens with decreasing temperature [47–50].

Less common than temperature studies at ambient pressure are experiments employing hydrostatic pressure, although dielectric measurements at high pressure were carried out nearly half a century ago [31,51–60]. Recently,

pressure has been employed as an experimental variable in broadband dielectric spectroscopy [12,40,44,61–96]. The relaxation time at ambient pressure can be maintained constant at elevated pressure P by raising the temperature T. Various combinations of P and T can be chosen for which the α-loss peak frequency ν_α (and τ_α) are the same. One important fact emerging from these pressure studies is that at a constant value of the structural relaxation time τ_α or frequency ν_α, the dispersion of the structural relaxation is constant [97–99]. In cases where the height of the α-loss peak, ε''_{max}, changes somewhat, the dispersions at a fixed ν_α have to be compared after the measured dielectric loss $\varepsilon''(\nu)$ is normalized by ε''_{max}. Very generally it is found that for a given material at a fixed value of τ_α, the relaxation function is constant, independent of thermodynamic conditions (temperature and pressure). Alternatively stated, temperature-pressure superpositioning works for the dispersion of the structural α-relaxation at constant τ_α. Lack of superposition may occur at frequencies sufficiently high compared with ν_α. Such deviation can be attributed to the contribution to dielectric loss from a resolved or unresolved secondary relaxation at higher frequencies, whose dielectric relaxation strength does not have the same P and T dependences as the α-relaxation.

In order to demonstrate convincingly that this is a general experimental fact of glass-formers, experimental data for many different materials and (for a particular material) experimental data for several dielectric relaxation times are presented herein. The glass-formers include both molecular liquids and amorphous polymers of diverse chemical structures. All show the property of temperature–pressure superpositioning of the dispersion of the structural α-relaxation at constant τ_α.

A. Molecular Glass-Formers

Numerous molecular glass-forming liquids that have narrow dispersions of the α-relaxation and have an excess wing on the high-frequency flank, but otherwise no resolved secondary relaxation in their dielectric spectra. There are experimental results [38,39,100–103] indicating that the excess wing is an unresolved Johari–Goldstein secondary relaxation [17,18,19,20,104]. The materials include cresolphthalein-dimethylether (KDE) [40], phenylphthalein-dimethylether (PDE) [71], propylene carbonate (PC) [72], chlorinated biphenyl (PCB62) [12], phenyl salicylate (salol) [73], 3,3′,4,4′-benzophenonetetracarboxylic dianhydride (BPTCDaH) [44], 1,1′-di(4-methoxy-5-methylphenyl)cyclohexane (BMMPC) [74]. For these materials, due to the unresolved secondary relaxation, a strong dependence of the shape of the dispersion on T and P (with τ_α varying) is especially evident; see, for example, refs. 12 and 40. The fact that at a fixed value of τ_α the dispersion of the α-relaxation is constant, independent of T and P, is demonstrated in Fig. 1a for KDE, Fig. 1b for PC, and Fig. 1c for PCB62

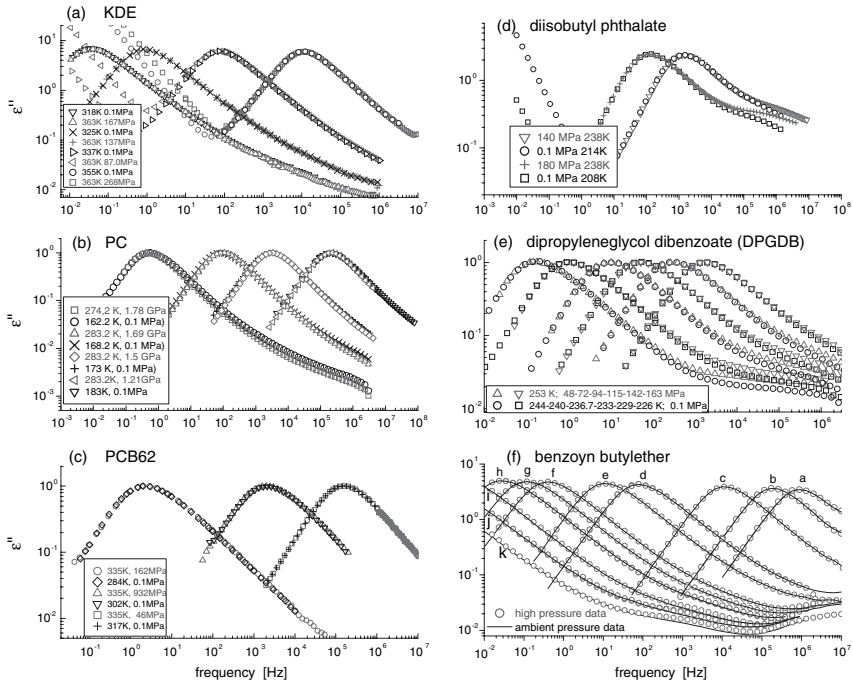

Figure 1. Dielectric loss data at various combinations of temperature and pressure as indicated to demonstrate the invariance of the dispersion of the α-relaxation at constant α-loss peak frequency ν_α or equivalently at constant α-relaxation time for (*a*) cresolphthalein-dimethylether (KDE) τ_α, (*b*) propylene carbonate (PC) (loss normalized to the value of the maximum of the α-loss peak), (*c*) chlorinated biphenyl (PCB62), (*d*) diisobutyl phthalate (DiBP), and (*e*) Dielectric loss of dipropyleneglycol dibenzoate (DPGDB). Loss normalized to the value of the maximum of the α-loss peak. The dc conductivity contribution has been subtracted. Triangles are isothermal measurements at $T = 253$ K and $P = 48$, 72, 94, 115, 142, 163 MPa (from right to left). Black symbols are isobaric measurements done at $P = 0.1$ MPa and $T = 244$, 240, 236.7, 233, 229, 226 K (from right to left). The spectrum at $T = 226$ K has been shifted along the x axis by multiplying frequency by a factor 1.3. (*f*) Dielectric loss of benzoyn isobutylether (BIBE) at different T and P. The dc conductivity contribution has been subtracted. Spectra obtained at higher P are normalized to the value of the maximum of the loss peak obtained at the same frequency at atmospheric pressure. From right to left: Black lines are atmospheric pressure data at $T = 271$ K (a), 263 K (b), 253 K (c), 240 K (d), 236 K (e), 230 K (f), 228 K (g), 226 K (h), 223 K (i), 220.5 K (j), 218 K (k). Symbols represent high-pressure data: $T = 278.5$ K and $P = 32$ MPa (a), 65 MPa (b), 118 MPa (c), 204 MPa (d), 225 MPa (e), 320 MPa (h), 370 MPa (j), 396 MPa (k); $T = 288.2$ K and $P = 350$ MPa (f), 370 MPa (g), 423 MPa (i), 450 MPa (j); $T = 298$ K and $P = 330$ MPa (d), 467 MPa (h).

(experimental details of these measurements can be found respectively in Refs.12, 40, and 72). In each figure, data are used to show that this property holds for more than one value of τ_α. The same results are found for PDE, BPTCDaH, BMMPC, and salol and are shown in Figs. 2, 3, 4, and 5, respectively.

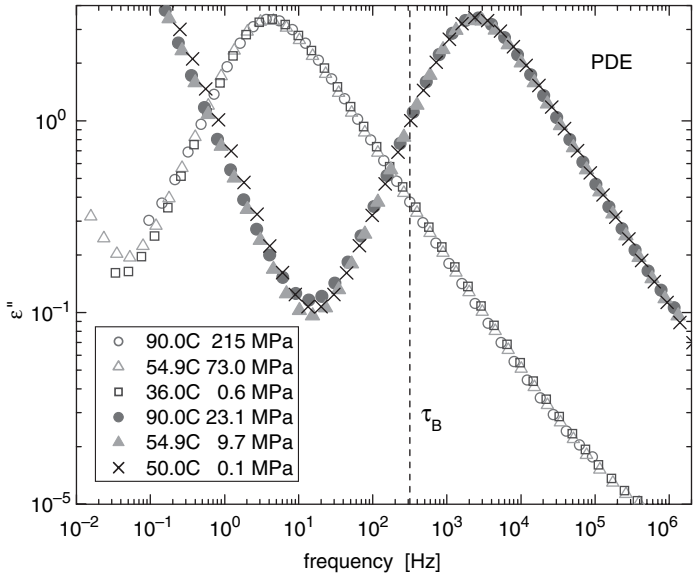

Figure 2. Dielectric loss data of phenylphthalein-dimethylether (PDE) at various combinations of temperature and pressure as indicated to demonstrate the invariance of the dispersion of the α-relaxation at constant α-loss peak frequency ν_α or equivalently at constant α-relaxation time τ_α.

Some molecular glass-formers have a resolved secondary relaxation whose peak frequency is practically pressure independent; these are not Johari–Goldstein (JG) processes (according to the definition given in Ref. 38). The slower JG relaxation is not resolved from the α-relaxation in the equilibrium liquid state, but in some cases it can be observed in the glassy state. Such liquids include 1,1′-bis(p-methoxyphenyl)cyclohexane (BMPC) [75], diethyl phthalate, (DEP) [76], di-*n*-butyl phthalate (DBP) [77], diisobutyl phthalate (DiBP) [77], di-isooctal phthalate (DiOP) [78], decahydroisoquinoline (DHIQ) [79], dipropyleneglycol dibenzoate (DPGDB) [80], benzoin-isobutylether (BIBE) [81], the epoxy compounds including diglycidyl ether of bisphenol-A (EPON828) [82], 4,4'-methylenebis(*N,N*-diglycidylaniline) (MBDGA) [83,84], bisphenol-A-propoxylate(1 PO/phenol)diglycidylether) (1PODGE) [85], *N,N*-diglycidyl-4-glycidyloxyaniline (DGGOA) [86], and *N,N*-diglycidyl-aniline (DGA) [86]. For all members of this class of glass-formers, a constant dispersion is associated with a fixed value of τ_α, independent of thermodynamic conditions (*T* and *P*). We show this (for more than one value of τ_α) with data in Fig. 1d for DiBP, Fig. 1e for DPGDB, and Fig. 1f for BIBE. The experimental details for these can be found in respectively Refs. 77, 80, and 81. The same

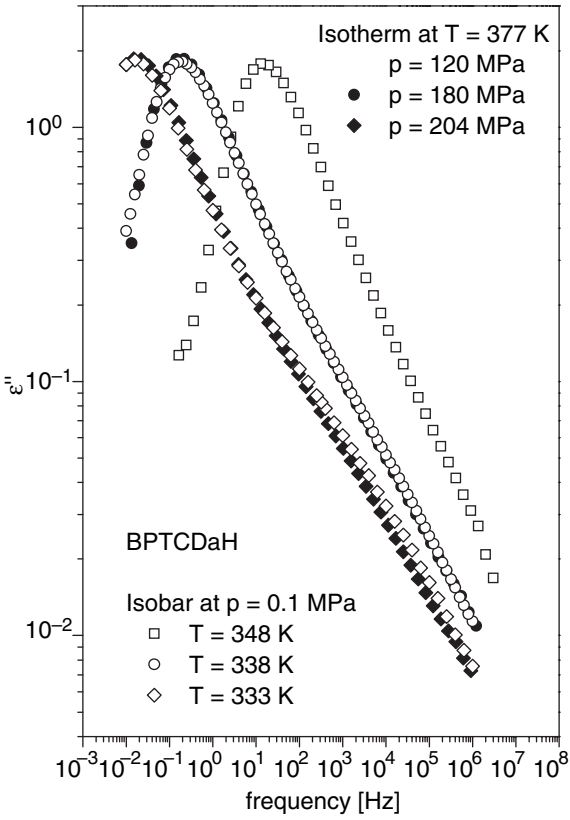

Figure 3. Dielectric loss data of 3,3′,4,4′-benzophenonetetracarboxylic dianhydride (BPTCDaH) at various combinations of temperature and pressure as indicated to demonstrate the invariance of the dispersion of the α-relaxation at constant α-loss peak frequency ν_α or equivalently at constant α-relaxation time τ_α.

property holds also for DiBP (Fig. 1d), BMPC (Fig. 6), DEP (Fig. 7), DiOP (Fig. 8), DHIQ (Fig. 9), EPON828 (Fig. 10), 1PODGE (Fig. 11), and MBDGA, DGGOA, and DGA (Fig. 12).

Earlier dielectric studies under elevated pressure [20,105–110] had found temperature–pressure superpositioning at constant τ_α in a few molecular glass-formers including ortho-terphenyl (OTP), di(2-ethylhexyl) phthalate, tricresyl phosphate, polyphenyl ether, and refined naphthenic mineral oil, although the temperature and pressure ranges are not as wide as achieved in more recent measurements.

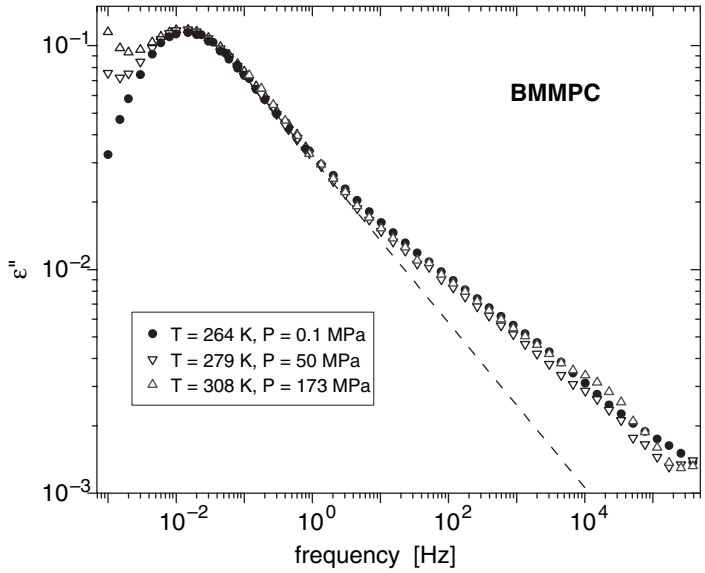

Figure 4. Dielectric loss data of 1,1′-di(4-methoxy-5-methylphenyl)cyclohexane (BMMPC) at various combinations of temperature and pressure as indicated to demonstrate the invariance of the dispersion of the α-relaxation at constant α-loss peak frequency ν_α or equivalently at constant α-relaxation time τ_α. The dashed line is the imaginary part of the one-sided Fourier transform of the KWW function with $\beta_{KWW} \equiv (1 - n) = 0.55$. The logarithmic ordinate scale makes evident the presence of an excess wing at higher frequencies.

B. Amorphous Polymers

Dielectric relaxation measurements under pressure have been carried out on several amorphous polymers, and for all cases studied the dispersion of the local segmental relaxation (i.e., the structural α-relaxation) conforms to temperature–pressure superpositioning at constant τ_α. These polymers include: polyvinylmethylether (PVME) [87]; poly(vinylacetate) (PVAc) [88]; poly(ethylene-*co*-vinyl acetate) (EVA, having 70 wt% vinyl acetate) [89]; polymethylphenylsiloxane (PMPS) [90]; poly(methyltolylsiloxane) (PMTS) [91]; 1,2-polybutadiene (1,2-PBD, also referred to as polyvinylethylene, PVE) [92]; poly(phenyl glycidyl ether)-*co*-formaldehyde (PPGE) [93]; 1,4-polyisoprene (PI) [94]; poly(propylene glycol) (molecular weight: 4000 Da), PPG-4000 [95]; poly(oxybutylene), POB [96]; and poly(isobutyl vinylether), PiBVE [111]. Constant dispersions at a fixed value of τ_α independent of thermodynamic conditions (T and P) are shown for more than one τ_α in Fig. 13a for PVAc, Fig. 13b for PMTS, Fig. 13c for PPGE, and Fig. 13d for POB. Experimental details for these measurements can be found in Refs. 88, 91, 93, and 96, respectively.

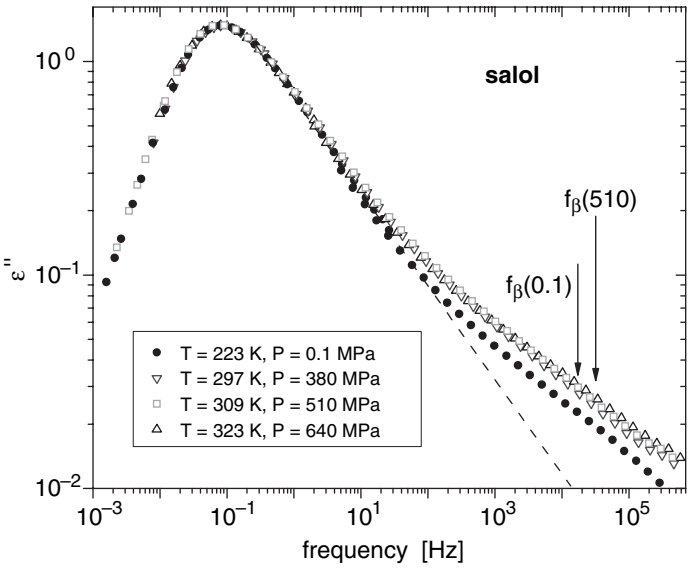

Figure 5. Dielectric loss data of phenyl salicylate (salol) at various combinations of temperature and pressure as indicated to demonstrate the invariance of the dispersion of the α-relaxation at constant α-loss peak frequency ν_α or equivalently at constant α-relaxation time τ_α. The dashed line represents extrapolation of the power law for frequencies just past the maximum.

Note that for POB there is a dielectrically active normal mode at lower frequencies, which has different P and T dependences than the local segmental mode. The T–P superposition at fixed τ_α holds also for PVME (Fig. 14), EVA (Fig. 15), PMPS (Fig. 16), PVE (Fig. 17), PPG-4000 (Fig. 18), and PiBVE (Fig. 19). For PMPS this superposition is maintained even when τ_α varies.

As illustrated in some of these figures, all the α-loss peaks are well-fitted by the one-sided Fourier transform of the KWW over the main part of the dispersion. Thus, the experimental fact of constant dispersion at constant τ_α can be restated as the invariance of the fractional exponent β_{KWW} (or the coupling parameter n) at constant τ_α. In other words, τ_α and β_{KWW} (or n) are co-invariants of changing thermodynamic conditions (T and P). If w is the full width at half-maximum of the dielectric loss peak normalized to that of an ideal Debye loss peak, there is an approximate relation between w and n given by $n = 1.047(1 - w^{-1})$ [112].

Hydrogen-bonded networks or clusters, if present, are modified at elevated pressure and temperature, changing the structure of the glass-former in the process. This occurs, for example, in glycerol [113], propylene glycol dimer and trimer (2PG and 3PG) [101,102], and *m*-fluoraniline [44]. These

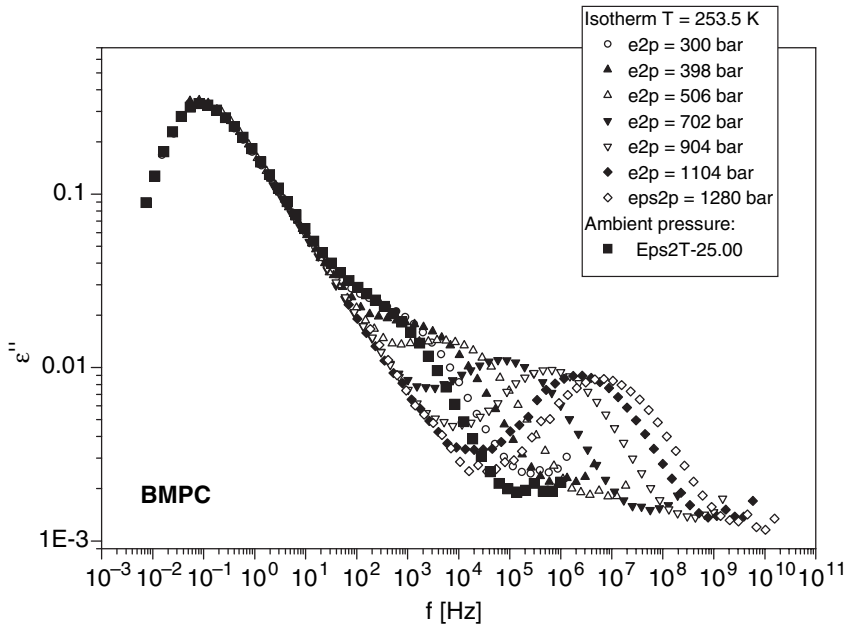

Figure 6. Master curve of the dielectric loss data of 1,1′-bis(*p*-methoxyphenyl)cyclohexane (BMPC). The spectra measured under pressure were shifted on the frequency scale to superpose with the α-loss peak at $T = 248$ K and ambient pressure. The secondary relaxation of BMPC is not a JG relaxation (its loss peak frequency is pressure-insensitive), and it is not temperature–pressure-superposable along with the α-loss peak.

hydrogen-bonded glass-formers do not obey temperature–pressure superpositioning at constant τ_α, since not just the relaxation time, but the material itself, is changing with changes in T and P. Such behavior is shown for glycerol and threitol in Fig. 20, 2PG in Fig. 21, and *m*-floraniline in Fig. 22. In higher members of the polyols, such as xylitol and sorbitol, the departure from *T–P* superpositioning at constant τ_α is small compared with the lower member glycerol. This is shown for xylitol in Fig. 23.

C. Implication of *T–P* Superpositioning of the α-Dispersion at Constant τ_α

We now discuss the impact of this general property on theories and models of the glass transition. The primary concern of most theories is to explain the temperature and pressure dependences of the structural relaxation time τ_α. The dispersion (n or β_{KWW}) of the structural relaxation is either not addressed or

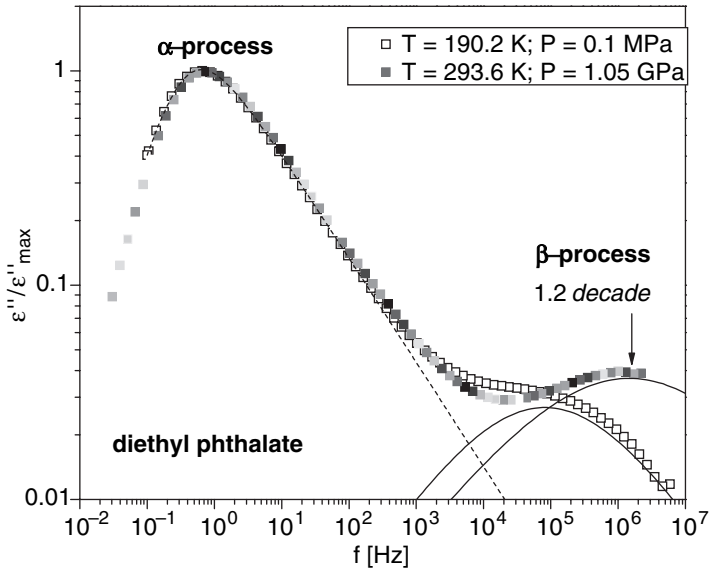

Figure 7. Dielectric loss data of diethyl phthalate (DEP) at various combinations of temperature and pressure as indicated to demonstrate the invariance of the dispersion of the α-relaxation at constant α-loss peak frequency ν_α or equivalently at constant α-relaxation time τ_α.

else considered separately with additional input not involved in arriving at τ_α. For example, the original free-volume models and the Adam–Gibbs model treat the variation of relaxation times with T and P but do not predict the distribution of molecular relaxation rates. Additional input such as a specific fluctuation and distribution of some parameter must be introduced to generate a distribution of relaxation times consistent with the empirical KWW time correlation function, as done in some modern versions of these theories. It is not difficult for any of model to find combinations of T and P such that the predicted $\tau_\alpha(T,P)$ is constant. However, it is unlikely that the same combinations will also keep the predicted dispersion or $\beta_{KWW}(T,P)$ constant. For one glass-former it may be possible to introduce additional assumptions to force both $\tau_\alpha(T,P)$ and $\beta_{KWW}(T,P)$ to be simultaneously constant. However, this would not be a worthwhile undertaking since $\tau_\alpha(T,P)$ and $\beta_{KWW}(T,P)$ are simultaneously constant for many glass-formers, with different physical and chemical structures and broadly different sensitivities to temperature and density [62,114,115]. Thus, the experimental observations (i.e., simultaneous constancy of $\tau_\alpha(T,P)$ and $\beta_{KWW}(T,P)$) has direct impact on the theoretical efforts to understand the glass transition, past and present. We are able to conclude that conventional theories and models, in which the structural relaxation time does not define or govern the dispersion of the

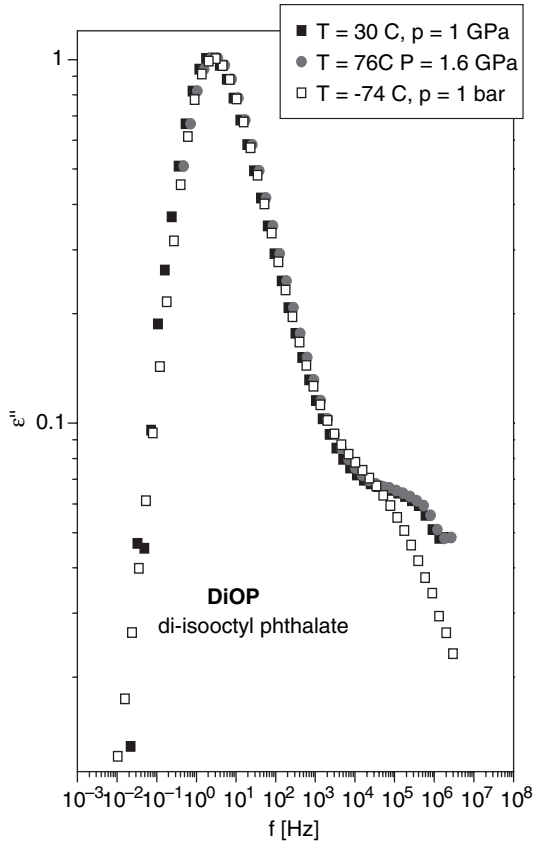

Figure 8. Dielectric loss data of di-isooctal phthalate (DiOP) at various combinations of temperature and pressure as indicated to demonstrate the invariance of the dispersion of the α-relaxation at constant loss peak frequency ν_α or equivalently at constant α-relaxation time τ_α.

structural relaxation, cannot explain the simultaneous constancy of $\tau_\alpha(T,P)$ and the dispersion of the α-relaxation or $\beta_{KWW}(T,P)$. Revision is required to bring them to consistency with this general experiment fact.

D. Invariance of the α-Dispersion to Different *T–P* at Constant τ_α Investigated by Techniques Other than Dielectric Spectroscopy

The spectra for molecular and polymeric glass-formers shown above to demonstrate the invariance of the α-dispersion to *T* and *P* at constant τ_α, were

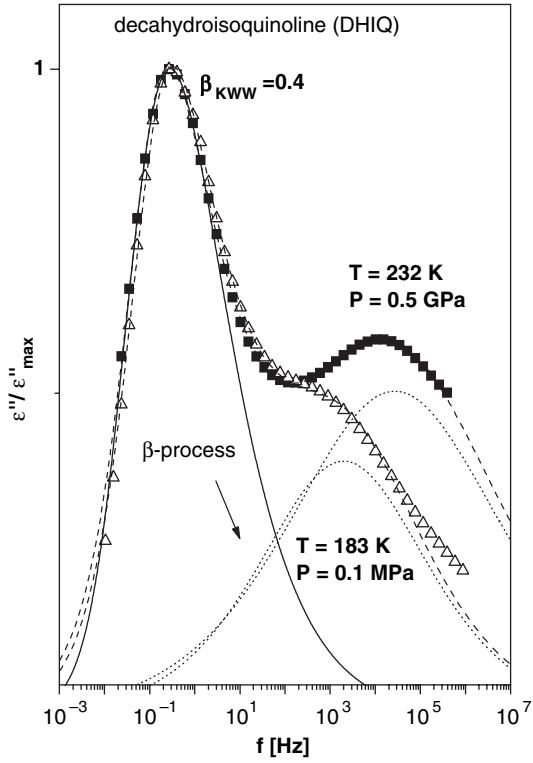

Figure 9. Dielectric loss data of decahydroisoquinoline (DHIQ) at various combinations of temperature and pressure as indicated to demonstrate the invariance of the dispersion of the α-relaxation at constant α-loss peak frequency ν_α or equivalently at constant α-relaxation time τ_α.

acquired by dielectric spectroscopy. This reflects the utility of dielectric spectroscopy in investigating broadband dynamics under pressure, particularly with recent instrumental developments. [62]. Therefore, an extensive database of broadband dielectric spectra of different materials in different *T–P* conditions is available, enabling an assessment of the *T–P* superpositioning. Although we believe the phenomena to be quite general, there is a paucity of data from other experimental techniques. However, some results are available, as described below.

For polymeric systems, only a few Photon Correlation Spectroscopy (PCS) studies have been carried out, and these were done more than 20 years ago. Within the experimental resolution, the shape of the α-relaxation was found to be essentially invariant to temperature and pressure at fixed τ_α, and time–

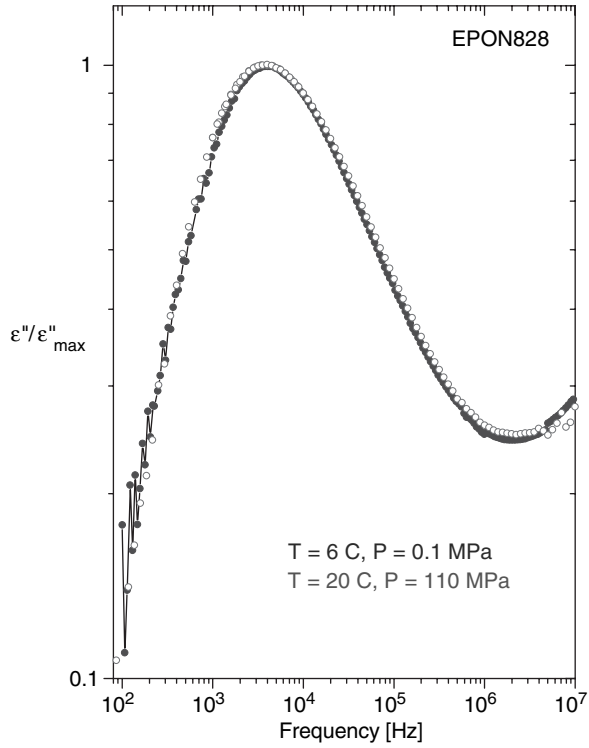

Figure 10. Dielectric loss data of diglycidyl ether of bisphenol-A (EPON828) at various combinations of temperature and pressure as indicated to demonstrate the invariance of the dispersion of the α-relaxation at constant α-loss peak frequency ν_α or equivalently at constant α-relaxation time τ_α.

temperature–pressure (*tTP*) superposition was invoked. The investigated systems were poly(ethylacrylate) [116,117], poly(methylacrylate) [118], and polystyrene [119]. A recent PCS experiment done on polypropyleneoxide also found that *tTP* superposition held. [120].

The available studies of molecular glass-formers are wider, for both materials and techniques. For ortho-terphenyl (OTP), the Kohlrausch parameters for the α-relaxation by PCS at different temperatures and pressures [121,122] have been reported. The stretching parameters β_{KWW} versus α-relaxation time τ_α for different T and P fall, within the experimental uncertainty, on a single curve, with β_{KWW} slightly decreasing with increasing τ_α. On the other hand, a shape invariance of the α-relaxation has been observed for OTP by specific heat spectroscopy under elevated pressure [123]. Additionally, experiments done on

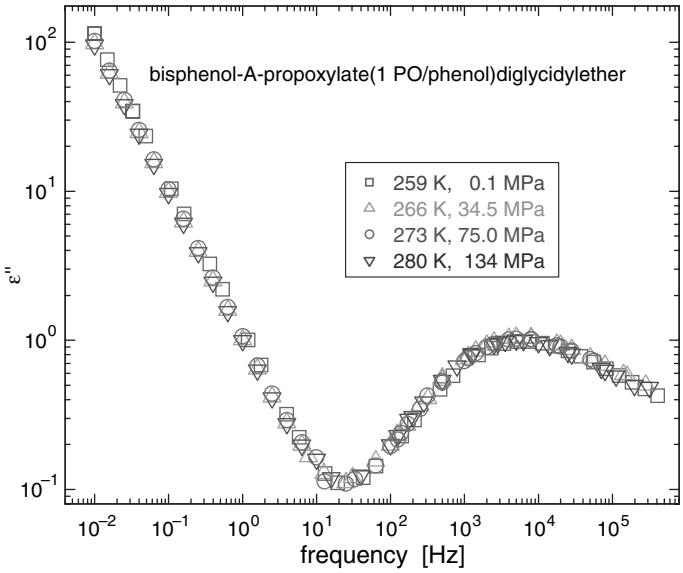

Figure 11. Dielectric loss data of bisphenol-A-propoxylate(1 PO/phenol)diglycidylether) at various combinations of temperature and pressure as indicated to demonstrate the invariance of the dispersion of the α-relaxation at constant α-loss peak frequency ν_α or equivalently at constant α-relaxation time τ_α.

OTP by neutron scattering at different *T* and *P* revealed a negligible dependence of the shape of the structural relaxation, while the static structure factor yielded a master curve only for isochronal conditions—that is, for constant relaxation time τ_α [124].

Salol is another system for which the invariance under pressure of the α-relaxation shape was reported. Recent PCS experiments [125,126] revealed that the correlation functions acquired at different pressures up to 180 MPa and at room temperature superposed. The stretching parameter β_{KWW} was 0.68, in agreement with the PCS measurements done at ambient pressure [127,128].

Very accurate PCS measurements for different T and P conditions were carried out on different molecular glass-forming systems by Patkowski and co-workers, including epoxy oligomers [129–131], and the van der waals liquids PDE [132,133], BMPC [134], and BMMPC [135]. In most of the investigated systems, master curves are obtained for $\beta_{KWW}(T,P)$ of the α-relaxation plotted versus $\tau_\alpha(T,P)$, with the value decreasing (broader dispersion) as the dynamics slow (longer $\tau_\alpha(T,P)$.). This is another evidence that the α-dispersion is directly related to the relaxation time.

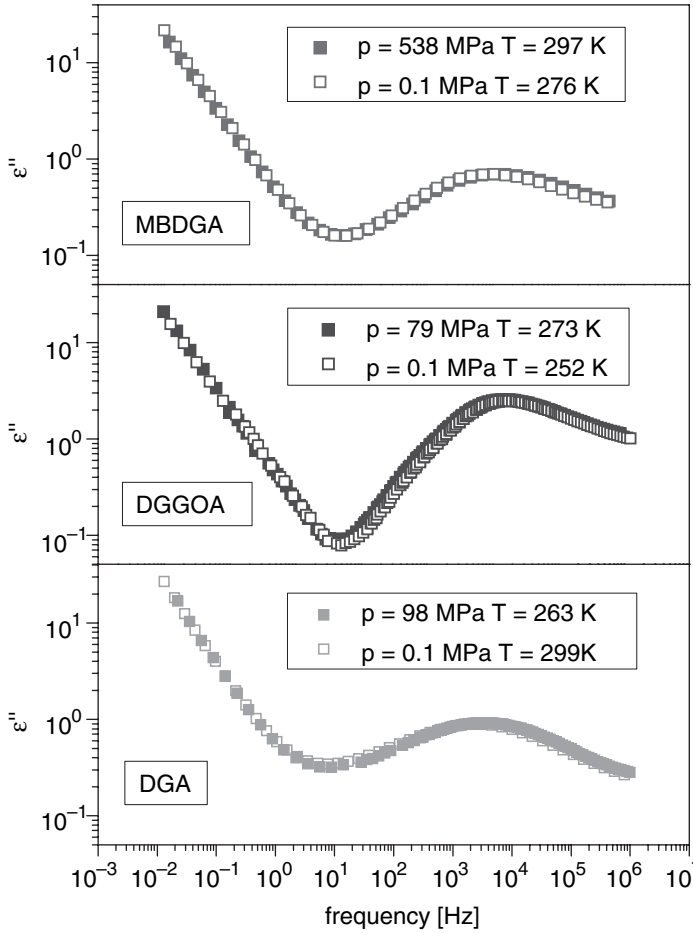

Figure 12. Dielectric loss data of MBDGA (top), DGGOA (middle), and DGA (bottom) at various combinations of temperature and pressure as indicated to demonstrate the invariance of the dispersion of the α-relaxation at constant α-loss peak frequency ν_α or equivalently at constant α-relaxation time τ_α. Open symbols represent the relaxation curves measured at ambient pressure, and solid symbols represent those at elevated pressures.

We can conclude that the result from dielectric spectroscopy—that the α-dispersion is invariant to T and P at constant τ_α—appears to be quite general, with respect to both the material and the experimental technique. The limitation is only that sufficiently broad spectra must be obtained under different conditions of temperature and pressure.

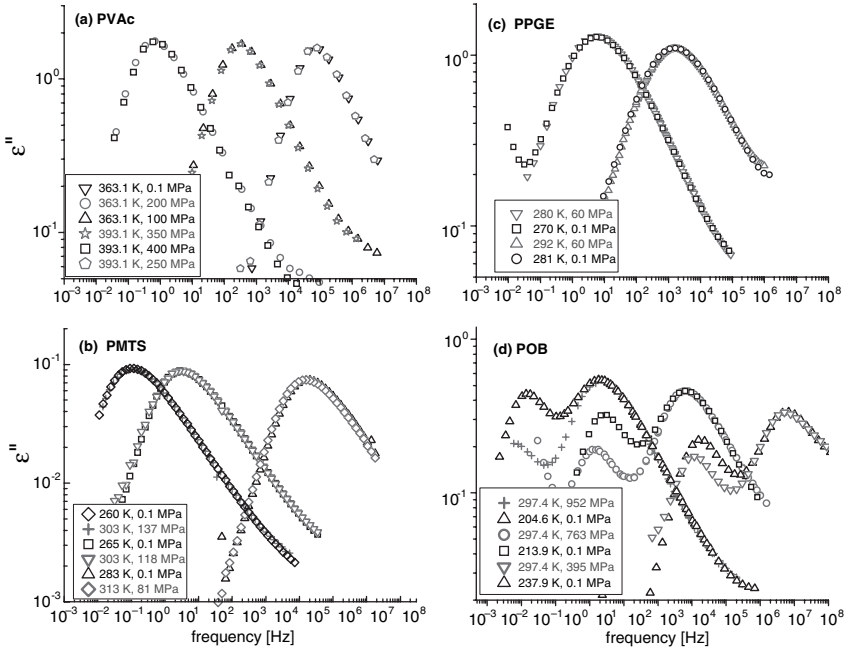

Figure 13. Dielectric loss data at various combinations of temperature and pressure as indicated to demonstrate the invariance of the dispersion of the α-relaxation at constant α-loss peak frequency ν_α or equivalently at constant α-relaxation time τ_α, for (*a*) poly(vinylacetate) (PVAc), (*b*) poly(methyltolylsiloxane) (PMTS), and (*c*) poly(phenyl glycidyl ether)-*co*-formaldehyde (PPGE); d)poly(oxybutylene) (POB). In all cases, spectra obtained at higher *P* are normalized to the value of the maximum of the loss peak obtained at the same frequency at atmospheric pressure.

III. STRUCTURAL RELAXATION PROPERTIES ARE GOVERNED BY, OR CORRELATED WITH, THE α-DISPERSION

Not only does τ_α uniquely define the dispersion, as shown herein, but also many properties of τ_α are governed by, or correlated with, the dispersion of the structural relaxation or the fractional exponent $\beta_{KWW}(=1-n)$ of the KWW function that describes it. Some examples of these properties have been described in reviews [2,22]. Here we mention briefly a few examples.

1. The steepness or "fragility" index, defined by $m \equiv d \log_{10}\tau_\alpha / d(T_g/T)|_{T_g/T=1}$, at ambient pressure increases with increasing n [45]. Glass-formers in general conform broadly to this correlation, although many exceptions are known, and in particular the correlation breaks down at elevated pressure [98]. Strict applicability may require restricting considerations

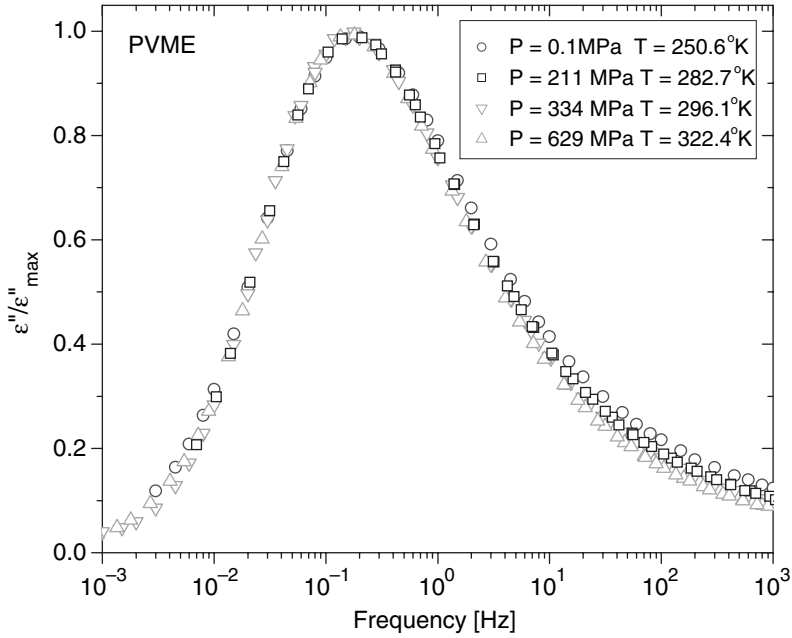

Figure 14. Dielectric loss data of polyvinylmethylether (PVME) at various combinations of temperature and pressure as indicated to demonstrate the invariance of the dispersion of the α-relaxation at constant α-loss peak frequency ν_α or equivalently at constant α-relaxation time τ_α.

to materials belonging to the same family, such as the polyols (glycerol, threitol, xylitol, and sorbitol) [136] or carbon-backbone amorphous polymers [46,137–139]. This is because, as discussed later, the temperature dependence of τ_α is governed not only by the dispersion, but also by the specific volume, V and entropy S. Chemically different glass-formers can have widely different dependence of τ_α on V [114,115]. Thus, the correlation between m and n can break down among chemically dissimilar glass-formers. An example is propylene carbonate, when considered together with glycerol, threitol, xylitol, and sorbitol. Among these, propylene carbonate has the narrowest dielectric relaxation dispersion (i.e., smallest n), but its m is larger than that of glycerol and threitol [36,140]. The correlation also breaks down in the same glass-former under different pressures [98]. In general, m decreases with P [141]. From the previous section, since n or the dispersion is invariant at $\tau_\alpha = 10^2$ s (a time customarily used to define T_g at any given pressure), the fact that m decreases with P means that the correlation between m and n necessarily breaks down.

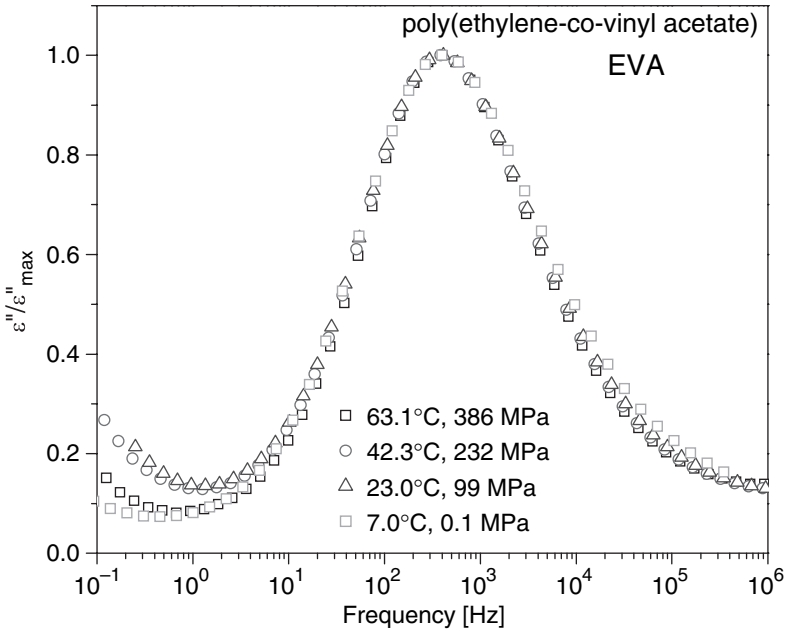

Figure 15. Dielectric loss data of poly(ethylene-*co*-vinyl acetate) (EVA, with 70 wt% vinyl acetate) at various combinations of temperature and pressure as indicated to demonstrate the invariance of the dispersion of the α-relaxation at constant α-loss peak frequency ν_α or equivalently at constant α-relaxation time τ_α.

2. Quasielastic neutron scattering experiments and molecular dynamics simulations on polymeric and nonpolymeric glass-formers have found that the dependence of τ_α on the scattering vector Q is given by $Q^{-2/(1-n)}$ [24,142–151]. Hence the Q dependence of τ_α is governed by the breadth of the dispersion or n. Such Q dependence of the relaxation time is also shared by other interacting systems including suspensions of colloidal particles [152], semidilute polymer solutions [153–155], associating polymer solutions [156,157], and polymer cluster solutions [158].

3. The temperature dependence of τ_α observed over more than 12 decades from sub-nanoseconds to 100 s cannot be fit by a single Vogel–Fulcher–Tammann–Hesse (VFTH) equation [159,160]. At short times and temperatures higher than T_A, τ_α has an Arrhenius dependence. Below T_A, τ_α has a VFTH dependence, $(\text{VFTH})_1$, which is no longer adequate when temperature falls below T_B. A second VFTH equation, $(\text{VFTH})_2$, has to be used to describe τ_α for $T < T_B$. At T_A, $n(T_A)$ is small. There is a significant increase of the rate of change of $n(T)$ with decreasing temperature when crossing T_B. The difference

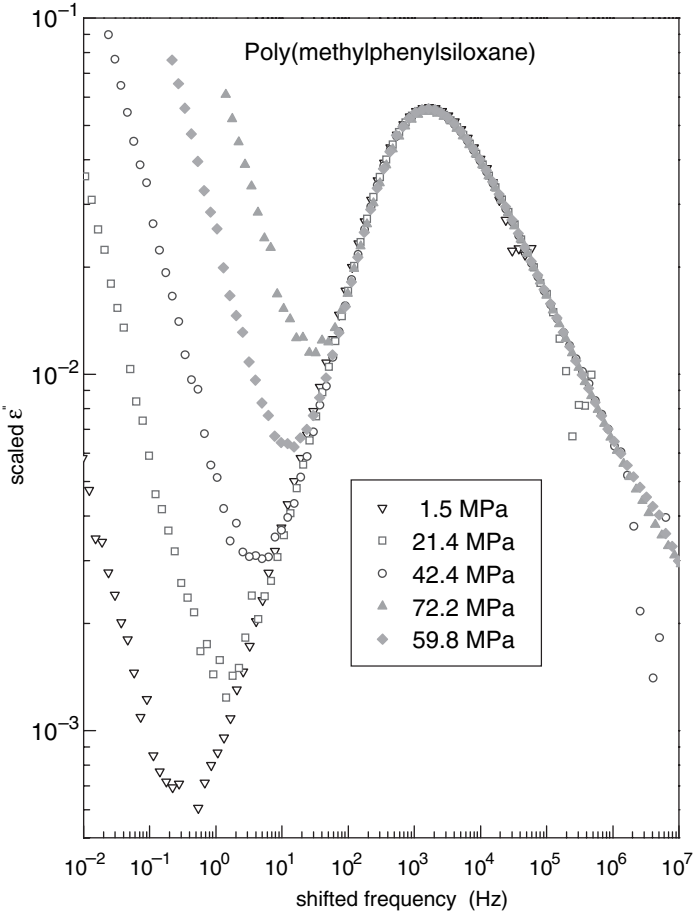

Figure 16. Dielectric loss curves of polymethylphenylsiloxane (PMPS) measured at a constant temperature ($T = 273$ K) and different pressures. The data have been shifted to superimpose onto the data for $P = 42.4$ MPa.

between $(VFTH)_1$ and $(VFTH)_2$ correlates with the width of the α-relaxation dispersion or $n(T_g)$, if T_g is defined uniformly as the temperature at which τ_α reaches an arbitrarily chosen long time, say 10^2 s [161–164]. The crossover from $(VFTH)_1$ to $(VFTH)_2$ was observed isobarically also at elevated pressures. The crossover temperature T_B generally increases with applied pressure P, but the value of τ_α or the viscosity at the crossover is the same for a given glass-former [141,165,166].Two examples, BMMPC and PCB62, are shown in Fig. 24 and 25, respectively. All glass-formers studied have the same dispersion

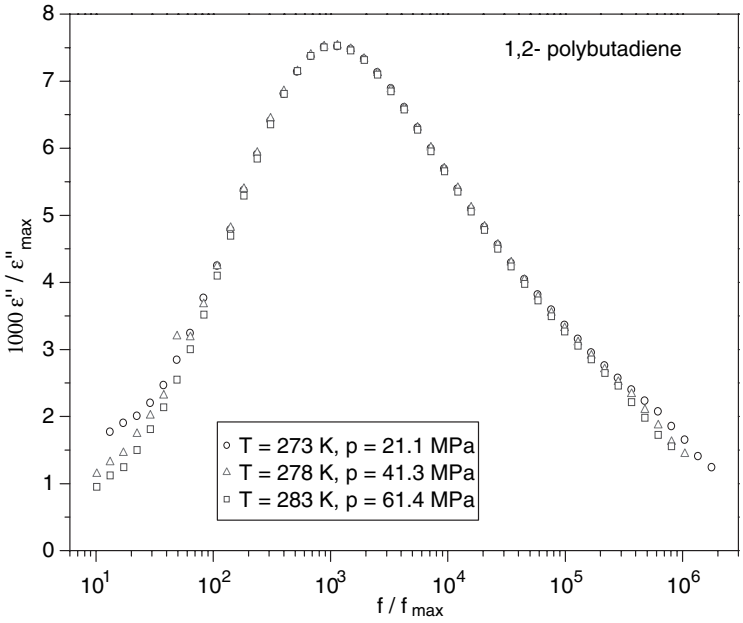

Figure 17. Dielectric loss data of 1,2-polybutadiene (1,2-PBD) at various combinations of temperature and pressure as indicated to demonstrate the invariance of the dispersion of the α-relaxation at constant α-loss peak frequency ν_α or equivalently at constant α-relaxation time τ_α.

at constant τ_α, independent of T and P, a general property discussed in Section II. Hence, the dispersion is invariant at the crossover from $(\text{VFTH})_1$ to $(\text{VFTH})_2$ when the latter is observed for different combinations of T and P.

4. The rotational diffusion coefficient, D_r, of a probe molecule in a glass-former follows the temperature dependence of the Debye–Stokes–Einstein (DSE) equation [167–171],

$$D_r \equiv \frac{1}{6\langle\tau_c\rangle} = \frac{kT}{8\pi\eta r_s^3} \tag{2}$$

Here η is the shear viscosity, $\langle\tau_c\rangle$ is the mean rotational correlation time, and r_s the spherical radius of the probe molecule. On the other hand, the translational diffusion coefficient, D_t, of the probe molecule is given by the Stokes–Einstein (SE) relation [167–171],

$$D_t = \frac{kT}{6\pi\eta r_s} \tag{3}$$

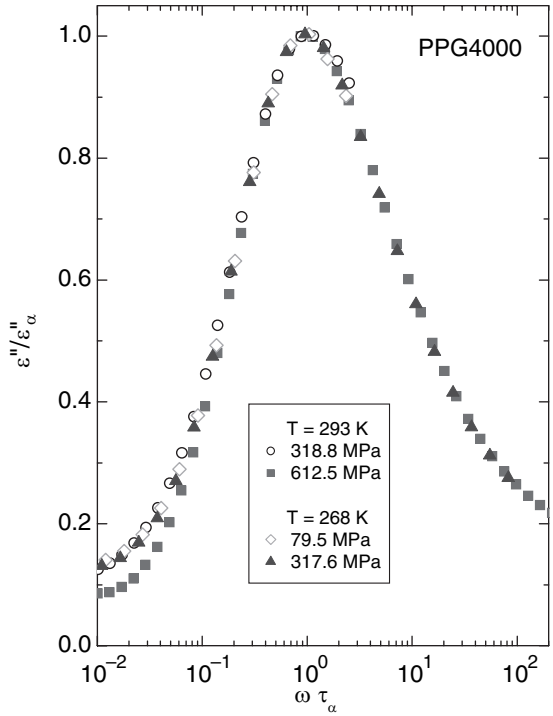

Figure 18. Dielectric loss data of poly(propylene glycol) (PPG-4000, molecular weight: 4000 Da) at various combinations of temperature and pressure as indicated to demonstrate the invariance of the dispersion of the α-relaxation at constant α-loss peak frequency ν_α or equivalently at constant α-relaxation time τ_α.

Thus, the combined SE and the DSE equations predict that the product $D_t\tau_c \equiv (D_t\tau_c)_{\mathrm{SE,DSE}}$ should equal $2r_s^2/9$. Measurements of probe translational diffusion and rotational diffusion made in glass-formers have found that the product $D_t\tau$ can be much larger than this value, revealing a breakdown of the Stokes–Einstein (SE) relation and the Debye–Stokes–Einstein (DSE) relation. There is an enhancement of probe translational diffusion in comparison with rotational diffusion. The time dependence of the probe rotational time correlation functions $r(t)$ is well-described by the KWW function,

$$r(t) = r(t) = r(0)\exp[-(t/\tau_c)^{\beta_{KWW}}] \tag{4}$$

The ratio $D_t\tau_c/(D_t\tau_c)_{\mathrm{SE,DSE}}$ evaluated at $T = T_g$ is a measure of the degree of breakdown of the SE and DSE relations for various combinations of probes

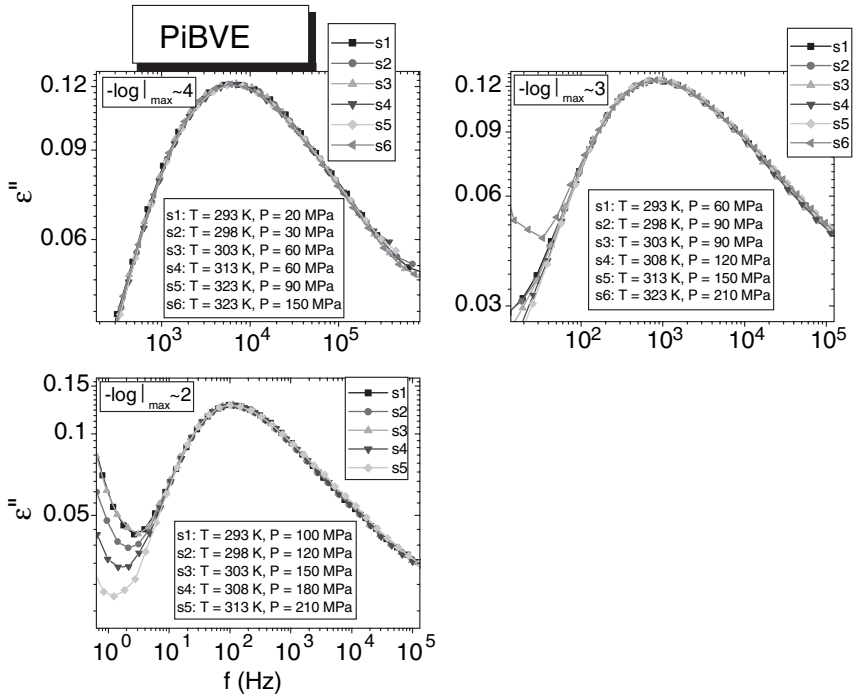

Figure 19. Dielectric loss data of poly(isobutyl vinylether) PiBVE at various combinations of temperature and pressure as indicated to demonstrate the invariance of the dispersion of the α-relaxation at constant α-loss peak frequency ν_α or equivalently at constant α-relaxation time τ_α, for three different τ_α or the corresponding loss peak frequency ν_α. Data supplied by G. Floudas [K. Mpoukouvalas, G. Floudas, B. Verdonck, and F. E. Du Prez, *Phys. Rev. E* **72**, 011802 (2005).].

and host glass-formers [167–171]. A strong correlation was observed at $T = T_g$ between the quantity $D_t\tau_c/(D_t\tau_c)_{\mathrm{SE,DSE}}$ and the dispersion of the probe rotational correlation functions $r(t)$ (see Fig. 26). A more enhanced probe translation compared with probe rotation is found for hosts having correlation functions that are more dispersive—that is, larger n or smaller β_{KWW} values. Hence, the dispersion is related to the degree of breakdown of SE and DSE relations, a general property of glass-forming liquids. The variation of the dispersion was traced to the difference between the probe rotation time and the host structural relaxation time [172].

When the probe is identical to the host, probe diffusion becomes self-diffusion in a neat glass-former. By extrapolating the results of probe/host systems, the breakdown of SE and DSE relations in neat glass-formers is expected, and the correlation between $D_t\tau_c/(D_t\tau_c)_{\mathrm{SE,DSE}}$ and $n \equiv (1 - \beta_{KWW})$

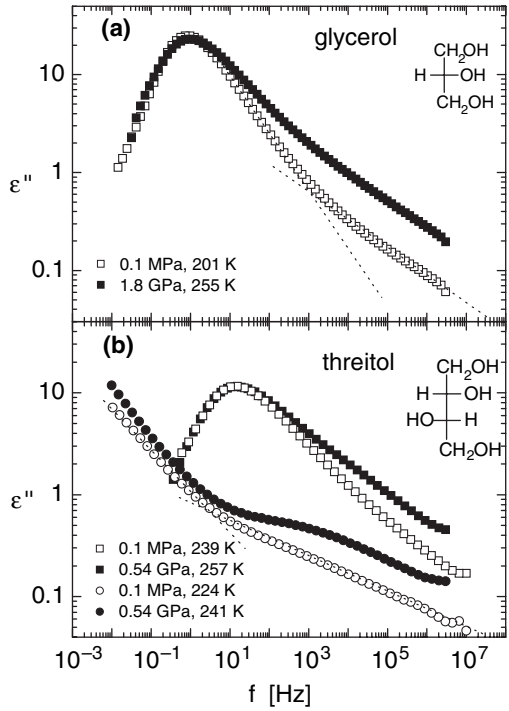

Figure 20. Dielectric loss data of glycerol and threitol at various combinations of temperature and pressure as indicated to demonstrate the departure of invariance of the dispersion of the α-relaxation at constant loss peak frequency ν_α or equivalently at constant α-relaxation time τ_α.

should still hold. Actually, the breakdown of SE and DSE relations in neat glass-formers was discovered more than three decades earlier in 1,3-bis-(1-naphthyl)-5-(2-naphthyl)benzene (TNB) and 1,2-diphenylbenzene (OTP) [160,173–177] and was recently reconfirmed using modern techniques [178].

The enhancement of translational/diffusional motions has been ascribed to spatially heterogeneous dynamics [178,179]. In this view, regions of differing dynamics give rise to nonexponential relaxation (dispersion) in ensemble average measurements. The decoupling between self-diffusion and rotation occurs because D_t is related to an average over $1/\tau$ of the distribution, emphasizing the fast dynamics, while τ_c is related to an average over τ of the distribution, which would be determined primarily by the slowest molecules. Experimentally, the product $D_t\tau_c$ of TNB is equal to $(D_t\tau_c)_{\mathrm{SE,DSE}}$ for $T \geq 1.28T_g$, and it increases montotonically with decreasing temperature to reach a value about 400 times $(D_t\tau_c)_{\mathrm{SE,DSE}}$. Within this view, an increasing product $D_t\tau_c$ is associated with the enlarging relaxation time dispersion (i.e.,

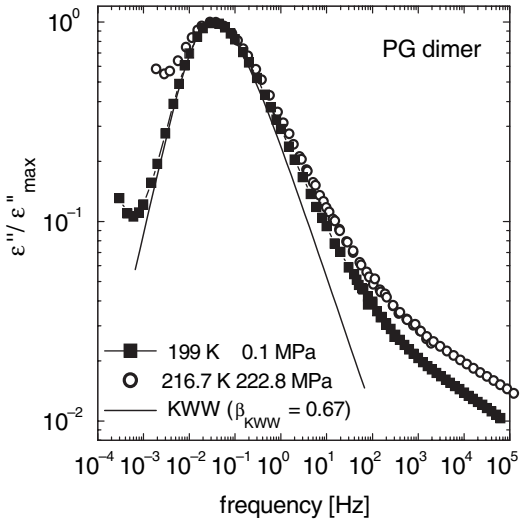

Figure 21. Dielectric loss data of PG dimer at various combinations of temperature and pressure as indicated to demonstrate the departure of invariance of the dispersion of the α-relaxation at constant loss peak frequency ν_α or equivalently at constant α-relaxation time τ_α.

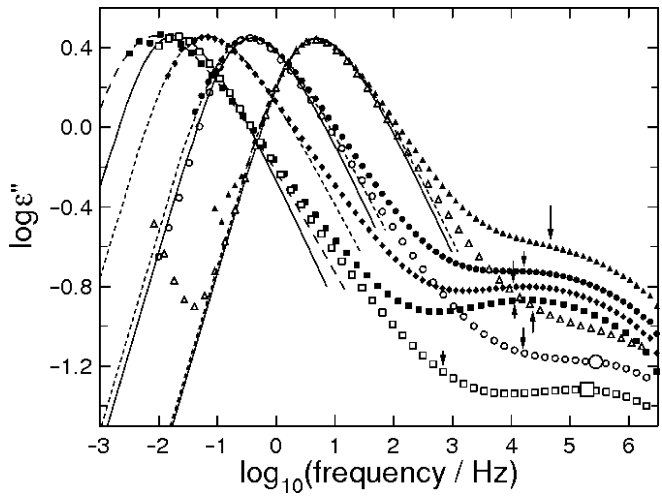

Figure 22. Dielectric loss spectrum of *m*-FA at 279 K and 1.69 GPa (■), 1.60 GPa (◆), 1.52 GPa data (●), and 1.4 GPa data (▲). Dielectric loss spectrum of mFA at ambient pressure and 174 K (□), 177 K data (○), and 180 K (△). The dashed lines are fits to the data at 279 K and under GPa pressures by the one-sided Fourier transform of the KWW function. The solid lines are similar fits to the ambient pressure data. The vertical arrows indicate the calculated primitive relaxation frequencies, ν_0, for all the data sets.

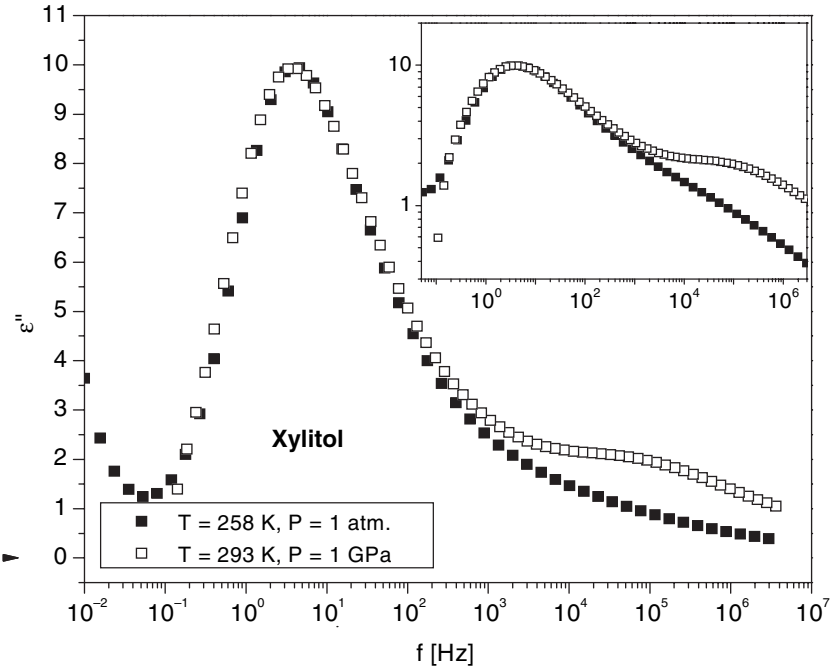

Figure 23. Dielectric loss data of xylitol at various combinations of temperature and pressure as indicated to demonstrate the much smaller departure of invariance of the dispersion of the α-relaxation at constant loss peak frequency ν_α or equivalently at constant α-relaxation time τ_α.

decreasing β_{KWW}) as T is lowered towards T_g. Therefore, this explanation requires a concomitant temperature dependence of the dispersion. However, dielectric measurements of the dispersion of the α-relaxation of TNB found it to be independent of temperature in the range $T_g < T < 1.23T_g$ [180]. Thus, the decoupling of rotational translational dynamics cannot be explained in the manner described by spatially heterogeous dynamics, which, like other properties including the α-dispersion *per se*, is a consequence of the many-molecule α-relaxation dynamics. Although the dispersion is consistent with spatial dynamic heterogenity, the former is not a derived consequence of the latter. Both are parallel consequences of many-molecule relaxation.

An alternative explanation is based on the dispersion and its dependence on the dynamic variables probed (i.e., rotation versus translation) [172]. The dispersion of rotational diffusion and of the shear viscoelastic response is broader than that of translational diffusion or the mean-square displacement of the molecule. It is a consequence of the cooperative dynamics that the dispersion of different dynamic variables for the same substance can be different and the

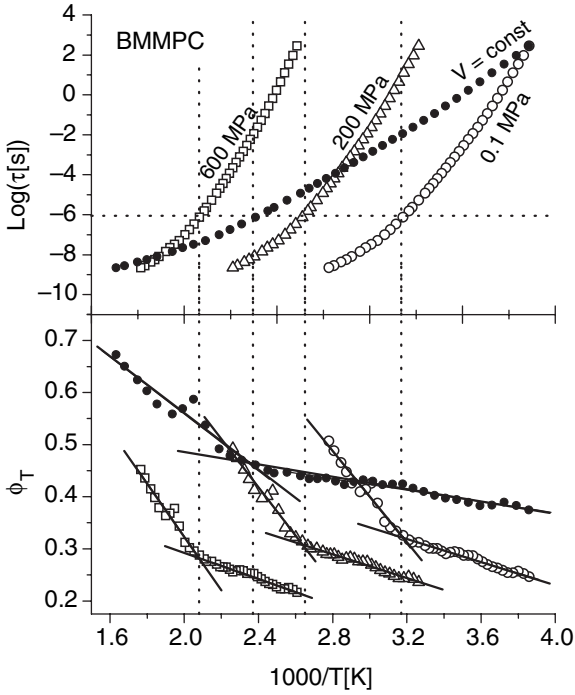

Figure 24. Upper panel: Dielectric relaxation time for BMMPC experimental data for 0.1 MPa, other isobars (200 and 600 MPa), and the isochore at $V = 0.9032$ ml/g were calculated. Dotted line indicates the average of $\log_{10}(\tau_B) = -6.1$ for the different curves. Lower panel: Stickel function, with low- and high-T linear fits, done over the range $-4.68 < \log_{10}(\tau[s]) < 3.85$ and $-8.55 < \log_{10}(\tau[s]) < -6.4$, respectively. Vertical dotted lines indicate the dynamic crossover.

dynamic variable having a broader dispersion usually has a stronger temperature dependence [181–186]. Thus, the breakdown of SE and DSE relations in glass-forming liquids is a special case of a general phenomenon [172,187].

5. The α-relaxation involves cooperative and heterogeneous dynamics of many molecules (or chain segments), which at any temperature define a length-scale L_{dh}. The dispersion of the α-relaxation is also a consequence of the many-body dynamics. Naturally we expect a larger L_{dh} to be associated with a broader dispersion, because both quantities directly reflect the intermolecularly cooperative dynamics. This correlation is borne out by comparing β_{KWW} with L_{dh} for glycerol, ortho-terphenyl, and poly(vinylacetate) as obtained by multidimensional ^{13}C solid-state exchange NMR experiments [188].

6. Amorphous polymers have relaxation processes transpiring at longer times and longer length-scales than the local segmental relaxation, which is the analog of the structural α-relaxation of molecular glass formers. For

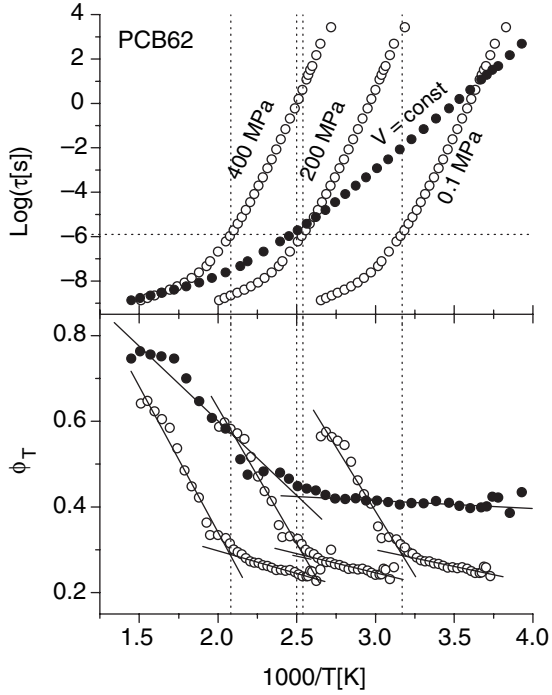

Figure 25. Upper panel: dielectric relaxation times for PCB62 experimental data for 0.1 MPa; other isobars and isochoric curve at $V = 0.6131$ ml/g were calculated. Dotted line indicates the average of $\log_{10}(\tau_B) = -5.9$ for the different curves. Lower panel: Stickel function, with low- and high-T linear fits, done over the range $-5.42 < \log_{10}(\tau[s]) < 2.169$ and $-8.87 < \log_{10}(\tau[s]) < -5.98$, respectively. The vertical dotted lines in both panels represent the dynamic crossover.

unentangled linear polymers, these processes are referred to as the Rouse modes. For entangled polymers, the long-time processes include the Rouse modes of chain units between entanglements and the terminal, entangled chain modes. It has been well documented that the Rouse and the terminal relaxation times have a weaker temperature dependence than τ_α of the local segmental relaxation, leading to breakdown of time–temperature superpositing in the viscoelastic response of amorphous polymers [189–209]. The width of the dispersion of the local segmental relaxation, or the β_{KWW} appearing in the exponent of the KWW fitting function, determines the difference in the temperature dependences. For example, from light scattering measurements, polystyrene has $\beta_{KWW} = 0.36$ [210] and polyisobutylene has $\beta_{KWW} = 0.55$ [211]. The breakdown of time–temperature superposition of viscoelastic data is much more pronounced in polystyrene than in polyisobutylene [190,191, 204,208].

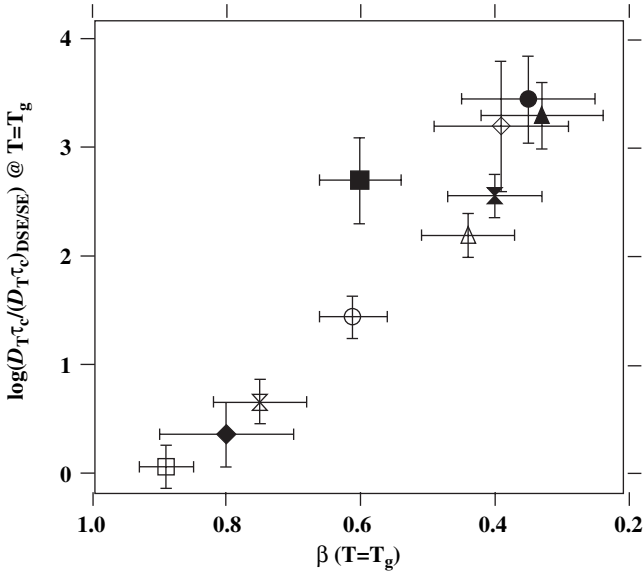

Figure 26. Correlation between enhanced translation $\log[D_t\tau_c)/(D_t\tau_c)_{\mathrm{SE,DSE}}$ at T_g and the KWW exponent of the probe rotational correlation function at T_g in four matrices: OTP, TNB, polystyrene (PS), and polysulfone (PSF). The probes are tetracene, rubrene, anthracene, and BPEA. The symbols represent PS/tetracene (closed circle), PS/rubrene (open circle), PSF/tetracene (closed triangle), PSF/rubrene (open triangle), OTP/tetracene (cloded square), OTP/rubrene (open square), OTP/antharcene (open diamond), OTP/BPEA (closed diamond), TNB/tetracene (closed hourglass), and TNB/rubrene (open hourglass). Figure adapted from data in the following references: M. T. Cicerone, F. R. Blackburn, and M. D. Ediger, *J. Chem. Phys.* **102**, 471 (1995); M. T. Cicerone and M. D. Ediger, *J. Chem. Phys.* **104**, 7210 (1996); F. R. Blackburn, C.-Y. Wang, and M. D. Ediger, *J. Phys. Chem.* **100**, 18249 (1996); M. D. Ediger, *J. Non-Cryst. Solids* **235–237**, 10 (1998)].

IV. THE PRIMITIVE RELAXATION AND THE JOHARI–GOLDSTEIN SECONDARY RELAXATION

In addition to the the structural α-relaxation, there are faster relaxation processes originating at earlier times. At short times, molecules are caged by neighboring molecules and cannot relax by reorientation or translation. The cage (or local liquid structure) is not fixed but fluctuates with time, giving rise to low loss which has no characteristic time scale [35,36,212]. This situation continues until some local independent (primitive) relaxation of the *entire* molecule (or a local segment in the case of a polymer) takes place, whereupon cages decay commences. The primitive relaxation should be observed as a secondary relaxation process, which is the precursor of the many-molecule relaxation dynamics. The latter evolves with time, becomes increasingly "cooperative"—

that is, involving more and more molecules (larger length-scale)—and eventually achieves the structural α-relaxation described by a KWW correlation function [Eq. 1]. This interpretation of the evolution of the dynamics is supported by experimental data for colloidal particles obtained by confocal microscopy [213]. Flexible glass-formers having internal degrees of freedom also exhibit intramolecular motions, which involve only some atoms in the the molecule. These intramolecular processes are also secondary relaxation, but they are not universal and are invariably faster than the primitive relaxation. Thus, if more than one secondary relaxation is observed for a glass-former, the slowest is the important JG relaxation.

Since the primitive relaxation involves the motion of the entire molecule and initiates the structural α-relaxation, the secondary JG relaxation to which it corresponds can have properties analogous to those of the structural relaxation. An example is the sensitivity of the secondary relaxation time to applied pressure, which is found in all JG relaxations but not in the non-JG secondary relaxations [38,101,102]. Rigid small-molecule glass-formers offer the best cases to test for the existence of the JG relaxation. There is no intramolecular degree of freedom in a rigid molecule, and hence any secondary relaxation must involve all atoms and thus comprise the JG (or CM primitive) relaxation. Johari and Goldstein found secondary relaxations in toluene and chlorobenzene, both rigid molecules [17–19]. Similarly, secondary relaxations have been found in polymers with no substantial side group (such as 1,4-polybutadiene, polyvinylchloride [214], and polyisoprene [35]), plastic crystals [215,216], phosphate-silicate glasses [217], the molten salt $0.4Ca(NO_3)_2$–$0.6KNO_3$ (CKN) [218], and metallic glasses [219–223]. These are all likely JG relaxations because they cannot be intramolecular motions. For glass-formers in general, rigid molecules or not, criteria were given [38] for identifying secondary JG relaxations that are the CM primitive relaxation. All criteria bear some relation to the properties of the structural relaxation. Naturally, the CM primitive relaxation time, τ_0, should correspond roughly to the experimentally observed JG relaxation time, τ_{JG}. However, in the context of the CM, the JG relaxation should not be interpreted as a Cole–Cole distribution of relaxation times in addition to the α-relaxation represented by the one-sided Fourier transform of the KWW function. The measured JG spectrum is the result of an evolution of dynamics that includes all processes starting at short times with the primitive relaxation, along with the continuous buildup of many-molecule dynamics with time, and ending up with the structural relaxation described by the KWW function. Multidimensional NMR, dielectric hole burning, light scattering, and solvation experiments [29,224,225] give evidence of such evolution of dynamics. For a review of other works see Ref. 29. These experiments have shown that the structural relaxation is dynamically heterogeneous. There are both rapid and slowly moving molecular units which exchange roles at a time $t \approx \tau_\alpha$.

The evolution of the many-molecule dynamics, with more and more units participating in the motion with increasing time, is mirrored directly in colloidal suspensions of particles using confocal microscopy [213]. The correlation function of the dynamically heterogeneous α-relaxation is stretched over more decades of time than the linear exponential Debye relaxation function as a consequence of the intermolecularly cooperative dynamics. Other multidimensional NMR experiments [226] have shown that molecular reorientation in the heterogeneous α-relaxation occurs by relatively small jump angles, conceptually simlar to the primitive relaxation or as found experimentally for the JG relaxation [227].

Correspondences between τ_0 and the observed JG relaxation times, τ_{JG}, are further discussed in a later section, wherein experimental data are reviewed which show that τ_{JG} approximately equals τ_0 of the CM for many glass-formers. One prominent experimental observation is that the separation between the JG and α-relaxation times in logarithmic scale, $[\log(\tau_\alpha) - \log(\tau_{JG})]$, correlates with the width of the α-relaxation dispersion or n [32,36,38]. This empirical correlation can be derived theoretically from the CM based on the result that $\tau_{JG} \approx \tau_0$.

V. THE JG RELAXATION AND ITS CONNECTION TO STRUCTURAL RELAXATION

From the view that the α-relaxation is the product of the cooperative dynamics originating from the JG or primitive relaxation, it is natural to expect that the properties of the JG relaxation will mimic those of the structural relaxation. We consider the relaxation time as well as the relaxation strength of the JG relaxation.

A. Pressure Dependence of τ_{JG}

The α-relaxation time τ_α increases with pressure at constant temperature although this sensitivity to pressure, or the density dependence of τ_α, varies among glass-formers, depending on their chemical structure. The JG relaxation time τ_{JG} also increases with applied pressure, although less so than τ_α. On the other hand, secondary relaxations that are not of the JG kind (involving intramolecular degrees of freedom) usually have little or no pressure dependence. Dipropyleneglycol dibenzoate (DPGDB) [80] and benzoin-isobutylether (BIBE)[80] are good examples. Of the two secondary relaxations in BIBE (Fig. 1f), the slower one is the JG relaxation. The increase of τ_{JG} with applied pressure and the lack of it for the faster secondary relaxation time are evident in the figure. Figure 1e shows only the slower JG secondary relaxation in DPGDB, which is sensitive to pressure, unlike the faster secondary relaxation (shown in Fig. 27).

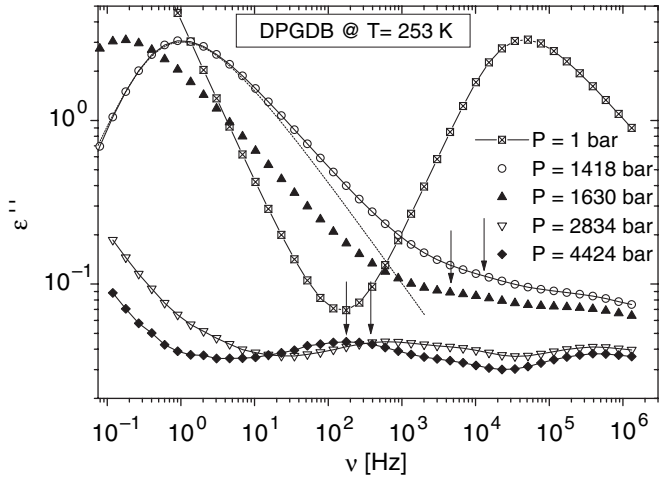

Figure 27. Dielectric loss of DPGDB versus frequency at 253 K under high pressure. The dotted line is the fit to the α-loss peak of data taken at 1418 bars by the KWW function and the value of coupling parameter n used in the fit is 0.37. The arrows indicate the locations of the calculated frequency ν_0 of the primitive process.

Glass-formers that have small differences between τ_α and τ_{JG} at T_g are useful for determining the pressure and temperature dependence of τ_{JG} above T_g because of the wide temperature range over which the JG relaxation can be observed in the liquid state. However, proximity of the two relaxations often obscures the weaker JG relaxation under the high-frequency flank of the α-relaxation; only an ''excess wing'' is observed in the dielectric loss spectrum. This situation occurs in many glass-formers, such as KDE, PDE, PC, PCB62, salol, BPTCDaH, and BMMPC, as previously discussed in Section II.A. The fact that the α-loss peak and the excess wing are superposable for different combinations of T and P at a fixed value of τ_α (see Fig. 1a–1c and 2–5) implies that the excess wing (i.e., the submerged JG relaxation) shifts with changes in pressure at constant temperature. This property is shown explicitly in Figs. 28 and 29 for the dielectric loss spectra of BMMPC and salol, respectively.

There are also glass-formers that have a resolved secondary relaxation that is not the JG relaxation according to the established criteria [38], but lack an apparent JG peak in their loss spectra at ambient pressure. These glass-formers include BMPC [75], dibutyl phthalate (DBP) [77], diethyl phthalate (DEP) [76], 2PG, 3PG [101,102], *m*-fluroaniline (*m*-FA) [44], and bis-5-hydroxypentylphthalate (BHPP) [228,229]. One criterion is the lack of a pressure dependence of their relaxation times, as shown for BMPC in Fig. 30. NMR measurements of molecular motion in BMPC had shown [230] that the

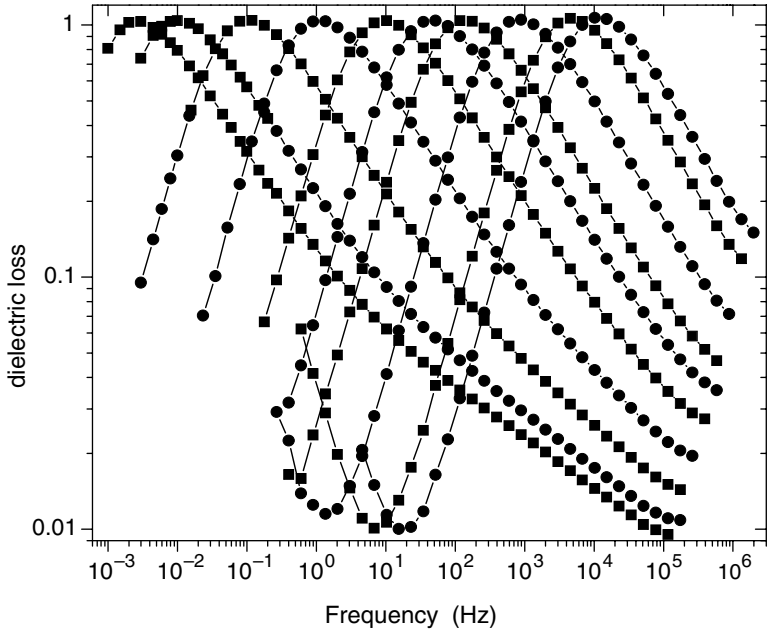

Figure 28. Dielectric loss for BMMPC at 288.8 K at pressures equal to 0.1 (rightmost curve), 12.0, 27.9, 51.8, 80.9 ($f_{max} = 0.03$ Hz), 101.7, 129.9, 185.5, and 218.7 MPa (lowest curve).

secondary relaxation is intramolecular in nature (arising from the rotation of the methoxyphenol moiety) and hence not the JG relaxation. In these glass-formers, the JG relaxation is unresolved from the structural relaxation peak at ambient pressure. However, in oligomers of propylene glycol, the JG relaxation has been resolved under the appropriate combination of pressure and temperature [101,102]. Figure 31 shows the dielectric spectrum for 3PG at $T = 220.5$ K (open symbols); with increasing pressure an excess wing develops between the α-relaxation and the pressure-invariant secondary relaxation. This excess wing eventually is transformed into a distinct peak. The pressure dependence of the resolved JG relaxation time and the lack of any P dependence for the faster secondary relaxation time are evident in Fig. 32. The fast secondary relaxation of *m*-FA seen at ambient pressure originates from the hydrogen-bonded clusters and not the entire *m*-FA molecule. Hence it is not the JG relaxation [44]. These hydrogen-bonded clusters are reflected by the presence of a prepeak in the static structure factor from neutron scattering at ambient pressure [231,232]. The hydrogen-bonded clusters are suppressed at high temperatures and elevated pressures, causing the disappearance of the fast secondary relaxation and the emergence of the JG relaxation peak [44]. A similar situation pertains for BHPP at elevated pressures and temperatures [229].

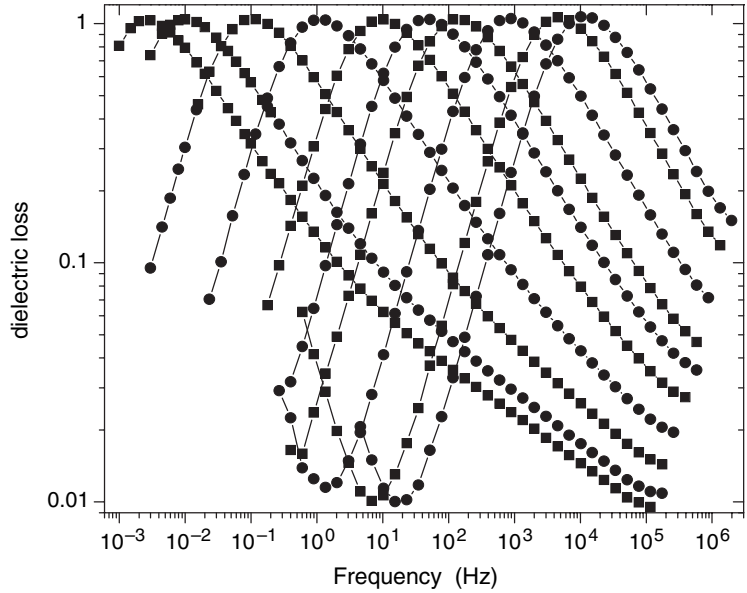

Figure 29. Representative dielectric loss curves for salol measured at 36°C and pressures equal to (from right to left) 0.334, 0.352, 0.383, 0.414, 0.431, 0.460, 0.495, 0.528, 0.566, and 0.590 GPa.

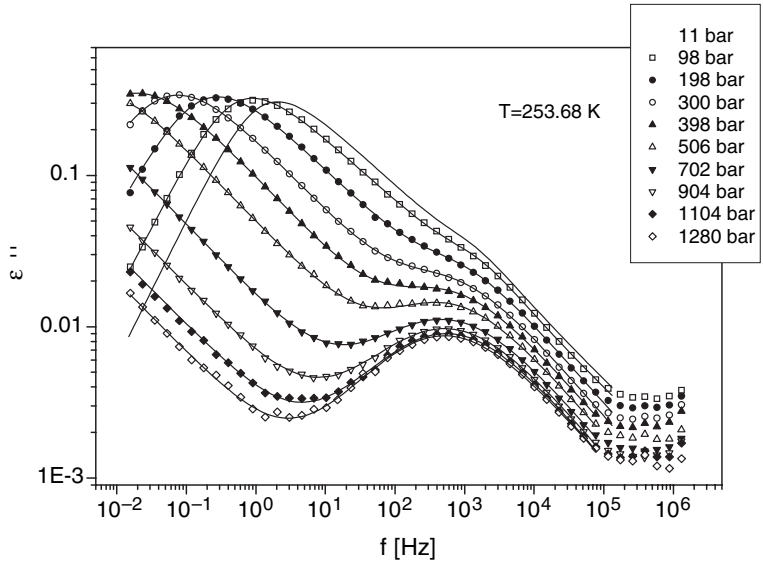

Figure 30. Representative dielectric loss spectra of BMPC obtained under isothermal conditions and applied pressure as indicated.

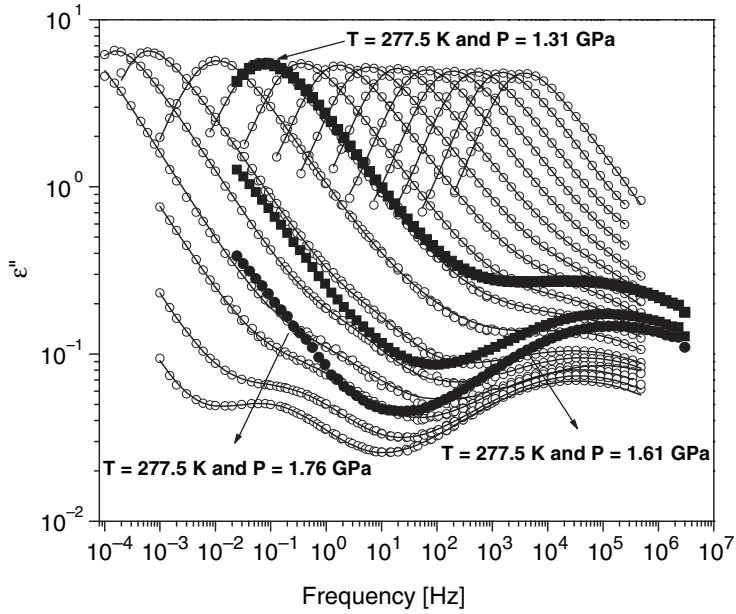

Figure 31. Dielectric loss of 3PG at $T = 220.5$K (open symbols), measured at pressures equal to (from right to left): 33.4, 61.9, 93.0, 120.7, 150.0, 180.2, 209.3, 237.5, 268.6, 297.2, 331.3, 373.4, 415.3, 447.2, 463.7, 510.2, and 591.3 MPa. The closed symbols are measured at $T = 277.5$ K and three pressures as indicated.

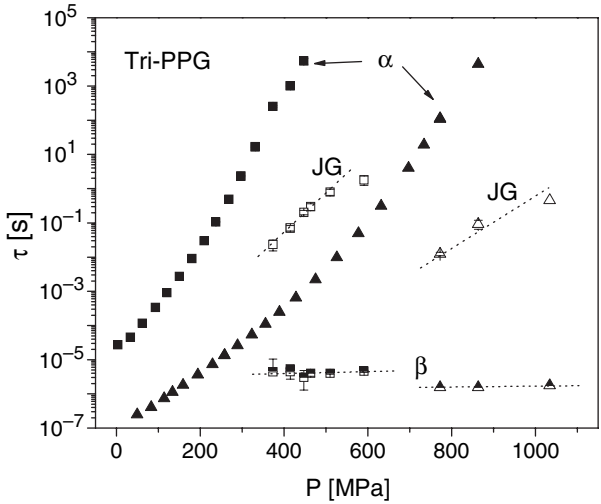

Figure 32. Relaxation times obtained from fitting the 3PG spectra at $T = 218.4$ (squares) and 245.2 K (triangles).

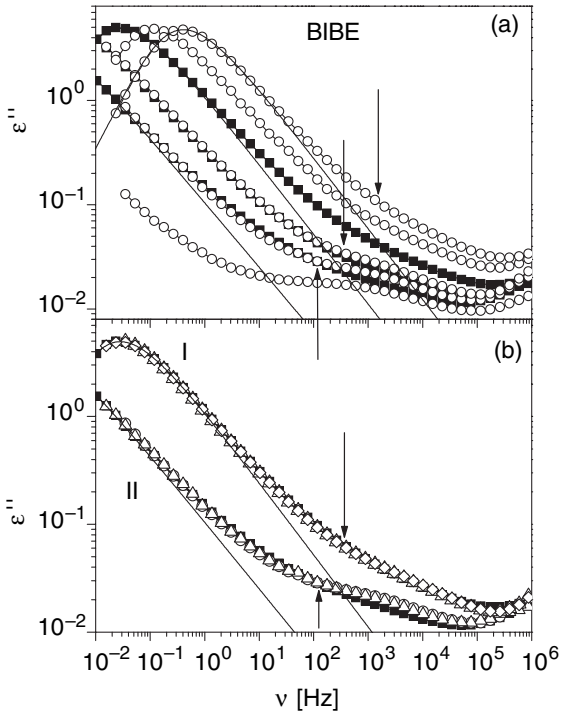

Figure 33. Dielectric loss of BIBE versus frequency at different pressures and temperatures. (*a*) Open circles: $T = 288.2$ K and $P = 3502$, 3699, 4234, 4507, 5165 bars (from right to left); solid squares $P = 1$ bar and $T = 226.1$, 223.0, 220.5 K (from right to left); solid lines are KWW fitting curves for α-process (coupling parameter $n = 0.33$–0.38). Arrows indicate the frequency location of JG process according to the CM predictions. (*b*) Comparison of different spectra with the structural peak in position I or II. The I peak includes: $T = 278.4$ K and $P = 3202$ bars (open triangles), $T = 298$ K and P = 4666 bars (open diamonds), and $T = 226.1$ K and $P = 1$ bar (solid squares). The II peak includes: $T = 278.4$ K and $P = 3699$ bars (open triangles), $T = 288.2$ K and $P = 4507$ bars (open circles), and $T = 220.5$ K and $P = 1$ bar (solid squares).

B. Invariance of τ_{JG} to Variations of T and P at Constant τ_α

In Section II, we have shown that for a given material the dispersion of the structural α-relaxation is the same for various combinations of T and P as long as τ_α is constant. From the same experimental data, τ_{JG} is also found to be invariant to changes in temperature and pressure at constant τ_α. BIBE and DPGDB in Figs. 1f and 1e, respectively, are examples of this invariance of τ_{JG}. A clearer demonstration for BIBE is given in Fig. 33. Although the ratio τ_{JG}/τ_α is constant, the entire dispersion encompassing the α-relaxation and the JG relaxation may not be exactly the same for different combinations of T and P. This is because the

relaxation strengths of the JG relaxation and the α-relaxation do not necessarily change in exactly the same manner with changes in T and P.

Many glass-formers have an unresolved JG relaxation, appearing as an excess wing in the loss spectrum. For these materials, the invariance of τ_{JG} to changes in temperature and pressure at fixed τ_α is manifested by the superpositioning of the α-loss peak together with the excess wing. Examples of such glass-formers include KDE, BMMPC, BMPC, salol, diglycidyl ether of bisphenol-A (Epon828), DEP,DBP, PCB62, and PDE (see examples in Figs.1a–1d and 2–5).

C. Non-Arrhenius Temperature Dependence of τ_β Above T_g

It is generally found that τ_β of all secondary relaxations, both JG and non-JG, has an Arrhenius temperature dependence in the glassy state; that is, $\tau_{JG} = \tau_\infty \exp(E_a/RT)$ with constant τ_∞ and E_a. The JG relaxation tends to merge with the α-relaxation above the glass transition temperature, T_g, as inferred by assuming that the Arrhenius temperature dependence persists into the equilibrium liquid state. The actual temperature dependence of τ_{JG} at temperatures above T_g is of central importance to any theoretical explanation of the origin of the JG relaxation. Unfortunately, above T_g the situation is less clear because of the difficulty in resolving the JG relaxation from the proximate α-process. By fitting ambient pressure dielectric spectra of the overlapping α- and β-peaks of sorbitol in this region to the sum of two functions, several groups have concluded that the Arrhenius dependence observed below T_g changes into a stronger temperature dependence above T_g [233–235]. Representative results are shown in Fig. 34 (open squares for α-relaxation and open diamonds for JG relaxation) [236]. The deduced β-relaxation has a temperature dependence above T_g which departs from the Arrhenius temperature dependence below T_g. Another example is ambient pressure dielectric data of poly(vinylacetate) [49,237], with deconvolution of the two relaxations achieved either by the superposition method or by the convolution method [238]. Such results, however, are somewhat inconclusive because the temperature dependence of the unresolved JG relaxation is deduced from a somewhat arbitrary fitting procedure. Moreover, the assumption that the JG relaxation has some distribution (e.g., Cole–Cole function) to be added on to the α-process (represented by an empirical Cole–Davidson or Havriliak–Negami distribution) assumes independence of the two processes; however, this is incompatible with the interpretation of structural relaxation as the evolution of the primitive (JG) dynamics. A clearer picture is offered by sorbitol, for which the JG peak is well-resolved for pressures above ~0.5 GPa over a range of temperatures above T_g [239]; representative results are shown in Fig. 34. The JG relaxation times can be determined directly (no deconvolution required) at high pressures, showing clearly that the temperature dependence changes from one Arrhenius relation below T_g to a more sensitive one above T_g. Similar results are found in dielectric measurements at high

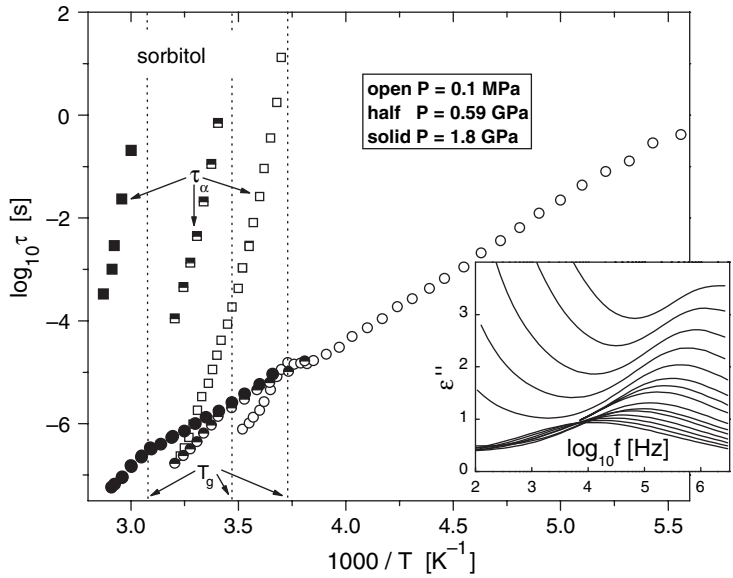

Figure 34. Isobaric α-relaxation times at $P = 0.1$ MPa (□), 0.59 GPa (half-filled squares), and 1.8 GPa pressure (■), along with the corresponding JG β-relaxation times at ambient (◯) and elevated pressure 0.59 GPa (half-filled circles) and (•) for sorbitol. The slope of τ_{JG} is independent of pressure, although it differs markedly for low versus high temperatures. Inset shows the JG peak in the dielectric loss at $P = 1.8$ GPa for temperatures from 273 K to 343 K, in 5-degree increments (bottom to top). The α-peak is too low in frequency to appear within the measured frequency range.

pressure on another polyol, xylitol [239], and in 17.2% chlorobenzene in decalin [67]. The implication is that a change in T dependence of τ_{JG} above T_g is a general feature of glass-forming liquids. The temperature dependence of τ_{JG} above T_g is much stronger than the dependence below T_g. Experiments at ambient pressure, in which the JG relaxation of dipropylglycol dibenzoate [240] and picoline mixed with tristyrene [241,242] were resolved both above and below T_g, also showed that τ_{JG} has a stronger temperature dependence in the equilibrium liquid state than in the glass.

For glass-formers that have an unresolved JG relaxation, which appears as an excess wing, the temperature dependence of τ_{JG} above T_g can be inferred from the shift of the excess wing with temperature. Since τ_α is non-Arrhenius above T_g and the excess wing is on the high-frequency side of the α-peak, the shift of the excess wing with temperature will also be non-Arrhenius, albeit less than that of τ_α. This non-Arrhenius behavior of the excess wing for $T > T_g$ has been shown for glycerol, propylene carbonate, propylene glycol [39], and KDE [40]. Thus, for all JG relaxations, hidden or resolved, τ_{JG} has different temperature dependences above and below T_g.

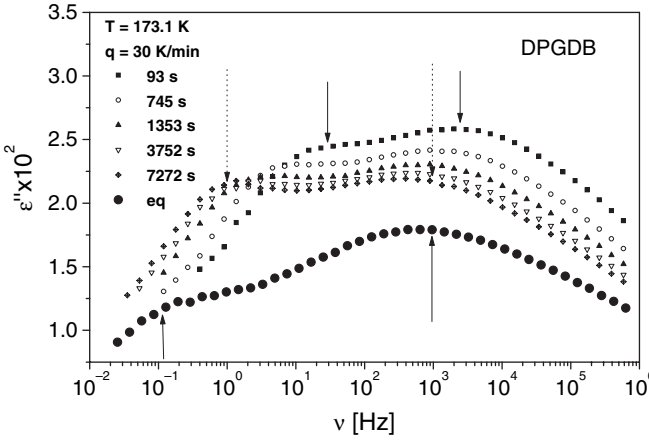

Figure 35. Time evolution of the secondary dielectric relaxation loss spectrum of DPGDB on isothermal annealing at 173.15 K after rapid cooling from 300 K. From top to bottom, the data were obtained after the sample has been annealed isothermally at 173.15 K for times, t_α, equal to 93 s, 745 s, 1353 s, 3752 s, and 7272 s elapsed after the thermal stabilization. Solid circles represent the spectrum obtained by slowly cooling the sample at 0.05 K/min. Vertical arrows show the frequencies of the maximum loss for the JG β- and the γ-processes.

D. Increase of τ_β on Physical Aging

Glasses usually densify on physical aging with a concomitant increase in the structural relaxation time. Early on it was noted by Johari [243] that the JG relaxation in the glass was affected by thermal history, such as the cooling rate used to vitrify the liquid or the aging time. A recent study [240] of the JG relaxation in dipropyleglycol dibenzoate (DPGDB) found the thermal history of the glass to exert a strong influence on the JG relaxation time. The increase in τ_{JG} with aging mimics the behavior of τ_α, as illustrated in Figs. 35 and 36. Although the change in τ_{JG} is less than that of τ_α, the effect on the JG β-relaxation is much greater than on the faster, non-JG γ-relaxation. Similar results have been found for xylitol [244] and sorbitol [245].

Since aging increases the separation of the α- and JG-relaxations, the excess wing seen in many glass-formers can be resolved into a distinct JG peak by long-time physical aging. This was shown for glycerol, propylene carbonate (PC), and propylene glycol (PG) [39,100,246], which all have an excess wing and no other secondary relaxation. The samples were annealed at constant temperature below T_g for up to five weeks, during which the excess wing was transformed into a shoulder; that is, a nascent JG relaxation peak. These changes of the dielectric loss of PC and PG with aging time are shown in Figs. 37 and 38 respectively. An even longer aging time of 3 months gives rise to a distinct peak, instead of the shoulder, in glycerol [247].

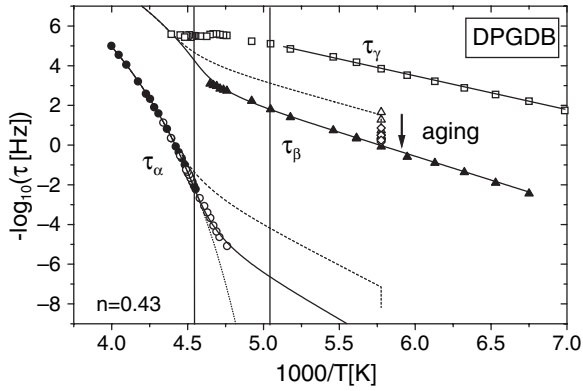

Figure 36. Relaxation map of DPGDB. Logarithm of the experimentally determined relaxation time versus 1000/*T*, of the α-process (filled and open circles, from fitting spectra and shift factors, respectively), JG β-process (filled triangles) and γ-process (open squares), compared to simulation data (lines) for α- and β-relaxation obtained by numerical solution of the Hodge model and the CM model, respectively. Solid lines refer to slow cooling (0.05 K/min), whereas dashed lines refer to fast cooling (30 K/min). Open triangles and diamonds are for the β-relaxation during the aging process, after a cooling at rate of 30 K/min and 9 K/min, respectively. Dotted lines represent the VFTH equation of the equilibrium liquid. Vertical lines (at $T_g = 220$ K and $T_x = 198.15$ K) delineate three regions from left to right for the slow-cooled system: equilibrium liquid region ($T = T_f$), "delayed" region ($T_g > T_f(T) > T_x$) where the system has fallen out of equilibrium but T_f changes with T, and the isostructural glassy state ($T < T_x$) where T_f is equal to 213.8 K and constant on the laboratory time scale.

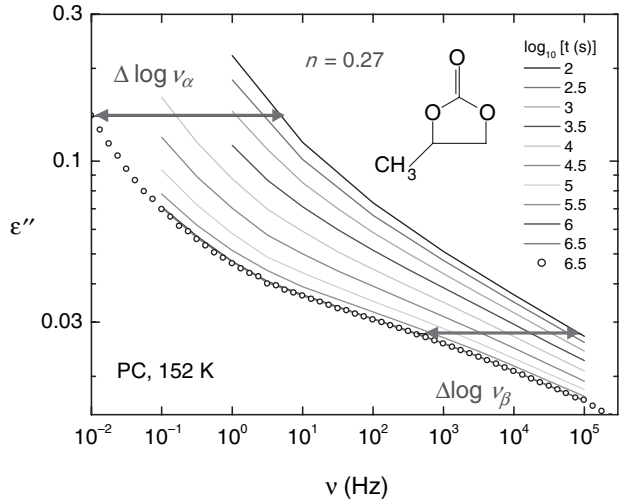

Figure 37. Shifts of the α-relaxation and the excess wing of propylene carbonate at 152 K after aging for the periods of time as indicated.

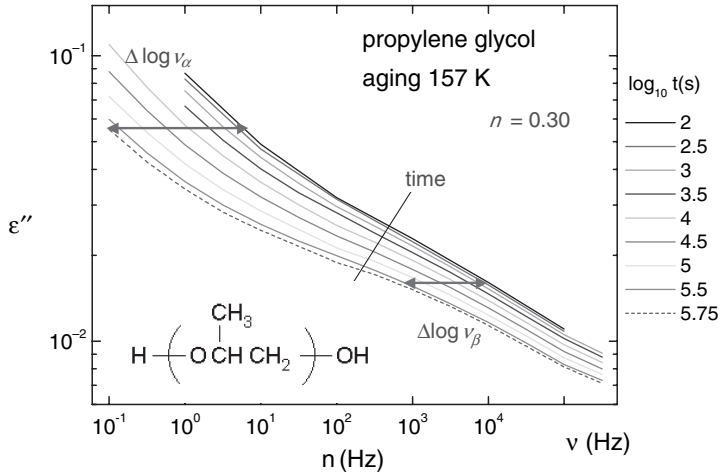

Figure 38. Shifts of the α-relaxation and the excess wing of propylene glycol at 157 K after aging for the periods of time as indicated.

2PG, DBP, dioctalphthalate (DOP), and several other glass-formers each have a resolved secondary γ-relaxation; however, these are not JG relaxations, as evidenced by the invariance of the relaxation times to pressure. In such materials, the JG relaxation must lie between the α- and γ-relaxations ($\tau_\alpha < \tau_{JG} < \tau_\gamma$), making its resolution more difficult than for PC and PG which have no γ-relaxation. Consequently, even the existence of an excess wing may be questioned, at least at ambient pressure. However, again, physical aging further separated the α- and JG-processes, enabling the excess wing to become clearly visible; results are shown for 2PG in Fig. 39 and DBP in Fig. 40. Note that the position of the γ-relaxation is unchanged with aging. This is strong evidence that the γ-relaxation has no relation to the glass transition. Properties of the γ-relaxation, such as a small decrease of its peak frequency with temperature, have been reported and an asymmetric double potential model proposed to explain them [248,249]. However interesting in their own right, it is important to distinguish among the various types of secondary relaxations. Notwithstanding the prominence of the γ-relaxation in some liquids (see, for example, the spectrum of DOP in Fig. 41), it has no influence on vitrification. In glass-formers such as DOP, physical aging (Fig. 42) or hydrostatic pressure are necessary to reveal the existence of the JG process as an excess wing.

E. JG Relaxation Strength and Its Mimicry of Enthalpy, Entropy, and Volume

The β-relaxations in 16.6 mol% chlorobenzene-decalin mixture [250], 5-methyl-2-hexanol [251], and D-sorbitol [233,252], are all of the JG kind. The relaxation

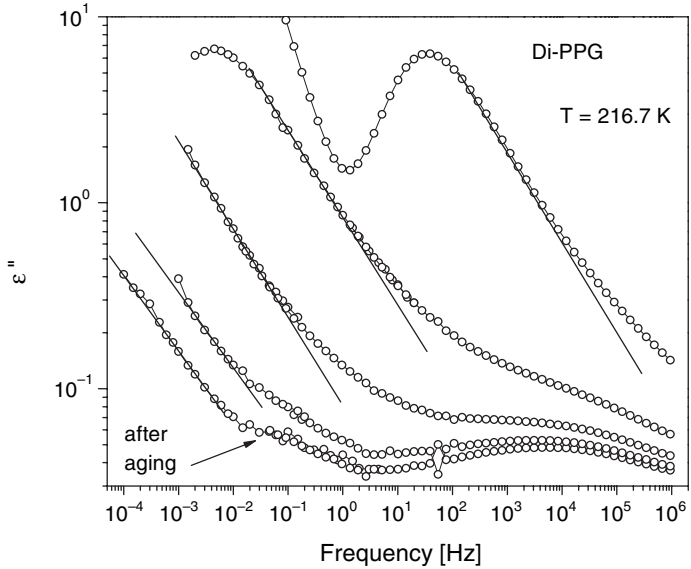

Figure 39. Dielectric loss for PPG dimer at pressures (from right to left) of 67.6, 248.7, 335.7, 520, and 510 MPa. The last one was measured after 12 hours of aging. There is a pressure-independent secondary peak at $\sim 10^4$ Hz, which exhibits a negligible response to aging.

strength, $\Delta\varepsilon_\beta$, of the JG relaxation in these glass-formers is found to change on heating through the glass transition temperature in a manner similar to that of the changes observed in the enthalpy H, entropy S, and volume V. The derivative of $\Delta\varepsilon_\beta$ with respect to temperature, $d\Delta\varepsilon_\beta/dT$, increases from relatively low values below T_g to higher values above T_g. This is the same behavior observed for the specific heat C_p and the thermal expansion coefficient, which are proportional to the derivatives dH/dT and dV/dT, respectively. The rotation angle for the motions underlying the JG relaxation, and hence $\Delta\varepsilon_\beta$, likely depends on the specific volume and the entropy. Thus, it is expected that the rate of change of $\Delta\varepsilon_\beta$ with temperature should be similar to that of these thermodynamic quantities. For the same reason, the angle of rotation or $\Delta\varepsilon_\beta$ is expected to depend on the thermal history of the glass, a denser glass having a smaller $\Delta\varepsilon_\beta$. It should be noted, however, that similar changes are observed also for some secondary relaxations that are not JG [253].

F. The Origin of the Dependences of Molecular Mobility on Temperature, Pressure, Volume, and Entropy Is in τ_{JG} or τ_0

The properties of the JG relaxation discussed in Sections **V.A–V.E** call to mind the properties of the structural α-relaxation associated with vitrification. The properties discussed in Sections **V.A**, **V.C**, **V.D**, and **V.E** indicate that pressure P,

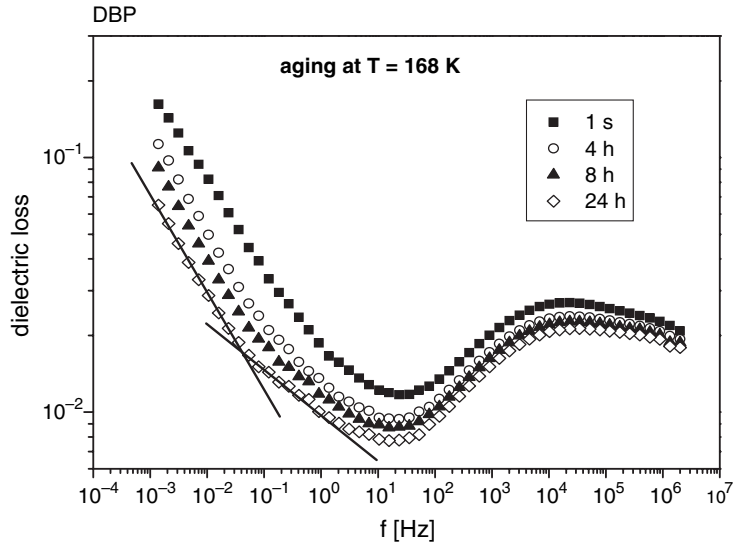

Figure 40. Dielectric loss of dibutylphthalate (DBP) at ambient pressures measured after aging for different periods of time as indicated. The excess wing becomes evident after aging for a sufficiently long time.

temperature T, and their conjugate variables, volume V and entropy S, govern the mobility of the JG relaxation in the equilibrium liquid state as well as in the glassy state. Since the JG relaxation transpires before the α-relaxation, we are led to conclude that pressure P (volume V) and temperature T (entropy S) first enter into the determination of molecular mobility at the level of the JG relaxation, well before the emergence of the α-relaxation. The dependences of the α-relaxation on temperature, pressure, volume, and entropy are derived from those of the JG relaxation after many-molecule dynamics have transformed the latter progressively with time into the former. Many molecules are involved in the α-relaxation, particularly at lower temperatures or higher pressures for which τ_α is longer. Evidence of the involvement of many molecules comes from the the heterogeneous dynamics engendering the dispersion. The width of the α-dispersion and the length-scale of the heterogenous dynamics are convenient measures of the intensity of the many-molecule dynamics. In contrast, the JG relaxation time, or more accurately the primitive relaxation time, corresponds to the individual and independent relaxation of molecules. The involvement of many molecules in the α-relaxation amplifies the original but weaker dependences of τ_{JG} or τ_0 on P (V) and T (S), and it naturally gives rise to the much stronger corresponding dependences of τ_α. The dependences of τ_α on P (V) and T (S) are the results of two contributing factors: (1) the many-molecule

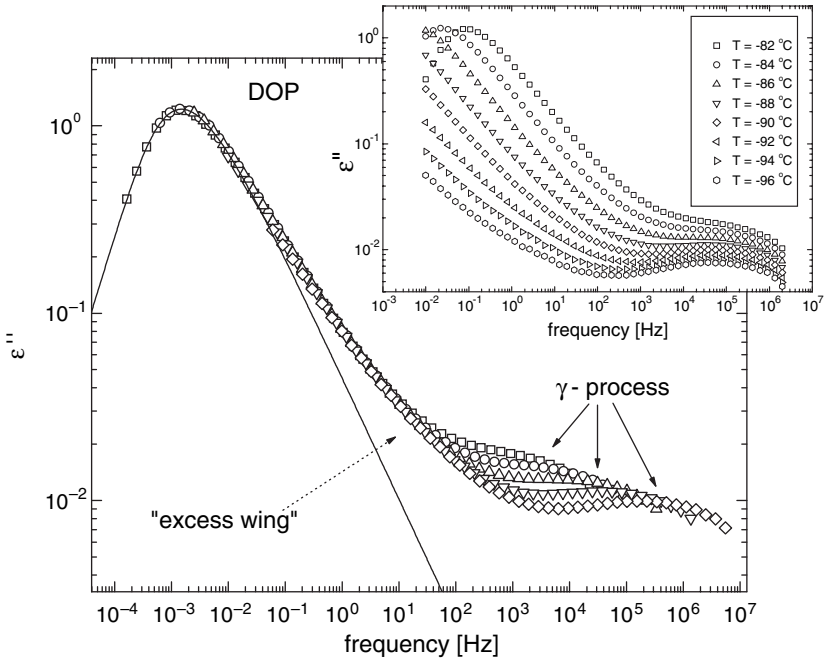

Figure 41. The inset shows isothermal dielectric loss spectra of DOP at ambient pressure. The γ-relaxation is the only resolved secondary relaxation. The main figure is obtained by time–temperature superposition.

dynamics manifested by the dispersion and (2) the originating dependences of τ_{JG} on the thermodynamic variables P (V) and T (S). These results suggest that a viable theory of glass transition has to start from the dependence of τ_{JG} or α_0 on pressure (volume) and temperature (entropy) and then implement the many-molecule dynamics to arrive finally at the α-relaxation.

Likewise, quantities derived from dependences of τ_α on P (V) and T (S), such as the ''steepness'' or the ''fragility'' index $m = d(\log_{10}\tau_\alpha)/d(T_g/T)\big|_{T=T_g}$, are determined by both thermodynamics and many-body dynamics. These two factors may not affect m in the same proportion. For example, in some glass-formers the many-molecule dynamics may not be severe (i.e., smaller n), but the dependences of τ_{JG} on the thermodynamic variables are strong, or vice versa. This scenario is observed for PC, KDE, and PDE, which have narrow dielectric dispersions (smaller n), but their m values are larger compared to other glass-formers [140]. Another example is the fact that m usually decreases with applied pressure. For any chosen τ_α, at elevated pressure the temperature can be raised to maintain τ_α constant. In particular, the P and T combinations can be chosen to

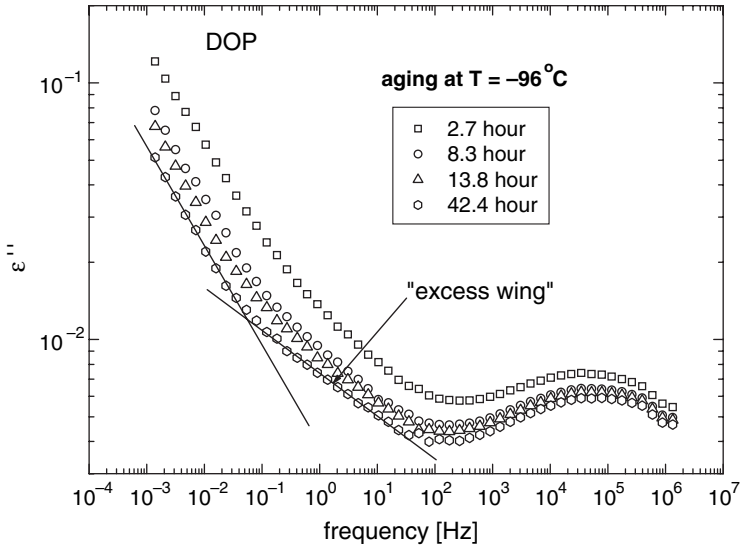

Figure 42. Dielectric loss for DOP at ambient pressures measured after aging for different periods of time as indicated. The excess wing becomes evident after aging.

have the same specific volume (isochoric condition). Since τ_α is the same, it follows from Section II that the dispersion is also the same, and hence the influence of many-molecule dynamics is the same for the three cases: at ambient pressure, at a fixed elevated pressure (isobaric condition), or at isochoric condition. The temperatures necessary to attain the same τ_α in all three cases are solely controlled by the thermodynamic factor. In Fig. 43, $\log_{10}(\tau_\alpha)$ is plotted against reciprocal temperature scaled by the respective T_g of the three cases. One can see that at any constant τ_α, the scaled reciprocal temperature T_g/T and the ''fragility'' index m of a glass-former change with thermodynamic condition. The fragility decreases with elevating pressure, and this decrease is spectacular when the glass-former is constrained to constant volume. These changes of m in the same glass-former illustrate the role of thermodynamic variables in determining τ_α and m, beyond the effects due to many-molecule dynamics (as reflected in the breadth of the dispersion). The classification of glass-formers according to their fragility is only useful to the extent that m is related in a straightforward fashion to a single fundamental factor. Unfortunately, our results indicate that this is generally not the case; at least two distinctly different factors, the thermodynamics and the dispersion, determine m and the nature of a T_g-scaled Arrhenius plot. Thus, notwithstanding its popularity, the use of m to classify glass-formers can lead to inconsistent conclusions.

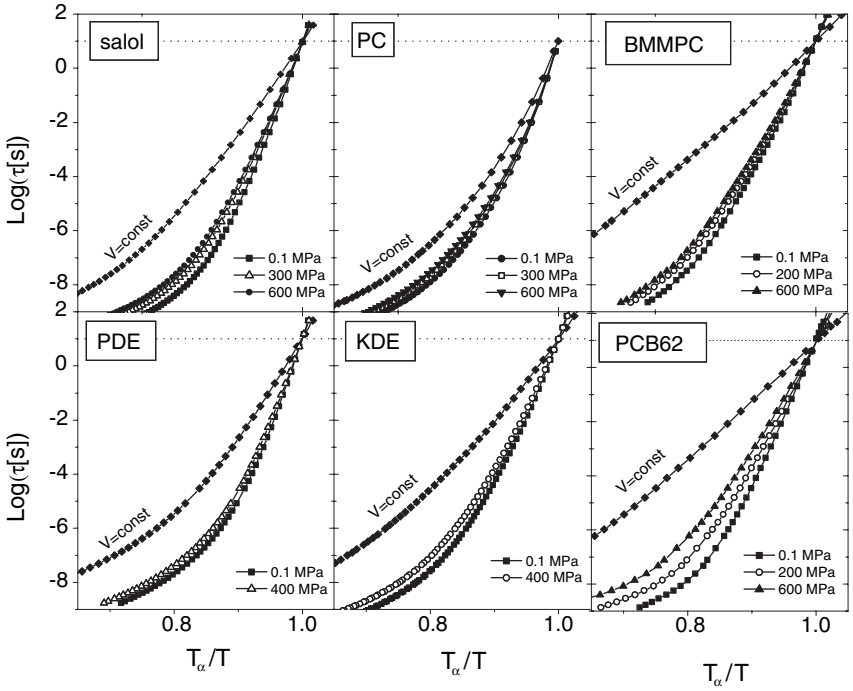

Figure 43. Isobaric dielectric relaxation times for salol, PC, BMMPC, PDE, KDE, and PCB62 versus T_α/T, where $\tau(T_\alpha) = 10$ s. Isochors were calculated at the volume at which $\tau = 10$ s at atmospheric pressure; $V = 0.7907$ (salol), 0.7558 (PC), 0.9067 (BMMPC), 0.7297 (PDE), 0.7748 (KDE), and 0.6131 (PCB62) ml/g. [Adapted from R. Casalini and C. M. Roland, *Phys.Rev. B* **71**, 014210 (2005).]

We have seen in Section V.B that the relation between the JG relaxation and the α-relaxation, expressed in terms of the ratio τ_α/τ_{JG}, is independent of the combination of P and T as long as τ_α is constant. This property in conjuction with the results of Section II lead to the following conclusion: For any given glass-former, τ_{JG}, in conjuction with the dispersion of the α-relaxation (or β_{KWW}), is invariant to changes in the thermodynamic variables P (V) and T (S), provided that τ_α is constant. In other words, τ_{JG} and β_{KWW} together uniquely define τ_α and vice versa, independent of the thermodynamic variables. This characteristic of τ_{JG} is another indication of the fundamental importance of the JG relaxation to the vitrification process. A theory of the glass transition is neither fundamental nor complete if it neglects the JG relaxation. Recalling the discussion in Section II, this statement also applies to models in which the dispersion of the α-relaxation is either ignored or is not uniquely defined by τ_α.

VI. THE COUPLING MODEL

A. Background

One of the manifestations of many-molecule dynamics is the dispersion of the structural α-relaxation or the Kohlrausch function [Eq. 1] used to represent the time correlation function with the fractional exponent, $\beta_{KWW} = (1 - n)$. We have discussed in previous sections that this dispersion is fundamental because it defines, governs, or correlates with the properties of the structural α-relaxation and even the JG relaxation. However, it is not easy to construct a theory or model that captures the many-molecule relaxation dynamics in real glass-formers and has predictions consistent with the experimental facts or that are falsifiable by experiment. Such a theory or model does not exist at the present time. This state of affairs is not surprising because the intermolecular potential in glass-forming liquids is anharmonic and motions of an Avogadro's number of molecules in phase space are chaotic and thus difficult to describe [254]. The problem is compounded by the fact that relaxation is an irreversible process and a method that can fully describe the many-molecule relaxation process and its evolution with time is lacking. Most theories of supercooled liquids and the glass transition avoid the issue and focus their attention on the connection between dynamics and thermodynamics [255]. In neglecting to address the many-molecule relaxation dynamics, these models suffer the consequence that the obtained dispersion of the α-relaxation does not define, govern, or correlate with other properties of the α-relaxation.

The authors of the present chapter, as well, have no solution to the complete many-molecule relaxation problem. Nevertheless, one of us did recognize the importance of many-molecule relaxation in interacting systems 26 years ago in initiating what is now known as the Coupling Model (CM). At that time and continuing until a few years ago, the CM has been concerned only with the terminal α-relaxation. No consideration was given to processes transpiring at early times. This conceptual model [256–262] indicated that the slowing down of the averaged α-relaxation rate is caused by interactions and constraints between molecules. Rigorous solutions of simple, coupled systems have given support to the premise of the CM and reinforced its generality. For instance, the energy relaxation in interacting arrays or lattices of nonlinear oscillators with anharmonic or dissipative coupling has been found to be slowed down by interactions and, under particular coupling conditions, to follow a stretched-exponential law [260–268]. Most importantly, in many cases a crossover from the faster single exponential relaxation to a stretched function was observed at a some crossover time [260–268]. Such a dynamic crossover should also take place in the case of glass-formers because many-molecule dynamics caused by intermolecular interaction cannot transpire instantly. Thus, the slowing down

starts at some time, t_c, the magnitude of which is determined by the strength of the molecular interaction potential. A system with weaker interaction has a longer t_c [24]. At infinitely weak interaction, there is no slowing down and $t_c \to \infty$. In the case of glass-formers, the many-molecule α-dynamics are heterogeneous and complicated, so that only averages over these heterogeneities are considered in the CM. A schematic description of the dynamic evolution can be described as follows: The CM recognizes that all attempts of relaxation have the same primitive (i.e., independent) relaxation rate $W_0 = \tau_0^{-1}$, but the many-molecule dynamics, starting at t_c, forestall all attempts of molecules to be simultaneously successful, resulting in faster and slower relaxing molecules or heterogeneous dynamics. However, when averaged, the effect is equivalent to the slowing down of τ_0^{-1} by another, time-dependent, multiplicative factor. The time-dependent rate $W(t)$ has the product form, $f(t)\tau_0^{-1}$, where $f(t)$ is a decreasing function with values less than unity. In particular, the slowing-down factor $f(t)^{-1}$ was found to be dependent on time according to a sublinear power law, and hence $W(t) \propto t^{-n}\tau_0^{-1}$, where n is the coupling parameter of the CM and $0 \leq n < 1$. The stronger the intermolecular interaction, the greater the slowing effect of the many-molecule dynamics and the larger the coupling parameter n. Therefore, the corresponding correlation function of the model is the Kohlrausch stretched exponential function [Eq. (1)], which holds only for $t > t_c$. At times shorter than t_c, there is no slowing down and the correlation function is the linear exponential,

$$\phi(t) = \exp(-t/\tau_0) \tag{5}$$

where τ_0 is the primitive relaxation time of a molecule, unimpeded by other molecules, and has normal properties such as the Q^{-2} dependence on the scattering vector Q. For polymers, because the repeat units are bonded along the chain, equation (5) has to be replaced by the Hall–Helfand function [269,270]. It was assumed that the crossover from $\phi(t) = \exp(-t/\tau_0)$ to the Kohlrausch function takes place continuously in a narrow neighborhood of t_c. All the above are supported by solutions of much simplified interacting or coupled systems [260–262], and the crossover leads to a relation between τ_α and α_0 given by

$$\tau_\alpha = (t_c^{-n}\tau_0)^{1/(1-n)} \tag{6}$$

Clear evidence of a crossover from the primitive relaxation to Kohlrausch relaxation was reported in several other systems, comprised of larger units than molecular glass-formers and having weaker interactions. The crossover times t_c of these systems are usually much longer than a picosecond (up to tens of microseconds) [24,152–158]. Vibrations and librations do not contribute to the measured quantity in this longer time regime, and the crossover of the correlation function can be clearly observed in these systems. Unfortunately, this is not the case for structural relaxation of inorganic, organic, and polymeric glass-formers,

which have shorter t_c on the order of picoseconds. Nonetheless, at sufficiently high temperatures, the structural relaxation dominates the intermediate scattering function obtained by neutron scattering experiments and molecular dynamics simulations of polymeric and small-molecule liquids, and the crossover can be seen at 1–2 ps [143,150,271–275]. The transport coefficients, including viscosity and conductivity, assume the Arrhenius temperature dependence of the primitive relaxation when the relaxation time becomes less than 2 ps [276]. These properties indicate that t_c is equal to about 2 ps for molecular and polymeric glass-formers. The Lennard-Jones potential, $V(r) = 4\varepsilon[(\sigma/r)^{12} - (\sigma/r)^6]$, is often used to model the intermolecular potential of molecular and polymeric glass-formers in molecular dynamic simulations. The unit of time from the Lennard-Jones potential is given by $(m\sigma^2/48\varepsilon)^{1/2}$, which gives $\sim$1 ps for typical parameters. The experimentally determined value of t_c is comparable to the Lennard-Jones unit of time [277]. The crossover from the primitive relaxation to Kohlrausch relaxation was seen also at about 1 ps in the many-ion dynamics of molten, crystalline and glassy ionic conductors [24].

The earlier works focused on the structural α-relaxation with the Kohlrausch correlation function, and they ignored the processes that precede it. In order of appearance, these processes include the vibrations inside cages (Boson peak), fluctuations of cages giving rise to the nearly constant loss, and cage decay due to the emergence of the local primitive relaxation, which is related to the Johari–Goldstein secondary relaxation (see below). The primitive relaxation is the building block of the many-molecule dynamics, which increase in length-scale with time to become the terminal α-relaxation with the maximal possible length-scale and the Kohlrausch function as its correlation function. Only recently, the Coupling Model (CM) has been extended beyond the Kohlrausch structural α-relaxation to incorporate some of the earlier processes [26,32–38,41,240,276,278,279]. Most important is the local primitive relaxation, which is an observable process occurring at times much shorter than τ_α. However, since the primitive relaxation is the initiator and building block of the ensuing many-molecule dynamics, it will not be resolved in the measured loss spectrum as a Debye process suggested by its exponential correlation function [Eq. (5)]. Nevertheless, the primitive relaxation frequency, $\nu_0 \equiv 1/2\pi\tau_0$, should correspond to the characteristic frequency of some observed features in the spectrum, which we shall see is the universal Johari–Goldstein secondary relaxation frequency. Thus, the primitive relaxation not only manifests itself as a genuine relaxation process at shorter times, but also plays the other distinctly different role when considering the Kohlrausch relaxation that leads to Eq. (6). It is important for the reader to recognize that there is no contradiction in the fact that the primitive relaxation plays two separate and distinctly different roles.

A definitive step in extending the CM is to include the relaxation processes occurring before the α-relaxation and to establish the existence of the primitive

relaxation at times shorter than τ_α. To do this, a connection is made between the primitive relaxation time τ_0 and the characteristic relaxation time of the Johari–Goldstein (JG) secondary relaxation τ_{JG}. In the literature, it is common to interpret the JG secondary peak in the spectrum as due to a local process having a Cole–Cole distribution of relaxation times. The CM interprets the spectrum differently, comprised of the primitive relaxation and thereafter the emerging many-molecule relaxation processes with length-scales that increase with time. However, we continue to use the term JG relaxation; henceforth, it should be interpreted in the sense of the CM. We are not identifying the primitive relaxation with a broad distribution of local processes, but only using the JG relaxation time τ_{JG} as an indicator or estimate of τ_0. Such a connection is expected from the similar characteristics of the two relaxation processes, including their local nature, involvement of essentially the entire molecule, common properties, and the fact that both serve as the precursor to the α-relaxation [38]. Multidimensional NMR experiments [226,280] have shown that the dynamically heterogeneous molecular reorientations of α-relaxation occur by relatively small jump angles with exponential time dependence, which is exactly the role played by the primitive relaxation of the CM. Furthermore, from one- and two-dimensional 2H NMR studies [227,281], the JG relaxation in toluene-d5 and polybutadiene-d6 also involves small angle jumps of similar magnitude at temperatures above T_g. This similarity in size of the jump angles of the primitive relaxation and the JG relaxation further supports the connection between these two relaxation processes. Hence,

$$\tau_{JG}(T,P) \approx \tau_0(T,P) \tag{7}$$

On combining Eqs. (6) and (7), we obtain a relation between τ_α and τ_{JG} given by

$$\tau_\alpha(T,P) = [t_c^{-n}\tau_{JG}(T,P)]^{1/(1-n)} \tag{8}$$

which should be valid for any temperature T and pressure P. A similar relation between the secondary relaxation time and the α-relaxation time but different in quantitative details was given by Cavaille et al. [282] in their model of relaxation in glass-formers.

The CM describes the evolution of the molecular dynamics chronologically as follows. At very short times all molecules are caged. Cages decay by local and independent (primitive) relaxation. At short times, only a few primitive relaxations are occurring and they appear separately in space as localized motions just like the JG relaxation. At times beyond τ_0 or τ_{JG}, more units tend to independently relax and when they can no longer be considered as isolated events, intermolecular interactions and mutual constraints impose a degree of cooperativity (or dynamic heterogeneity) on the motions. The degree of dynamic heterogeneity and the corresponding length-scale continues to increase with time as more and more units participate in the motion, as suggested by the

evolution of the dynamics of colloidal particles with time seen by confocal microscopy [213]. These time-evolving processes contribute to the observed response at time longer than τ_0 or τ_{JG} and are responsible for the broad dispersion customarily identified as the JG relaxation. After sufficiently long times, $t \gg \tau_0$ or τ_{JG}, the *fully* cooperative α-relaxation with the averaged correlation function having the Kohlrausch form [Eq. (1)] is attained. In this terminal regime, the α-relaxation has the maximum dynamic heterogeneity length-scale, L_{dh}. Naturally we expect a larger L_{dh} is associated with a broader dispersion or a larger n, because both quantities are proportional to the intensity of the many-molecule dynamics. This correlation is borne out by comparing n with L_{dh} for glycerol, ortho-terphenyl, and poly(vinylacetate) obtained by multidimensional ^{13}C solid-state exchange NMR experiments [188]. These experiments found that at about $T = T_g + 10$ K, the number of molecules per slow domain is 390 monomer units for poly(vinylacetate), 76 molecules for ortho-terphenyl, and only 10 molecules for glycerol. The coupling parameter n deduced from the Kohlrausch fit to the dielectric spectra near $T = T_g$ is 0.53, 0.50, and 0.29 for poly(vinylacetate) [49], ortho-terphenyl [233], and glycerol [36,100], respectively. NMR experiments also confirm that the distribution of relaxation rates is narrower for glycerol than it is for either poly(vinylacetate) or ortho-terphenyl [188].

In the extended CM, the JG relaxation is just part of the continuous evolution of the dynamics. The JG relaxation should not be represented by a Cole–Cole or Havriliak–Negami distribution, as customarily assumed in the literature, and considered as an additive contribution to the distribution obtained from the Kohlrausch α-relaxation. Nevertheless, the JG relaxation may be broadly defined to include all the relaxation processes that have transpired with time up until the onset of the Kohlrausch α-relaxation. Within this definition of the JG relaxation, experiments performed to probe it will find that ''essentially'' all molecules contribute to the JG relaxation and the motions are dynamically and spatially heterogeneous as found by dielectric hole burning [180,283] and deuteron NMR [284] experiments. This coupling model description of the JG relaxation may help to resolve the different points of view of its nature between Johari [285] and others [180,226,227,280,281,283,284].

The broad width of the JG relaxation can be accounted for by the broad transition from the cage dynamics (revealed by the nearly constant losses) to the fully cooperative Kohlrausch relaxation [36]. In fact, it is important to recall that the time scale where JG relaxation takes place usually exceeds t_c, especially in molecular glass-formers, whereas the onset of many-molecule dynamics starts at $t_c \approx 2$ ps. So, when $t_c \ll \tau_0 \ll \tau_\alpha$, the molecules are essentially all caged at short time and then a gradual development of cooperativity occurs when increasing numbers of molecules are ready to reorient independently. In the region $t_c \ll t \ll \tau_\alpha$ all the molecules are attempting to make independent

relaxation, but not all of them are successful because of the interaction with or the constraints by the surrounding molecules. The most probable relaxation time τ_{JG}, related to the few molecules that have the chance to independently reorient, should be close to τ_0, the primitive relaxation time of the independent reorientation if molecular interactions would be negligible. Evidently, the primitive and the JG relaxation processes are not identical, but they are closely related. Therefore the check of a correspondence between the JG relaxation time and the primitive relaxation time τ_0 is of paramount importance to test the predictions of the CM in glass-forming systems.

B. The Correspondence Between τ_0 and τ_{JG}

In the previous subsection, we have provided conceptually the rationale and experimentally some data to justify the expectation that the primitive relaxation time τ_0 of the CM should correspond to the characteristic relaxation time of the Johari–Goldstein (JG) secondary relaxation τ_{JG}. Furthermore, it is clear from the CM relation, $\tau_\alpha = (t_c^{-n}\tau_0)^{1/(1-n)}$, given before by Eq. 6 that τ_0 mimics τ_α in behavior or vice versa. Thus, the same is expected to hold between τ_{JG} and τ_α. This expectation is confirmed in Section V from the properties of τ_{JG}. The JG relaxation exists in many glass-formers and hence there are plenty of experimental data to test the prediction, $\tau_{JG}(T,P) \approx \tau_0(T,P)$. Broadband dielectric relaxation data collected over many decades of frequencies are best for carrying out the test. The fit of the α-loss peak by the one-sided Fourier transform of a Kohlrausch function [Eq. (1)] determines n and τ_α, and together with $t_c \approx 2$ ps, τ_0 is calculated from Eq. 6

$$\tau_0 = (t_c)^n(\tau_\alpha)^{1-n} \tag{9}$$

The result is then compared with τ_{JG} of the resolved JG relaxation appearing at higher frequencies in the isothermal or isobaric spectrum. Remarkably, for all small molecule and polymer glass-formers tested, including those mentioned in this chapter, the relation

$$\tau_{JG}(T,P) \approx \tau_0(T,P) = t_c^n[\tau_\alpha(T,P)^{1-n}] \tag{10}$$

with $t_c = 2$ ps holds [32,33,34,36,39,40,41,80,240]. Here we demonstrate this with three examples of the correspondence between the calculated τ_0 and the experimental τ_{JG} in the dielectric loss spectra of the small-molecule glass-formers DPGDB (Fig. 27), and BIBE (Fig. 33), and the polymer polyisoprene (Fig. 44).

The separation between $\nu_0 \equiv 1/2\pi\tau_0$ and $\nu_\alpha \equiv 1/2\pi\tau_\alpha$, (in units of hertz) on a logarithmic scale is given by

$$\log_{10}\nu_0 - \log_{10}\nu_\alpha = n(10.9 - \log_{10}\nu_\alpha) \tag{11}$$

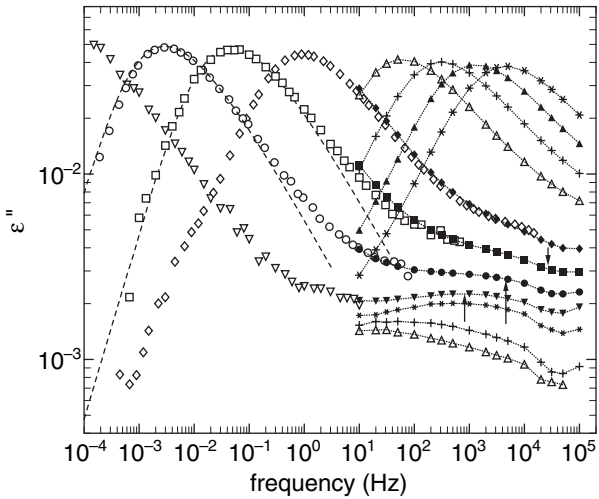

Figure 44. Dielectric loss spectra of PI. The data at 216.0 K (◇), 211.15 K (□), 208.15 K (◯), and 204.15 K (▽) were obtained using the IMass Time-Domain Dielectric Analyzer. All the other data, which start at 10 Hz and continue up to 100 kHz, were taken with the CGA-83 Capacitance Bridge. There is good agreement of the CGA-83 data at 216.7 K (◆), 212.7 K (■), 208.7 (•), and 204.7 K (▼) with the IMass data at 216.0 K (◇), 211.15 K (□), 208.15 K (◯), and 204.15 K (▽), respectively, after the latter have been shifted horizontally by an amount determined from the VFTH temperature dependence of the α-relaxation frequency, in order to account for the slight differences in temperature. The other eight spectra were obtained only using the CGA-83. The spectra that show α-loss maxima correspond (from right to left) to $T = 236.7$ (∗), 232.7 (▲), 228.7 (+) and 224.7 K (△). The lower three CGA-83 curves, which show β-loss peaks, were taken (starting from the bottom) at 169.7 (△), 181.7 (+), and 200.7 K (∗). The vertical arrows mark the locations of the calculated primitive relaxation frequencies, ν_0, at (from right to left) 212.7 K (■), 208.7 K (•), and 204.7 K (▼). The locations of these ν_0 should be compared with the secondary relaxation peaks at these temperatures.

If $\nu_0 \approx \nu_{JG}$ holds, then we have

$$\log_{10}\nu_{JG} - \log_{10}\nu_\alpha \approx n(10.9 - \log_{10}\nu_\alpha) \tag{12}$$

which says that the separation between ν_{JG} and ν_α is smaller for smaller n at constant ν_α. Hence, glass-formers with small n will have ν_{JG} too close to ν_α and their JG relaxations will be hidden by the high-frequency flanks of the more intense α-loss peaks. The JG relaxation is unresolved and appears as an excess wing instead. In fact, for many such glass-formers, the calculated primitive relaxation frequency, ν_0, falls within the excess wing.

Some small n glass-formers show also a secondary relaxation with peak frequency ν_γ much higher than ν_0. If these secondary relaxations were the JG relaxations, then the data would be counter examples to $\nu_0 \approx \nu_{JG}$. However, in all such cases, the position of these secondary relaxations do not change much

or at all on applying pressure, and hence they are not the JG relaxation. The JG relaxation is still in the excess wing with its relaxation time ν_{JG} located in between ν_α and ν_γ. In some cases, the excess wing can be transformed to a resolved JG relaxation by applied pressure or by physical aging like that found in dipropylene glycol and tripropylene glycol [101,102] (see Figs. 31 and 32). The resolved JG relaxation time ν_{JG}, unlike ν_γ, is pressure-dependent and is approximately the same as the calculated ν_0. *m*-Fluoroaniline (*m*-FA) is another example of this class of glass-formers, but it stands out because we have a clue on the origin of the additional secondary relaxation. Elastic neutron scattering measurement and computer simulation of *m*-FA [231,232] have found the presence of hydrogen-bond-induced clusters of limited size in *m*-FA at ambient pressure and temperature of dielectric measurement. The resolved secondary relaxation in *m*-FA originates from the hydrogen-bond-induced clusters and hence is not the JG relaxation involving the entire *m*-FA molecule. Neutron scattering experiments have also found that the hydrogen-bond-induced clusters are suppressed under high pressure and elevated temperature. If the additional secondary relaxation were indeed coming from the hydrogen-bond-induced clusters, the dielectric relaxation spectrum taken at high pressure and elevated temperature would be different from that at ambient pressure and lower temperatures. By performing high-pressure/high-temperature dielectric relaxation measurements on *m*-FA, we find changes in the entire spectrum as a consequence of the suppression of the hydrogen-bond-induced clusters and alteration of the physical structure [44]. The α-loss peak is broadened, the excess wing is curtailed to the extent that its existence is in doubt, and a new secondary relaxation emerges to replace the one seen at ambient pressure (see Fig. 22). The spectrum on the whole resembles that of the closely related molecular glass-former, toluene, the secondary relaxation of which is definitely the JG relaxation because (a) toluene is a rigid molecule and (b) its characteristic frequency is nearly the same as the calculated ν_0 (indicated by the upward pointing vertical arrow in Fig. 45). The characteristic frequency of the new secondary loss peak of *m*-FA also is in good agreement with the calculated ν_0 (indicated by the downward pointing vertical arrow in Fig. 22) and is pressure-dependent. Thus, the secondary relaxation that emerges after the hydrogen bonded clusters have been suppressed at high temperature and pressure is a genuine JG relaxation. The results of *m*-FA indicate that, for other glass-formers having similar dielectric spectrum (i.e., narrow α-loss peak, presence of an excess wing, and a resolved secondary relaxation at higher frequencies), the well-resolved secondary relaxation should not be identified as the JG relaxation. The secondary relaxations in some of these glass-formers, such as di-*n*-butyl phthalate (DBP) [77] and di-ethyl phthalate [76], do not arise from hydrogen-bonding, and unlike *m*-FA they are not suppressed by high pressure and temperature. However, the lack of pressure dependence in their

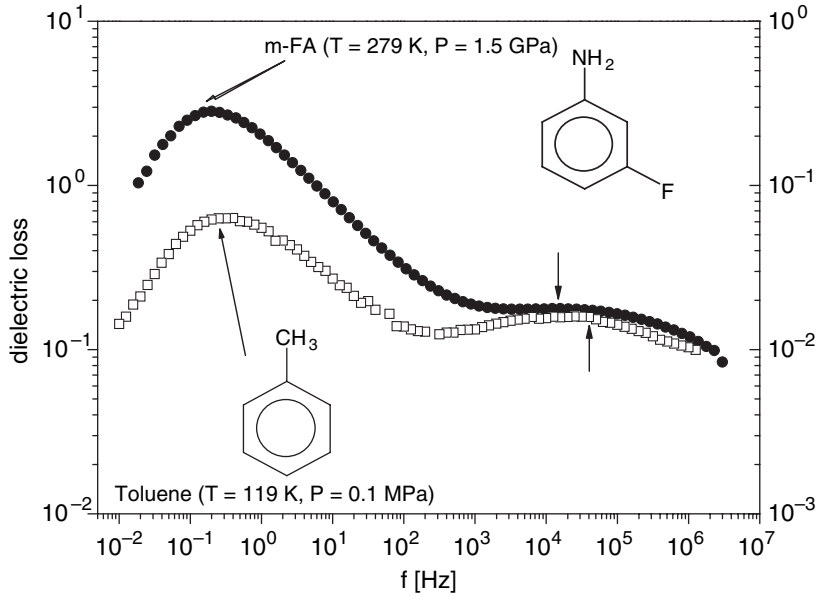

Figure 45. The dielectric loss spectrum of m-FA at high pressure and temperature compared with toluene at ambient pressure. The α-loss peak frequency is nearly the same in the two cases. The vertical arrows indicate the calculated primitive relaxation frequencies, ν_0, for the two cases.

relaxation times is another good indication that they are not the JG relaxation. The genuine JG relaxation of DBP is identified with a new excess wing, which emerges after physical aging for a period of time (see Fig. 40). These examples are sufficient for us to warn against the practices of either (a) referring to all observed secondary relaxations as JG relaxations without applying any criterion or (b) the other extreme of not distinguishing the secondary relaxation that bears relation to the structural α-relaxation from others that do not. Both extremes are unreasonable and detrimental to the search of secondary relaxations that may play a fundamental role in glass transition.

Polymers that have bulky repeat units can have multiple secondary relaxations. If more than one secondary relaxation is found, then the slowest one has to be the JG relaxation, assuming that the latter is resolved. Excellent illustrations of this scenario are found by dielectric relaxation studies of aromatic backbone polymers such as poly(ethylene terephthalate) (PET) and poly(ethylene 2,6-naphthalene dicarboxylate) (PEN) [43]. The calculated τ_0 from the parameters, n and τ_α, of the α-relaxation are in good agreement with the experimental value of τ_{JG} obtained either directly from the dielectric loss spectra or from the Arrhenius temperature dependence of τ_{JG} in the glassy state extrapolated to T_g. The example of PET is shown in Fig. 46.

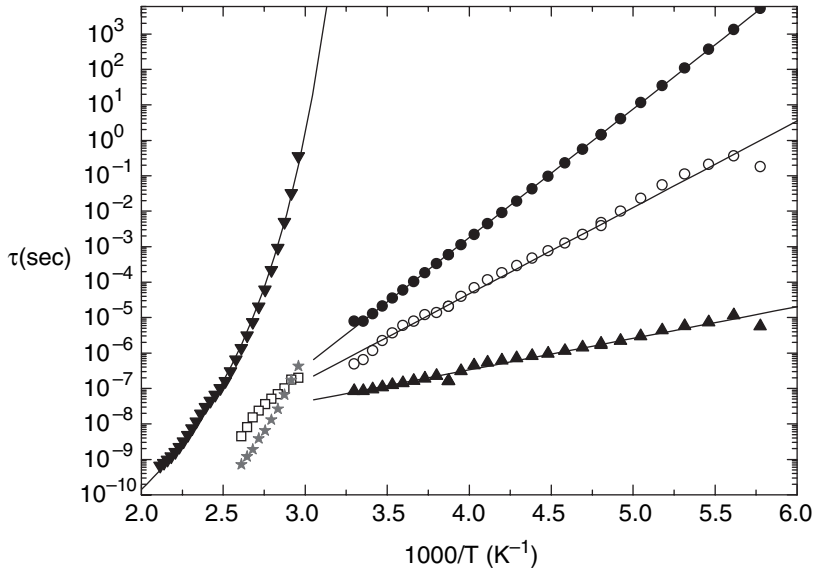

Figure 46. Relaxation map of PET showing the primary relaxation and three secondary relaxations. The calculated primitive relaxation time are represented by stars. [A. Sanz, A. Nogales, and T. Ezquerra, paper presented at the 5th International Discussion Meeting on Relaxation in Complex Systems, July 7–13, 2005 and to be published in J. Non-Cryst. Solids 2006.]

C. Relation Between the Activation Enthalpies of τ_{JG} and τ_α in the Glassy State

In the previous section, at temperatures above T_g, the Johari–Goldstein relaxation time has been shown to correspond well to the primitive relaxation time, and both are related to the structural α-relaxation time by Eq. (10). This equation should continue to hold at temperatures below T_g. However, testing this relation in the glassy state is difficult because of either the scarcity or the unspecified thermal history of the data on the α-relaxation time τ_α. In fact, a reliable characterization of the structural relaxation can be acquired only at equilibrium, and such condition is rarely satisfied below T_g. Glassy systems are nonergodic, and their properties can depend on aging time and thermal history. Anyway, for glasses in isostructural state with a constant fictive temperature T_f, both τ_α and τ_0 as well as τ_{JG} should have Arrhenius T-dependences with activation enthalpies E_α, E_0, and E_{JG} respectively. Eq. (10) leads us to the relation

$$(1-n)E_\alpha = E_0 = E_{JG} \tag{13}$$

between the activation enthalpies. This relation was predicted by another model of relaxation in glass-formers [282,286–288], although it differs from the CM in quantitative details. When checking this prediction, it is important to bear in mind that the JG relaxation times τ_{JG}, obtained at all temperatures to determine E_{JG}, are derived from experiment under isostructural condition with T_f being held constant. A wrong conclusion could result from data of τ_β obtained in glassy states having different T_f coming from different cooling rates, annealing temperatures, and waiting times. In fact, it has been demonstrated in physical aging experiments [289] that the structural states induced in three different types of thermal history (isothermal, isochronal, and isostructural) are very different. Thus, to verify Eq. (13), it is important to know the thermal history and the fulfillment of isostructural condition. This was done for dipropylene glycol dibenzoate (DPGDB) [240]. Knowing E_α of the isostructural state and $n = 0.43$, the product $(1 - n)E_\alpha$ has the value of 48.4 kJ/mol. On the other hand, by fitting the experimental JG β-relaxation times (Fig. 36) in the lower- temperature region to an Arrhenius equation, its activation energy E_{JG} has the value of 48.0 ± 0.6 kJ/mol. There is good agreement between $(1 - n)E_\alpha$ and E_{JG}.

Unfortunately, most of the articles concerning JG relaxations do not report any information about thermal history, and one cannot be sure if the relaxation times were derived isostructurally. The simple relation [Eq. (13)], has been tested for other systems where genuine JG relaxations have been reported in the literature, although the thermal history followed to reach the glassy state is not given. The results are shown in Fig. 47 [80], where the product $(1 - n)E_\alpha$ is plotted against the experimentally measured activation energy E_{JG} of the JG β-relaxation. A linear regression of data yields an angular coefficient of 0.99 ± 0.01, meaning a remarkable agreement between experiments and model predictions, in spite of possible errors due to unknown thermal history of the glassy state. The data reported in Fig. 47 include the glass-formers reported in Ref. 34, some low-molecular-mass van der Waals glass-formers (like OTP, isopropyl benzene, and toluene), some hydrogen-bonding systems (like glucose and *n*-propanol), the mixture benzyl chloride in toluene, and the polymer PMMA. Additionally, Fig. 47 displays also the JG β-relaxation of some epoxy compounds having a multiple secondary relaxation scenario (only the slowest secondary relaxation is the genuine JG) [290,291], the data of the JG β-relaxation for the polymer PET [292], and the recently discovered JG β-relaxation of polyisoprene [35].

D. Explaining the Properties of τ_{JG}

(*i*). *Pressure Dependence and Non-Arrhenius Temperature Dependence Above* T_g. The CM equation

$$\tau_\alpha(T, P, V, S) = [t_c^{-n}\tau_0(T, P, V, S)]^{1/(1-n)} \approx [t_c^{-n}\tau_{JG}(T, P, V, S)]^{1/(1-n)} \quad (14)$$

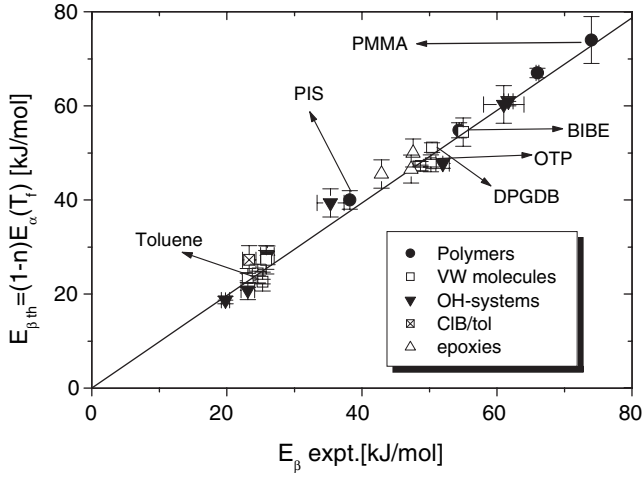

Figure 47. Linear correlation between the experimental activation energy in the glassy state for the JG β-relaxation process (abscissa) and the activation energy predicted by the CM for the primitive relaxation (ordinate). Symbols for simple van der Waals molecules, H-bonded systems, polymers, chlorobenzene/toluene mixture, and epoxy oligomers are shown in the figure. The solid line is a linear regression of data (linear coefficient 0.99 ± 0.01).

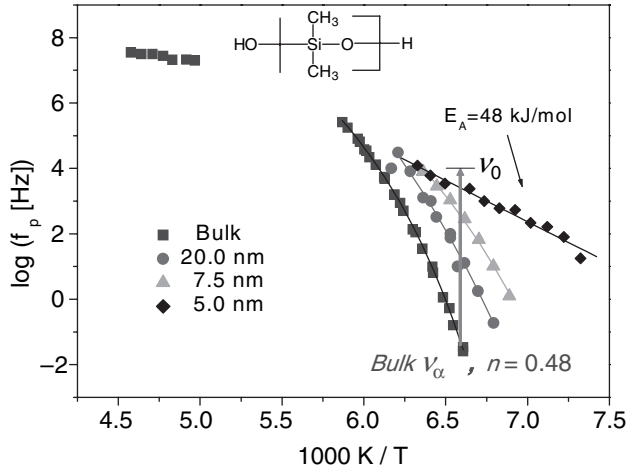

Figure 48. Loss peak frequency, f_p, of PDMS in bulk or in nanopores.

relates τ_{JG} to τ_α. Here we write out explicitly all the possible dependences of the relaxation times on the thermodynamic variables P, V, and T and entropy S, which are related by $(\partial S/\partial P)_T = -(\partial V/\partial T)_P$ [293]. From Eq. (14), the properties of the JG relaxation discussed in Section V can be immediately explained. For example, the properties of τ_{JG}, including the pressure dependence and the non-Arrhenius temperature dependence (in the equilibrium liquid state), all readily follow from the corresponding properties of τ_α and vice versa from their relation. Any dependence of τ_α is stronger than the corresponding dependence of τ_{JG} because, in Eq. (14), the former is obtained from the latter by raising it to the power $1/(1-n)$, which is larger than one.

(*ii*) *Physical Aging*. The same is true for the increase of relaxation times on physical aging of the glassy state. Let us denote by $\tau_{JG}(0)$ and $\tau_\alpha(0)$ the two relaxation times at $t = 0$ when the aging experiment starts, and by $\tau_{JG}(t_{\rm age})$ and $\tau_\alpha(t_{\rm age})$ the two relaxation times after $t_{\rm age}$. From Eq. (14), we see that the shift factors of the two relaxation times are then related by

$$\log[\tau_\alpha(t_{age})/\tau_\alpha(0)] = \frac{\log[\tau_{JG}(t_{age})/\tau_{JG}(0)]}{1-n} \tag{15}$$

The shift factor of τ_α is larger than that of τ_{JG} by the factor $1/(1-n)$. This quantitative prediction is consistent with the physical aging data of propylene carbonate (Fig. 37), propylene glycol (Fig. 38), and glycerol (not shown). As can be seen from the dielectric aging data and the value of n of propylene carbonate and propylene glycol in Figs. 37 and 38, the relation between two shift factors (indicated by the lengths of the horizontal arrows) are consistent with the Eq. (15). In principle, the Kohlrausch parameter, and therefore the coupling parameter n, could be dependent on $t_{\rm age}$ in Eq. (15) [294]. Anyway, it is noteworthy that in a recent aging experiment done on similar samples [244], negligible changes of the Kohlrausch parameter were reported during aging, thereby strengthening the substantial validity of Eq. (15).

A glass is in a nonequilibrium state. At temperatures not far below T_g and when the structural α-relaxation time is not too long, given time the structure changes, driving the glass toward the equilibrium liquid state. It is the structural α-relaxation that can change the structure of the glass during aging. The JG or the primitive relaxation is local, and by itself it cannot effect structural changes. In a recent article [244], the dielectric loss data of several glasses obtained after they have been aged for different lengths of time, $t_{\rm age}$, were analyzed using two assumed equations to describe the changes of the dielectric loss ε'' at any frequency ν and the loss peak frequency ν_α with $t_{\rm age}$. These equations were successful in fitting the dependence of ε'' on $t_{\rm age}$ for many frequencies ν higher than ν_α, although two adjustable parameters $\varepsilon_{\rm st}$ and $\varepsilon_{\rm eq}$ have to be used in the fits for each ν. The accomplishment led

the authors of Ref. 244, to state: ''It is the structural rearrangement during aging, which in a direct way (by shifting the α-peak to lower ν) influences $\varepsilon''(t_{age})$ in the α-peak region and in a more indirect way (by varying the structural ''environment'' felt by the relaxing entities) in the other regions.'' By ''other regions,'' these authors mean the excess wing or the JG relaxation. We agree with this statement because in Section V the relaxation time of the JG relaxation (either resolved or hidden under the excess wing) has been shown to be pressure dependent in the equilibrium liquid state and ν_{JG} is therefore density-dependent. After the glass has been densified by aging for the time period t_{age}, ν_{JG} is shifted along with ν_α to lower frequencies. However, we do not agree with the conclusion of the authors that the excess wing and the JG relaxation shift to lower frequencies by exactly the same amount as ν_α for all t_{age}. This conclusion was drawn from their good fits to the data, but the fits involve two adjustable parameters ε_{st} and ε_{eq} for each ν. The aging data of propylene carbonate (PC) and propylene glycol used in their fits are the same as that shown in Figs. 37 and 38, where we can see directly without any fit that the excess wing does not shift by the same amount as the high-frequency flank of the α-loss peak. The difference between the two shifts is not large because PC has $n = 0.27$ [see Eq. (15)], which may explain the success of the fits performed in Ref. 244, particularly with the luxury of two adjustable parameters for each ν. Xylitol has a larger $n = 0.46$, and the shift of the α-loss peak toward lower frequencies is more significant than the resolved JG relaxation. Aging xylitol at 243 K, the $\varepsilon''(t_{age})$ data for $\nu = 1$ kHz belongs to the JG relaxation. On the other hand, the $\varepsilon''(t_{age})$ data for ν lower than 10 Hz are in the domain of the α-loss peak. The authors of Ref. 244 pointed out an anomaly in their fits to the xylitol data: The observed decreases of $\varepsilon''(t_{age})$ with increasing t_{age} for $\nu = 1$ kHz and 100 kHz are much milder than that of $\varepsilon''(t_{age})$ for ν less than 10 Hz. This anomalous behavior is likely due to the fact that actually the shift of ν_{JG} with aging time is smaller than that of ν_α, and the good agreement of fit with data is probably due to redundant free parameters.

Although the structural change in aging is effected by the α-relaxation, in the glassy state the JG or primitive relaxation is still the elementary process from which the structural α-relaxation is formed out of many-molecule dynamics. The following describes how aging proceeds by feedback between the changes of the α-relaxation and the JG or the primitive relaxation with time. Let aging start at $t = 0$. After a small increment of time, Δt_1, there is a small change in the structure or fictive temperature T_f effected by the structural α-relaxation with relaxation time $\tau_\alpha(t=0)$ given by $\tau_\alpha(t=0) = [t_c^{-n}\tau_{JG}(t=0)]^{1/(1-n)}$. Since the JG or the primitive relaxation is sensitive to the structure through volume and entropy, their relaxation times $\tau_{JG}(\Delta t_1)$ or $\tau_0(\Delta t_1)$ at $t = \Delta t_1$ increase slightly from $\tau_{JG}(t=0)$ or $\tau_0(t=0)$, in response to the change of the fictive temperature

from T_f to $T_f - \Delta T_{f1}$. In the next time period $[\Delta t_1, \Delta t_1 + \Delta t_2]$, the structural is further changed by the structural α-relaxation with relaxation time now given by $\tau_\alpha(\Delta t_1)$, which is given by $\tau_\alpha(\Delta t_1) = [t_c^{-n}\tau_{JG}(\Delta t_1)]^{1/(1-n)}$. The new fictive temperature is $T_f - \Delta T_{f1} - \Delta T_{f2}$. The JG or primitive relaxation responds to this step change of structure and are further increased to $\tau_{JG}(\Delta t_1 + \Delta t_2)$ or $\tau_0(\Delta t_1 + \Delta t_2)$ at $t = \Delta t_1 + \Delta t_2$. Repeating this argument many times to reach the aging time t_{age}, the results for $\tau_\alpha(t_{\text{age}})$ and $\tau_{JG}(t_{\text{age}})$ are determined. This description illustrates the feedback between the changes of τ_α and τ_{JG} during aging, but still the primitive or the JG relaxation is the precursor of the structural relaxation at all times.

(*iii*) *Invariance of* τ_{JG} *to Variations of T and P at Constant* τ_α. We have seen in Section II that the dispersion of the α-relaxation (or n) is invariant to different combinations of temperature and pressure so long they keep τ_α constant. Accepting this as an empirical fact, Eq. (14) immediately explains the experimental finding discussed in Section V.B that τ_{JG} is also invariant to changes in temperature and pressure while τ_α is maintained constant.

The T and P dependences of τ_α of many glass-formers can be recasted as the dependence of $\log(\tau_\alpha)$ on the product variable, $T^{-1}V^{-\gamma}$ [114,115]. Here V is the specific volume and γ is a material-specific constant, which is found to vary over a broad range $0.14 \leq \gamma \leq 8.5$ for the glass-formers investigated to date. Combining this with the invariance of τ_{JG} to changes in T and P while maintaining τ_α constant, it follows that $\log(\tau_{JG})$ must also be a function of $T^{-1}V^{-\gamma}$ However, when rewritten as functions of $T^{-1}V^{-\gamma}$, the established relation between τ_α and τ_{JG},

$$\tau_\alpha(T^{-1}V^{-\gamma}) = [t_c^{-n}\tau_0(T^{-1}V^{-\gamma})]^{1/(1-n)} \quad \text{or} \quad [t_c^{-n}\tau_{JG}(T^{-1}V^{-\gamma})]^{1/(1-n)} \tag{16}$$

still holds. This is a CM prediction that both τ_α and τ_{JG} (or τ_0) depend on the same variable $T^{-1}V^{-\gamma}$, but their dependences are different and related by the equation above. This prediction has not yet been tested due to lack of data of resolved JG relaxation over large range of variations of T and P at the present time. Nevertheless, dielectric relaxation data of a few polymers, showing not only the α-relaxation but also the longer time normal chain modes [94,96], offer quantitative tests of the prediction that τ_α and τ_0 are different functions of the same product variable $T^{-1}V^{-\gamma}$ and they are related by Eq. (16). This is because, in the application of the CM to polymer dynamics and viscoelasticity [25,191,202,205,206,208,209,295], the normal modes and the local segmental mode have the same primitive monomeric friction coefficient $\zeta_0(T^{-1}V^{-\gamma})$. Based on this, the breakdown of thermorheological simplicity of the viscoelastic spectrum of amorphous polymers discussed in Section III, (paragraph 4), was

explained based on the difference between the coupling parameter n_α and n_n of the local segmental mode and the normal modes, respectively. While τ_α is governed by the friction coefficient,

$$\zeta_\alpha(T^{-1}V^{-1}) = [\zeta_0(T^{-1}V^{-1})]^{1/(1-n_\alpha)} \tag{17}$$

τ_n is governed by

$$\zeta_n(T^{-1}V^{-\gamma}) = [\zeta_0(T^{-1}V^{-\gamma})]^{1/(1-n_n)} \tag{18}$$

Thus, τ_α and τ_n are both functions of $T^{-1}V^{-\gamma}$, but their dependences on $T^{-1}V^{-\gamma}$ are different. Usually, n_α is larger than n_n, and certainly in the case of $n_n = 0$ for the Rouse normal modes of unentangled polymers. Thus, a stronger dependence of τ_α on $T^{-1}V^{-\gamma}$ than τ_n is predicted by the two equations given above. The prediction can be tested quantitatively after the values of n_α and n_n have been determined by analysis of the dielectric spectra. In fact, dielectric relaxation measurements of the α-relaxation and the normal mode were obtained for various T and P combinations on polypropylene glycol (PPG), 1,4-polyisoprene (PI), and poly(oxybutylene) (POB)[94,96]. Both τ_α and τ_n were shown to yield master curves when plotted against the parameter $T^{-1}V^{-\gamma}$ with the same value of γ. However, the dependences of τ_α and τ_n on $T^{-1}V^{-\gamma}$ are not the same. Neither is their dependences on V at constant T, or on T at constant P. The experimental findings were explained by the CM equations, Eqs. (17) and (18) [207]. The values of n_α and n_n were determined from the dielectric spectra, and the stronger dependences of τ_α on $T^{-1}V^{-\gamma}$ than τ_n were accounted for quantitatively.

E. Consistency with the Invariance of the α-Dispersion at Constant τ_α to Different Combinations of T and P

According to the CM interpretation of the evolution of dynamics with time, the primitive relaxation is the fundamental building block of the many-molecule dynamics that ultimately ends up in the α-relaxation with its correlation function having the Kohlrausch form [Eq. (1)]. Experimental data have shown that the origin of the dependences of molecular mobility on T, P, V, and S is in τ_{JG} or τ_0. The corresponding dependences of the α-relaxation time τ_α are not original but derived from those of τ_{JG} or τ_0 and given by the CM equation, Eq. (14). Different combinations of T and P can certainly be found to maintain τ_{JG} or τ_0 constant. As a consequence of Eq. (14), n must be the same in order that τ_α can be kept constant for all these combinations of T and P. Thus, the invariance of the α-dispersion to different combinations of T and P at constant τ_α, found experimentally in many glass-formers (see Section II), can be derived from the CM.

F. Relaxation on a Nanometer Scale

Supercooled liquids confined in nanometer-size glass pores may not be chemically bonded or physically interacting with the walls if the surfaces of the walls has been rendered passive by treatment such as with silane. There are several studies of the relaxation of the nanoconfined liquids in silanized glass pores. Examples include the liquids 1,2-diphenylbenzene (also known as *ortho*-terphenyl (OTP)) [296–297,298], salol [299], and the polymers poly(dimethyl siloxane) and poly(methylphenyl siloxane) [300,301]. Under such conditions, the molecules nearer the smooth wall have larger reduction of intermolecular coupling because their neighboring molecules on the side of the wall have been removed. Another factor that contributes to the reduction of intermolecular coupling is when the pore size becomes comparable or smaller than the many-molecule dynamics length-scale, and hence reduces the extent of the many-molecule dynamics inside the pores. Possible lower density of the liquid in the pores than in the bulk directly affects the primitive relaxation time through its dependence not only on density but also on the coupling parameter, because the molecules are further apart. Reduction of intermolecular coupling in the CM means that the coupling parameter $n(T)$ becomes smaller than the bulk value $n_b(T)$. Had this effect been the only factor, the dispersion of the liquid in the pore will be narrower than in the bulk. However, there is an additional complication. The cooperative dynamics of molecules situated at various distances from the wall are necessarily affected differently and thus n is position-dependent. The overall observed relaxation dispersions of confined liquids are additionally broadened by the spatial distribution of the molecules in the pores. This is a dominant effect on the observed dispersion because all molecules inside the pore are sampled by experiment, and it could eclipse the effect of the reduction of $n(T)$ of the molecules at distances nearer the smooth wall. Hence, we cannot obtain the reduced values of $n(T)$ of molecules nearer the wall from the experimentally observed width of the dispersion of the liquid confined in pores. Nevertheless, we expect that $n(T)$ to decrease with the decreasing size of the pores. The CM equation can be rewritten as $\tau_\alpha = \tau_0(\tau_0/t_c)^{n/(1-n)}$ or $\tau_\alpha = \tau_{JG}(\tau_{JG}/t_c)^{n/(1-n)}$. Since τ_0 or τ_{JG} is usually much larger than $t_c = 2$ ps and $n/(1-n)$ is a monotonic decreasing function with decreasing n, $\tau_\alpha(T)$ of nano-confined liquids decreases on decreasing the size of the pores. Consequently, the difference between τ_α and τ_0 or τ_{JG} becomes smaller [298,302,303]. This trend is shown in Fig. 48 by the dielectric relaxation data of PDMS confined in silanized glass pores of various sizes. If in sufficiently small pores $n \to 0$, then $\tau_\alpha \to \tau_0$ or τ_{JG}, and the characteristics of the α-relaxation will not be very different from that of the JG relaxation. The location of the primitive frequency ν_0 corresponding to τ_0 calculated from the bulk τ_α and $n = 0.48$

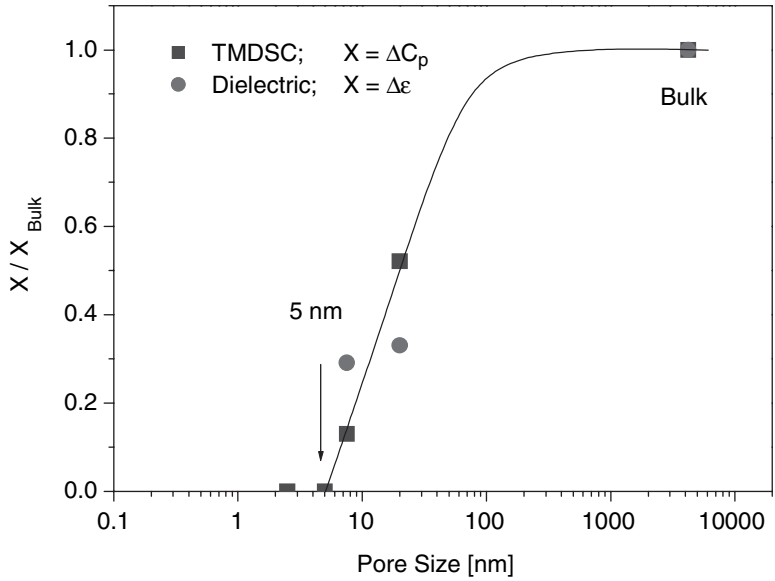

Figure 49. Dielectric strength $\Delta\varepsilon$ as well as the thermal capacity ΔC_p of the α-relaxation of PDMS normalized to the bulk values are plotted against pore size. The data show mark decrease of $\Delta\varepsilon$ and ΔC_p from the bulk value on decreasing the pore size.

values at one temperature is indicated in Fig. 49, and note that they differ by about five orders of magnitude. On the other hand, τ_α of PDMS in 5-nm pores at the same temperature is only a factor of 4 longer than τ_0, and its temperature dependence is weaker than τ_α of bulk PDMS, having an apparent activation enthalpy of 48 kJ/mol commonly found for JG relaxation of polymeric glass-formers. Moreover, the dielectric strength $\Delta\varepsilon$ as well as the thermal capacity ΔC_p of the α-relaxation undergo a marked decrease from the bulk value on decreasing the pore size as shown in Fig. 49. At 5 nm, the dielectric strength and ΔC_p of the α-relaxation are significantly smaller than the same quantities of bulk PDMS. They become similar to that observed for the JG relaxation of bulk glass-formers, in comparison with the α-relaxation [304], indicating once more that in nanometer-size pores the α-relaxation is not much different from the JG relaxation. The data of OTP confined in silanized nano-pores and comparison with τ_0 is shown in Fig. 50. Again, there is good indication that at small pore size, τ_α tends to be close to τ_0. The results in Figs. 48–50 demonstrate the veracity of the primitive relaxation and its relaxation time τ_0. They are actually observed as the α-relaxation and τ_α when the size of the glass-former is scaled down to a few nanometers. This transformation of the α-relaxation of the bulk glass-former to the primitive or

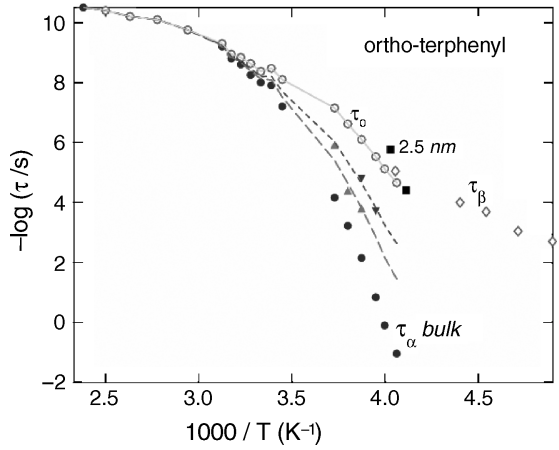

Figure 50. Temperature dependencies of the various relaxation times of OTP. Filled circles are α-relaxation times of bulk OTP obtained by photon correlation spectroscopy; open diamonds are JG relaxation times obtained by dielectric spectroscopy; open circles are the primitive relaxation times τ_o of bulk OTP calculated by Eq. (10). The photon correlation spectroscopy relaxation times of OTP confined in 7.5-nm pores (▲); 5.0-nm pores (▼); 2.5-nm pores (■).

the JG relaxation occurs because the many-molecule dynamics in the bulk are suppressed when the size is reduced to the nanometer scale.

Similar effects were found in thin poly(methylphenylsiloxane) (PMPS) films with thickness of the order of 1.5 to 2.0 nm intercalated into galleries of silicates (Fig. 51) [302,303,305]. The observed α-relaxation time τ_α in the PMPS film is much shorter than in the bulk at the same temperature. The root-mean-squared end-to-end distance of the PMPS chains is estimated to be of the order of 3 nm, which is about twice the thickness of the films. It can be expected that there are significant induced orientations in the chains due to severe chain confinement. This, together with the extremely small thickness of the film, suggests that we may now have large reduction of intermolecular coupling of the local segmental relaxation. Hence, in the thin film, the coupling parameters n may be reduced to approach zero value, and the observed α-relaxation time $\tau_\alpha(T)$ becomes nearly equal to the primitive relaxation time $\tau_0(T)$ calculated from the parameters, $\tau_\alpha(T)$ and n, of bulk PMPS. This expected change of $\tau_\alpha(T)$ is supported by the experimental data shown in Fig. 51 [302], like in the case of PDMS confined in nanometer-size glass pores discussed in the previous paragraph. Another similar case is thin supported polystyrene films [306]. The changes of $\tau_\alpha(T)$ on decreasing film thickness from 90 nm to 6 nm are similar to that found in PDMS confined in glass pores when the pore size is decreased from the bulk to 5 nm (Fig. 49) or in PMPS thin films (Fig. 51).

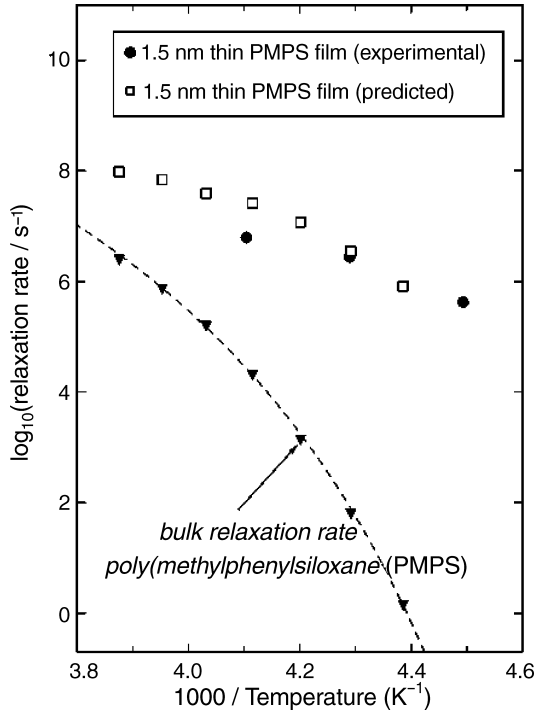

Figure 51. Temperature dependencies of the various relaxation times of PMPS obtained by dielectric spectroscopy. (▼) α-Relaxation rates of bulk PMPS. (•) α-Relaxation rates of 1.5-nm thin films of PMPS. (□) Primitive relaxation rate of bulk PMPS calculated by Eq. (10).

Some studies of the dynamics of thin polymer films go beyond the local segmental relaxation to include the modes of longer length scales, such as the Rouse modes, and the terminal modes if the polymer is entangled. In bulk amorphous polymers, it is well established experimentally that the temperature and pressure dependences of the more global viscoelastic modes are different from that of the local segmental relaxation [25,94,96,189,193,202,206, 207,295,307–309]. In considering the viscoelastic data of thin polymer films, one should be mindful of these facts in bulk polymers. When analysing or interpreting the data of thin films, it is logical to require the theory or model used to be able to account for, or at least consistent with, these known bulk polymer properties. Otherwise, the theory constructed for thin films will not be worthwhile. The Coupling Model (CM) satisfies this requirement (see Section III, paragraph 6). Extended to consider polymer thin films, the CM predicts an increase of the mobility of the local segmental motions as discussed in the prededing section, but predicts the lack of such a change for the mobility of the

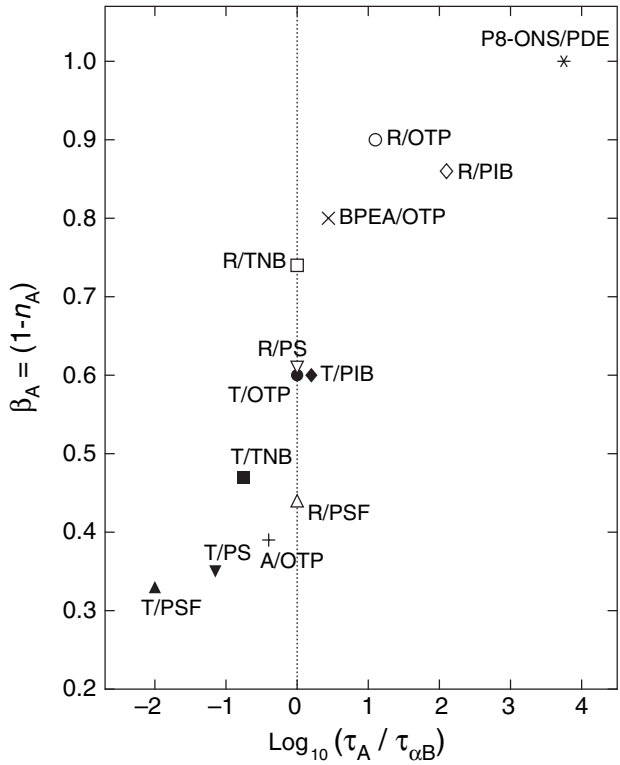

Figure 52. Plot of the stretch exponent β_A of the probe correlation function against the ratio, $\tau_A/\tau_{\alpha B}$, of the probe correlation time τ_A to the host α-relaxation time $\tau_{\alpha B}$. T/PS denotes the probe tetracene (T) in the host polystyrene (PS). Other probes are anthracene (A), BPEA, rubrene (R), and the PS spheres (PS-ONS). The other hosts are polysulfone (PSF), tri(naphthal benzene) (TNB), orhto-terphenyl (OTP), polyisobutylene (PIB), and phenylphthalein-dimethylether (PDE).

Rouse modes and the diffusion of entire polymer chains [303]. These predictions of the CM are in accord with experiments and computer simulations cited in Refs. 303 and 310.

Since the discovery more than a decade ago of the deviation from the bulk glass-transition temperature due to confinement of glass-formers in nanometer spaces [311–313], many experiments have shown that there can be significant changes of T_g as well as other dynamic properties in the nanoconfined materials. However, the changes vary greatly depending on the nature of the interfaces, the chemical structure of the nanoconfined glass-former, the experimental methods used, and, in the case of polymers, the length scale of the dynamics probed [314–317]. Just for T_g alone, it can decrease, increase, or remain the same depending upon the experimental or simulation conditions. As concluded in the

most recent and comprehensive review [317a], "... the existing theories of T_g are unable to explain the range of behaviours seen at the nanometre size scale, in part because the glass transition phenomenon itself is not fully understood." We fully agree with the above quoted remark by Alcoutlabi and McKenna, and furthermore we can identify the reason why the existing theories of T_g fail to explain the range of behaviors of nanoconfinement. Most theories of dynamics of nanoconfinement are based on conventional theories of glass transition for bulk materials. But, as has been shown in previous sections, conventional theories and models of glass transition are not able to account for some general dynamic properties of bulk glass-formers. What causes the conventional theories to be deficient already for bulk glass-formers is the lack of an adequate treatment of the many-molecule dynamics or at least taking into account the dispersion of the structural α-relaxation as a fundamental element. Thus, it is unsurprising to find that, when applied to nanoconfinement, the conventional theories have limited success in explaining the range of behaviors of nanoconfinement. On the other hand, the coupling model is able to explain the range of behaviors seen at the nanometer size scale [317b].

G. Component Dynamics in Binary Mixtures

In general, when two miscible glass-formers A and B are mixed, the dynamics of the component molecules A and B are changed from that in their respective pure states. The problem of predicting the dynamics of each component has attracted much attention particularly in miscible mixtures of two polymers. Perhaps the first published model addressing the component dynamics of binary polymer blends was by Roland and Ngai (RN) [318–324]. The coupling model's description of homopolymer dynamics was extended to blends by incorporating dynamic heterogeneity, due both to the intrinsic mobility differences of the components and to the local compositional heterogeneity from concentration fluctuations. The dynamics of any relaxing species in a blend is determined by its chemical structure, as well as by the local environments, since the latter govern the intermolecular cooperativity and the associated coupling parameters of the relaxation. Thus, the relaxation of a given species reflects its intrinsic mobility and the degree of intermolecular coupling (measured by the coupling parameter n) imposed by neighboring segments (molecules, if the mixture is composed of nonpolymeric glass-formers), the latter obviously fluctuates and is composition dependent. The important ansatz of the blend model is that each environment i of A is associated with a coupling parameter, n_{Ai}, the magnitude of which depends on the intermolecular constraints on A imposed by the molecules in the environment. The correlation function is given by

$$\Phi_{Ai}(t) = \exp[-(t/\tau_{Ai})^{1-n_{Ai}}] \tag{19}$$

with the relaxation time τ_{Ai} given by

$$\tau_{Ai} = [t_c^{-n_{Ai}}\tau_0]^{1/(1-n_{Ai})} \tag{20}$$

This ansatz can be rationalized by some theoretical considerations [325,326].It is also supported by the experimental data at very low concentrations of the component *A* where the study is reduced to the dynamics of the probe *A* in host *B*. Each probe molecule experiences the same environment, which eliminates the complications from concentration fluctuations. We have mentioned in Section III, paragraph 4, that the probe rotational correlation function indeed has the Kohlrausch form. The differential between the probe rotational time τ_A and the host α-relaxation time $\tau_{\alpha B}$ is gauged by their ratio, $\tau_A/\tau_{\alpha B}$. As expected, the slower the host *B* compared with the probe *A*, the larger the coupling parameter, $n_A \equiv (1 - \beta_A)$, obtained from the stretch exponent β_A of the measured probe correlation function. The experimental data are shown in Fig. 52. For more details, see Ref. 172.

Another support of the CM ansatz for blends come from molecular dynamics simulations. Molecular dynamics simulations of a binary LJ liquid thin film confined by frozen configurations of the same system has been performed [327]. The film thickness was 15.0 in units of the length parameter of the Lennard-Jones potential, with the film center at a distance $z = 7.5$ from the confining walls. An important feature of the simulation is the interaction of the mobile particles in the film with the immobile particles comprising the confining walls. Interaction between the mobile and the immobile particles occurs via the Lennard-Jones potential, the same as between mobile particles. The particles in the immediate vicinity of the wall are highly constrained (i.e., strongly coupled) because of the neighboring immobile particles of the wall (the analog of the component *B* that has much higher T_g in mixture with *A*). Thus, the ansatz of the blend model leads to the expectation that particles in layers closer to the wall will have a large *n*. The advantage of simulation is that the self part of the intermediate scattering function, $F_s(q,z,t)$, can be calculated for any layers at a distance z from the wall. All particles at the same distance from the wall are equivalent. Remarkably, for all z, $F_s(q,z_1,t)$ has the Kohlrausch form,

$$F_s(q,z,t) = A(z)\exp - [t/\tau(z)]^{1-n(z)} \tag{21}$$

with $n(z)$ decreasing with increasing distance z from the wall, and at the center of the film it become the same as the coupling parameter of bulk binary LJ liquid. Furthermore, the relaxation time $\tau(z)$ and the coupling parameter $n(z)$ obtained from the simulation were shown [302] to follow the relation $\tau(z) = [t_c^{-n(z)}\tau_0]^{1/[1-n(z)]}$ approximately for all z, with the *same* primitive relaxation time τ_0 for all z. Thus, the dynamics of the layers are consistent

with the CM ansatz for component dynamics of blends. When all particles in the confined thin film are included in the calculation, the intermediate scattering function, $F_s(q,t)$, does not have the Kohlrausch stretched exponential time dependence. Instead it exhibits a long-time tail, which when Fourier transformed causes asymmetric broadening toward low frequencies. This effect is similar to the dielectric frequency dispersion of a polymer blended with a less mobile component, such as PVME mixed with polystyrene [328], and described by the blend model by a superposition of Kohlrausch functions with different n_i and τ_i.

Various observed phenomena have been explained by the blend model, such as component dynamics differing qualitatively from that of the pure components, thermorheological complexity, unusual concentration dependences, asymmetric broadening of the relaxation function, and the emergence of a secondary relaxation peak. For a review see Ref. 329, where supporting evidence for the change of coupling parameter of a component in the blend and its distribution due to concentration fluctuations are given. In the intervening years, other models of component dynamics in polymer blends have been proposed. Fischer and co-workers (FZ) [330,331] developed a model that specifically addressed in terms of subvolumes the effect of local composition on the glass transition temperature. Kumar and co-workers [332,333] extended the FZ concentration fluctuation model. While concentration fluctuations still give rise to subvolumes, each governed by a local glass temperature, Kumar et al. invoke the idea that experimental probes of the dynamics only sense composition fluctuations that occur over a certain cooperative volume. Rather than a constant length scale, the cooperative volume is governed by the local composition. Lodge and McLeish [334,335] observed that, when making comparisons to experimental results, the cooperative length scale required to fit the data is too large, on the order of 10 nm or more in both the models of Fischer et al. and Kumar et al. Lodge and McLeish proposed an alternative model based on the Kuhn length, l_K, of the polymer chain. The segmental relaxation rate of a segment of component A, in a binary blend of polymers A and B, is determined by the composition of its local volume with a length scale of l_K of A. Because of chain connectivity, this local volume is, on average, richer in A units than the average bulk concentration ϕ_A (''self-concentration'' effect). This enhanced local concentration of A is given by $\alpha_{\text{eff}} = \phi_A + \phi_{sA}(1 - \phi_A)$, where ϕ_{sA} is the ''self-concentration'' of A, determined by the volume fraction occupied by A repeat units in a volume of size $(l_K)^3$. Concentration fluctuations and the dispersion of component dynamics have not been taken into consideration because the objective of the Lodge and McLeish model is to predict the component relaxation times. For polymer blends, the proposal of taking into consideration of ''self-concentration'' effect is reasonable, although not necessarily in the manner proposed by Lodge and McLeish. However, this effect cannot be the ultimate factor that governs component dynamics in

polymer blends. This is because the ''self-concentration'' effect is absent in mixtures of nonpolymeric molecular glass-former, and yet their component dynamics are similar in many respects to polymer blends.

Understandably, the component dynamics in binary mixtures are more complicated to unravel than the dynamics of a neat glass-former. The solution to the problem will require additional inputs, making it more difficult to test any proposed theory against the observed component dynamics stringently. Actually, a cogent as well as stringent test of any theory of mixtures already exists without even having to compare the predictions of the theory with the observed component dynamics. We just have to ask the question, What does the theory predict when the concentration of one component vanishes and the mixture is reduced to a neat glass-former? Many general properties of neat glass-formers have been given in the previous sections, and the test is whether the predictions of the theory in the neat glass-former limit are consistent with these properties. One outstanding example is the invariance of the dispersion of the structural α-relaxation to different combinations of temperature and pressure while τ_α is kept constant. In the blend theory of Fischer et al., it is assumed that within each subvolume the shape of the complex dielectric sucseptibility for one component is the same as that of the component in the pure state and can be described by the empirical Havriliak–Negami function. Thus, the blend theory of Fischer et al. is built upon a theory of glass transition of neat glass-formers in which the dispersion and the relaxation time τ_α of the α-relaxation are independent inputs, *a priori* bearing no relations with each other. Hence, there is no guarantee that they are co-invariants for different combinations of T and P. The emphasis of the blend theories of Kumar et al. and Lodge and McLeish is on predicting the component relaxation times and not on the dispersions of the components. Obviously these two theories have not much to say about (a) the dispersion of a component in its pure state and (b) the fact that many general properties of τ_α of pure glass-formers are either governed by or correlated with the dispersion, as shown throughout this chapter. When the concentration of one component in a binary blend is small, the problem is transformed to the study of the dynamics of a probe molecule in a host glass-former. This is a simpler problem than component dynamics in a blend because of the absence of concentration fluctuation. Nevertheless, the extent of deviation of the probe dynamics from the Stokes–Einstein and the Debye–Stokes–Einstein relations (see Fig. 26) and the frequency separation between the α- and β-relaxations of the probe molecule (see Fig. 53) is correlated with the dispersion of the probe molecule. None of these properties in simpler situations can be addressed by the three blend theories discussed in this paragraph. The logical basis of these theories can be questioned because they attack a more complicated problem (i.e., the component dynamics in a blend) before resolving or at least addressing the outstanding phenomenologies found in a simpler problem (i.e., the dynamics of neat glass-formers or a probe molecule). On the

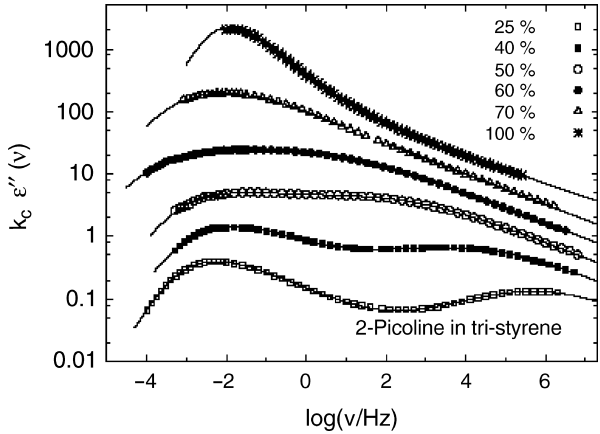

Figure 53. The dielectric loss of 2-picoline in mixtures with tri-styrene at different concentrations obtained at different temperatures but similar α-relaxation times of the 2-picoline component. For clarity, each spectrum is shifted by a concentration-dependent factor k_c. Data from T. Blochowicz and E. A. Rössler, *Phys. Rev. Lett.* **92**, 225701 (2004).

other hand, this criticism does not apply to the Coupling Model (CM) constructed for component dynamics in blends. It is an extension of the CM for the dynamics of neat glass-former and probe dynamics in a host glass-former, polymeric or nonpolymeric, the general properties of which have either been explained or shown to be consistent with the predictions of the CM.

Anomalous component dynamics in blends and mixtures have been observed which cannot be explained by the models of Fischer et al., Kumar et al., and Lodge and McLeish [329]. A recent example is the anomalous dynamics of d_4PEO found in the d_4PEO/PMMA polymer blends [336]. While this anomaly cannot be understood by the other models, it has an immediate explanation from the CM [337].

The CM has a quantitative relation between the α-relaxation frequency ν_α and the Johari–Goldstein (JG) relaxation frequency ν_{JG} or the primitive relaxation frequency ν_0 given by Eqs. (10)–(12), which accounts well for the experimental data of many neat glass-formers. For any fixed value of ν_α, the separation between the α-relaxation and the JG relaxation, $\log(\nu_{JG}) - \log(\nu_\alpha)$, is proportional to n. The change of dynamics of a lower T_g component A when mixed with another component B occurs partly due to an increase of its most probable coupling parameters, n_A, according to the CM. The increase of n_A is larger at higher concentration of the component B because of the increasing numbers of the less mobile molecules B in the neighborhoods of the A molecules. The immediate consequence of this precept of the CM theory for blends, in conjunction with the CM relation $\log_{10}\nu_{JG}^{(A)} - \log_{10}\nu_\alpha^{(A)} \approx n_A(10.9 - \log_{10}\nu_\alpha^{(A)})$,

is that the separation distance, $\log_{10}\nu_{JG}^{(A)} - \log_{10}\nu_{\alpha}^{(A)}$, between the α-relaxation and the JG relaxation of component A at constant $\log_{10}\nu_{\alpha}^{(A)}$, should increase with increasing concentration of component B. On the other hand, the most probable coupling parameters, n_B, of the higher T_g component B will decrease with increasing concentration of the component A. From the same CM relation, the separation distance, $\log_{10}\nu_{JG}^{(B)} - \log_{10}\nu_{\alpha}^{(B)}$, between the α-relaxation and the JG relaxation of component B at constant $\log_{10}\nu_{\alpha}^{(B)}$ should decrease with increasing concentration of the lower T_g component A. These are predictions that can be either verified or falsified by experimental measurements. In the following we shall cite some examples in which these predictions have been verified.

(*i*) *The JG and the α-Relaxations of Poly(n-butyl methacrylate) in Poly(n-butyl-methacrylate-stat-styrene) Random Copolymers*. The copolymers of poly(*n*-butyl methacrylate) (P*n*BMA) and polystyrene (PS) is one example [338,339]. Here P*n*BMA is the lower T_g component A. Neat P*n*BMA has $n = 0.47$ and a JG relaxation. On increasing the styrene content from 0 to 66 mol% in the copolymer, a monotonic increase of n_{A} of the P*n*BMA component leads to a concomitant increase in the separation of the JG relaxation from the segmental relaxation, both of the P*n*BMA component. This changes were observed in the dielectric relaxation experiment.

(*ii*) *The JG and the α-Relaxations of Poly(vinyl methyl ether) in Blends with Polystyrene*. Neat poly(vinyl methyl ether) (PVME) does not have a resolved JG relaxation. In the mixture with polystyrene (PS) that has a higher T_g, an increase of n_A of the PVME component is expected. For blends with large enough PS concentrations, the distance, $\log_{10}\nu_{JG}^{(A)} - \log_{10}\nu_{\alpha}^{(A)}$, will be sufficient large for the JG relaxation of PVME to be resolved as a distinct peak. This prediction is borne out by dielectric relaxation data for blends with 70% or higher PS concentrations [340]. For these compositions, a new relaxation loss peak appears, at a frequency intermediate between that of the α-peak and the high-frequency non-JG secondary relaxation peak of the PVME component. The new peak has an Arrhenius temperature dependence at temperatures below T_{gA} of the PVME component, and its dielectric strength increases with temperature (see Fig. 5 of Ref. 340). These characteristics indicate that the relaxation is indeed a JG process. The isochronal dielectric data at 1 kHz for 70% PVME mixed with 30% poly(2-chlorostyrene) [341] also show a resolved JG secondary relaxation, and a similar explanation applies.

(*iii*) *The JG and the α-Relaxations of Picoline in Mixtures with Tri-styrene or Ortho-terphenyl*. Neat picoline is a small molecule glass-former A having a smaller $n = 0.36$ [241,242,342]. As a result and in accordance with Eq. (12), its JG relaxation is not well separated from the α-relaxation, showing up as an excess wing. When mixed with a higher-T_{g} glass-former B such as tri-styrene or OTP [241,242], the JG β-relaxation of picoline was resolved at sufficiently high

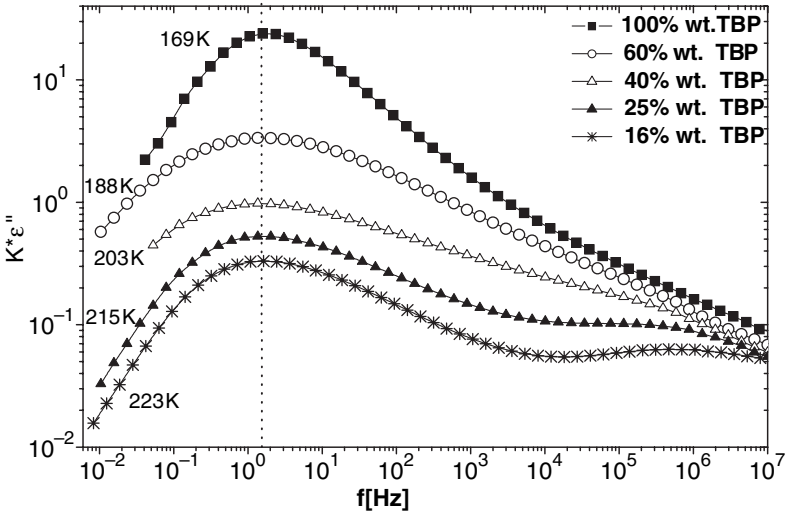

Figure 54. Dielectric loss spectra with the same maximum peak frequency for different concentrations of *tert*-butylpyridine (wt%) in tristyrene. For clarity, each spectrum is shifted vertically by a concentration dependent factor K. $K = 7$, 2, 1.3, 1, and 0.98 for 100%, 60%, 40%, 25%, and 16% TBP, respectively. The x axis is the real measurement frequency, except for the spectra of 100% and 16% TBP, where horizontal shifts of frequency by factors of 1.75 and 0.80, respectively, have been applied.

concentrations of B molecules. The separation between the JG β-relaxation and α-relaxation of the picoline component, $\log_{10}\nu_{JG}^{(A)} - \log_{10}\nu_{\alpha}^{(A)}$ at constant $\log_{10}\nu_{\alpha}^{(A)}$, was observed to increase monotonically with concentration of B in the mixtures (Fig. 53). The experimental data are in accord with the predictions of the CM [342]. Exactly the same behavior was recently found in the JG β-relaxation and α-relaxation of *tert*-butylpyridine, a polar rigid molecule with low $T_g = 164$ K, when mixed with the apolar tri-styrene ($T_g = 232$ K) by Kessairi et al. [343] Sample data are shown in Fig. 54.

(*iv*) *The JG and the α-Relaxations of Sorbitol in Mixtures with Glycerol.* A dielectric study of mixtures of sorbitol with glycerol [344] reported on the changes of the dynamics of both the α-relaxation and the JG relaxation of sorbitol, the component B that has a higher T_g than glycerol, the component A. Neat sorbitol has a larger $n = 0.52$, along with a resolved JG relaxation well separated from the α-relaxation [235]. The CM predicts increasing reduction of the coupling parameter n_B of sorbitol on increasing the concentration of the more mobile glycerol molecules, and decreasing separation, $\log_{10}\nu_{JG}^{(B)} - \log_{10}\nu_{\alpha}^{(B)}$, between the α-relaxation and the JG relaxation of the sorbitol component B at constant $\log_{10}\nu_{\alpha}^{(B)}$. The experimental data was shown to be in accord with the CM prediction [136]. Similar results are found in mixtures of xylitol with water

[345]. The separation between the α-relaxation and the JG relaxation of xylitol at constant $\log_{10}\nu_\alpha^{(B)}$ of xylitol is reduced with addition of water.

H. Interrelation Between Primary and Secondary Relaxations in Polymerizing Systems

Linear polymers or polymer networks are built upon small molecular repeat units by bonded interactions. These bonded interactions reinforce the intermolecular constraints on the primitive motion and increase the coupling parameter n or equivalently the width of the dispersion of the structural α-relaxation. The comparison of the dynamics of a monomer with the oligomers and the higher-molecular-weight linear polymers or networks formed by physical or chemical cross-links is a worthwhile undertaking because essentially the chemical structure of the repeat unit remains the same. The change in the intermolecular constraints or the coupling parameter of the CM is made evident experimentally by the change of the dispersion of the structural α-relaxation. The polyols—glycerol, threitol, xylitol and sorbitol—have the number of carbon atoms on the "backbone" increase from 3 to 6, and their n values are 0.29, 0.36, 0.46, and 0.52, respectively. Concomitant with the increase of n, the separation between the α-relaxation and the JG relaxation, $\log_{10}\nu_{JG} - \log_{10}\nu_\alpha$, is observed to increase as expected by the CM [36]. A similar trend is found in a series of propylene glycols: its dimer, trimer, heptamer, and poly(propylene oxide) [278].

The same is found in a series of oligo(propyleneglycol) dimethyl ethers [346], where again both n and $\log_{10}\nu_{JG} - \log_{10}\nu_\alpha$ increases with molecular weight. However, there is hardly any change in the "fragility" index m. This finding is another indication that m is not a fundamental quantity and its correlation with n or the dispersion can break down as cautioned before in Section III, paragraph 1. Naturally there is no correlation between $\log_{10}\nu_{JG} - \log_{10}\nu_\alpha$ and m. This was mentioned by Mattsson et al. [346], and for this aspect they cited Ref. 32, implying that that this reference proposed a correlation between $\log_{10}\nu_{JG} - \log_{10}\nu_\alpha$ and m. This implication is inappropriate because throughout Ref. 32 as well as in this chapter, the emphasis is on the correlation between $\log_{10}\nu_{JG} - \log_{10}\nu_\alpha$ and n.

Tri-styrene has been mentioned before in this section. It has a much narrower α-relaxation dispersion [242] compared with that of higher-molecular-weight polystyrene. Tristyrene has no resolved JG relaxation because n is small and hence the separation distance, $\log_{10}\nu_{JG} - \log_{10}\nu_\alpha$, is small. On the other hand, polystyrene has a resolved JG relaxation [194,347] because it has a broad α-relaxation dispersion and $n = 0.64$ from photon correlation spectroscopic measurement [210].

The changes of molecular dynamics from the starting material of low-molecular-weight epoxy resins to the fully polymerized state during polymerization reaction are well brought out by the large number of experimental studies of the evolution of the primary and secondary relaxations over the past

two decades by many researchers [207,348–375]. The most widely studied starting material is diglycidyl ether of bisphenol-A (DGEBA) under the trade name EPON828. The neat diepoxide EPON828 is an example of molecular glass-formers that have two secondary relaxations and polymerization offers an excellent opportunity of showing the difference in their properties and which one is the true JG relaxation as well as elucidating the changing relation between the JG relaxation and the α-relaxation with the degree of polymerization. There is a tremendous amount of published work on the evolution of the primary and the two secondary relaxations with reaction time, or the number of covalent bonds formed. Dielectric spectra of epoxy systems have been measured at various stages of the polymerization process and the properties of the secondary and primary relaxations as well as their changes from stage to stage are known. In time order, the stages are given as follows: (1) the neat EPON828 [290] or another neat glass-forming tri-epoxy triphenylolmethane triglycidyl ether (TPMTGE) with trade name Tactix742 [291]; (2) the unreacted mixtures of EPON828 with aniline, cyclohexylamine (CHA), or *p*-aminodicyclohexylmethane (PACM), or unreacted mixtures of Tactix742 with the monoamines 3-chloroaniline or 4-chloroaniline [355,357,358,361,364–367]; (3) the partially polymerized products at different instants of reaction; and (4) the completely polymerized product. The observed molecular dynamics at each stage as well as the changes from one stage to another present multiple challenges for interpretation and explanation. The results are general, independent of the structure of the starting molecular liquids and the polymerizing or cross-linking agents used. Here we present one example to discuss the evolution of the dynamics in several stages. Additional examples can be found in a recent work [207].

The relaxation map of Fig. 55 shows the temperature dependence of the most probable relaxation times τ_α, τ_β, and τ_γ of neat EPON828 obtained. The dielectric α-loss peak of neat EPON828 was well-fitted by the one-sided Fourier transform of the KWW function with $n = 0.47$. It is temperature-independent near T_g and together with $\tau_\alpha(T)$, the corresponding $\tau_0(T)$ is calculated by Eq. (10). The calculated values of $\tau_0(T)$ at $T = 256$ and 259 K near T_g are shown in Fig. 55 by the two solid inverted triangles. They are in good correspondence with the value of $\tau_\beta(T)$ obtained by extrapolating the data below T_g to these two temperatures, and thus the good correspondence between $\tau_0(T)$ and $\tau_\beta(T)$ is verified in neat EPON828, as well as in Tactix 742 (not shown), like found in other molecular and polymeric glass-formers. This indicates that slow β-relaxation in EPON828 and Tactix742 is truly of the JG kind. On the other hand, the γ-relaxation appearing at higher frequencies seems to be related to intramolecular motions involving mainly the epoxide end groups.

On mixing 1 mol of EPON828 with 1 mol of aniline (which has a lower T_g) and before reaction starts, τ_α of the EPON828 component becomes shorter as

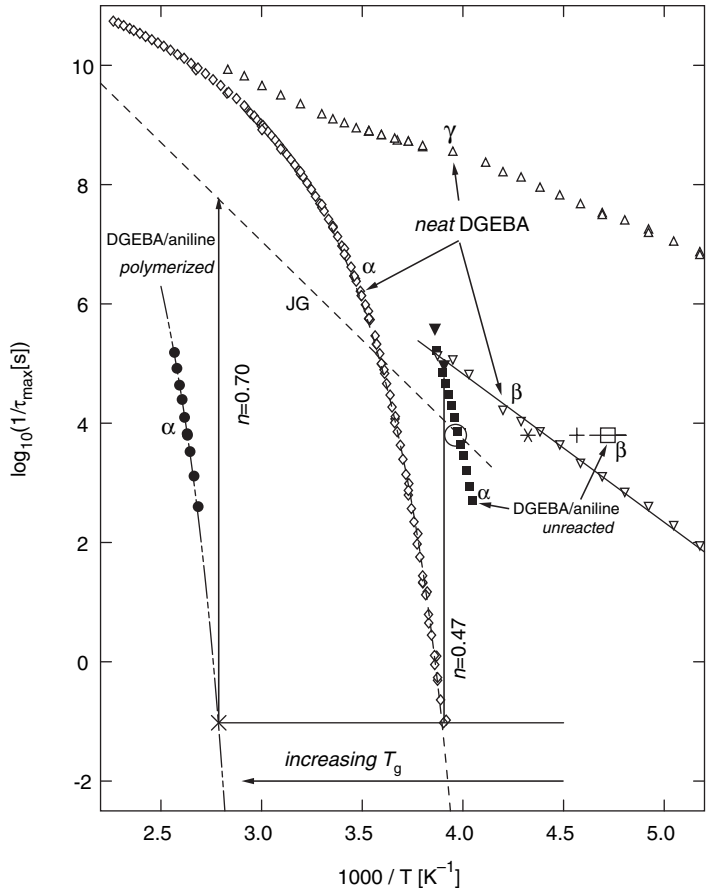

Figure 55. The relaxation map for neat EPON828, for an unreacted mixture of one mole of EPON828 with 1 mole of aniline, and for partially polymerized and completely polymerized EPON828/aniline mixtures. There are two secondary relaxations in addition to the primary α-relaxation. Shown are the reciprocals of the α-relaxation time τ_α, the JG β-relaxation time τ_β, and the non-JG relaxation time τ_γ. The two solid inverted triangles indicate $1/\tau_0$ of neat EPON828 calculated at two temperatures just above its T_g. For the legends of other symbols and lines, as well as for the references from which the data are taken, see text.

expected in the presence of the more mobile aniline molecules. More interesting is that the JG relaxation time τ_β also becomes shorter in the unreacted mixture, while the γ-relaxation time τ_γ is basically insensitive to mixing before reaction starts. These changes of τ_α and τ_β are shown in Fig. 55. The fact that τ_β of EPON828 changes in the presence of aniline is another example of the JG relaxation mimicking the behavior of τ_α discussed in Section V.

After reaction has started and polymers with increasing molecular weight are formed, τ_β increases monotonically with time, mimicking the changes of τ_α, although the changes of τ_α are much larger. This trend is demonstrated in Fig. 55 by τ_β and τ_α of the fully polymerized product represented by the dashed line and the solid circles, respectively. There is an increase of the configurational restriction of molecular motion and a decrease of the specific volume with the number of covalent bonds formed during polymerization, causing a decrease of configurational entropy or free volume. Hence the changes of τ_β in parallel to τ_α during polymerization can be considered as another evidence of the sensitivity of the JG relaxation time to (configurational) entropy or free volume long before the α-relaxation transpires. Accompanying the increase of τ_α with formation of polymer networks or linear-chain polymers from small epoxy resin molecules is the increase of the width of the dispersion of the α-relaxation time. When interpreted in terms of the CM, this is equivalent to the increase of the coupling parameter n of the cooperative many-molecule α-relaxation. The CM predicts that the separation between the JG relaxation and the α-relaxation given by $(\log\tau_\alpha - \log\tau_\beta)$ increases with coupling parameter n or N, the number of covalent bonds formed by reaction. This prediction is in qualitative agreement with the changes in the relation between the two relaxation times at all stages of the experiment. This is illustrated in Fig. 56 for the completely polymerized product, where the experimentally determined separation distances $(\log\tau_\alpha - \log\tau_\beta)$ corresponds to the large value of $n = 0.70$ (compared with $n = 0.47$ of EPON828) and the broad width of the α-relaxation.

I. A Shortcut to the Consequences of Many-Molecule Dynamics and a Pragmatic Resolution of the Glass Transition Problem

From the numerous experimental evidences accumulated over the years including those discussed in this chapter, there is no doubt that (free) volume and (configurational) entropy play important roles in determining the structural relaxation time. Recent experiments with applied pressure have already shown that the relative importance of temperature and volume can vary greatly from one glass-former to another [114]. Glass-formers of different chemical composition and physical structures exist in great numbers. A theory that can account quantitatively the temperature, pressure, volume, and entropy contributions to the structural relaxation rate for *any* glass-former has to be extremely difficult to come by. Besides, as we have shown throughout this chapter, many dynamic and kinetic properties of the glass-forming substances cannot be explained by a theory based on these thermodynamic variables alone. Dispersion of the structural α-relaxation has to be considered as another factor because, as we have seen from multiple experimental facts, it either governs or correlates with the dynamic and kinetic properties of the α-relaxation, and even the relation

of the α-relaxation to its precursor, the Johari–Goldstein (JG) β-relaxation. Experiments have shown that α-relaxation is dynamically heterogeneous, involving slowly and fast relaxing molecules exchanging roles in time scales of the order of the α-relaxation time [27,29,213]. These are clear evidences that many-body dynamics are involved in the α-relaxation. Since the dispersion of the α-relaxation is some average of the heterogeneous dynamics, it is clear that the dispersion of the α-relaxation originates from the many-molecule dynamics. Therefore, a viable theory of glass transition must incorporate the many-molecule dynamics. Unfortunately, many-molecule relaxation is an unsolved problem at the present time. A workable theory of glass transition has to take into account the many-molecule dynamics as well as the influence of the thermodynamic variables on a fundamental basis. Considering the difficulties to implement these two aspects of the problem, a perfectly rigorous theory that can explain all the salient properties will not be available for some time to come. In the mean time, it is not a bad idea to have an imperfect or even a schematic theory that can assimilate the fundamental factors and has predictions that are consistent with all the experimental facts. A schematic theory based on the Coupling Model (CM) is proposed as follows.

From the evidences given before, the JG relaxation time τ_{JG}, or equivalently the primitive relaxation time τ_0 of the CM, is temperature, pressure, volume, and entropy dependent and has the VFTH temperature dependence at temperatures above T_g. Thus, T, P, V, and S have entered into the determination of molecular mobility of the JG or the primitive relaxation. Time being a natural variable, along with the fact that τ_{JG} or τ_0 precedes τ_α, implies that the source of the dependence of molecular mobility on T, P, V, and S originates from τ_{JG} or τ_0. The T, P, V, and S dependences inherent in the JG or the primitive relaxation is passed onto the α-relaxation through the cooperative many-molecule relaxation process occurring at later times. The T, P, V, and S dependences of τ_α is stronger than that of τ_{JG} because the α-relaxation stems from cooperative dynamics involving more than one molecule with length scale that increases with decreasing temperature, while the JG or the primitive relaxation is a local process arising from the independent relaxation of individual molecules. Construction of the schematic theory starts by first simply writing down the dependence of τ_{JG} or equivalently τ_0 on T,P,V,S, explicitly as $\tau_{JG}(T,P,V,S)$ or $\tau_0(T,P,V,S)$, without providing the actual dependence. For any particular glass-former, the dependence is best obtained from experiment data on the JG relaxation, if available, or deduced from that observed on the α-relaxation via Eq. (10). Until a theory that can provide accurate account of $\tau_{JG}(T,P,V,S)$ becomes available for that glass-former, realistically this is the best that one can do. Next we implement the many-molecule dynamics, which eventually gives rise to the α-relaxation. Due to the absence of a theory of the many-molecule dynamics from first principles, we use the shortcut to τ_α by the relation between

τ_α and τ_0 or τ_{JG} by Eq. (14) of the CM. To carry on further, we need to know the coupling parameter n appearing in the fractional exponent, $1-n$, of the Kohlrausch function. Numerous experimental data and molecular dynamics simulations have shown at long times that the observed correlation functions are invariably well approximated by the Kohlrausch function. Thus, there is no need to have a theory that just assures us that the correlation function is approximately a Kohlrausch function but nothing else. Moreover, no existing theory can gives us the exact coupling parameter n for any real glass-former anyway. We just shrewdly take what the experiment gives us for the value of n by fitting the dispersion of the α-relaxation to the Kohlrausch function, at any temperature or pressure [376]. Since t_c has already been determined to be approximately 2 ps for molecular liquids and polymers, the relation between the measured τ_α and τ_0 or τ_{JG} is quantitative and completely specified. We write it out here again, including dependence on other variables Q, such as the scattering vector of neutron scattering,

$$\tau_\alpha(T,P,V,S,Q) = [t_c^{-n}\tau_0(T,P,V,S,Q)]^{1/(1-n)} \quad \text{or} \quad [t_c^{-n}\tau_{JG}(T,P,V,S,Q)]^{1/(1-n)} \tag{22}$$

Eq. (22) gives quantitatively τ_α, as well as its dependences on the thermodynamic variables and other parameters Q, from τ_0 or τ_{JG}. Since the exponent, $1/(1-n)$, is larger than one, it is clear that τ_α has a stronger dependences on *T, P, V,* and *S* than the corresponding dependences of τ_0 or τ_{JG}. The normal dependence of τ_0 or τ_{JG} on Q is modified by the superlinear power, $1/(1-n)$. The result is that τ_α having an unfamiliar or anomalous Q dependence. If Q is the scattering vector of neutron scattering, then the normal Q^{-2} dependence of τ_0 will become the anomalous $Q^{-2/(1-n)}$ dependence of τ_α observed in experiments [144–151]. The isobaric dependence of τ_0 or τ_{JG} on *T, P, V,* and *S* is the origin of the deviation of molecular mobility from Arrhenius temperature dependence in the equilibrium liquid state, which is magnified in τ_α. Possible dependence of n on temperature can make the temperature dependence of τ_α even more complicated, such as the need of more than one VFTH equation to fit it [159,160], while only one is sufficient for τ_0 [48,162]. As demonstrated before, when used judiciously, Eq. (22) can explain other observed properties of τ_α and the transport coefficients such as viscosity, diffusion coefficient, and dc conductivity, especially the anomalous ones. The origin of several observed correlations between n and the properties of τ_α, as well as the ratio (τ_{JG}/τ_α), are easily traced back to the dependence of τ_α on n in Eq. (22).

Admittedly, the schematic theory described above is far short of a rigorous solution to the problem. It does not provide any method to calculate n and $\tau_{JG}(T,P,V,S)$ or $\tau_0(T,P,V,S)$. Nevertheless, simple as it is, the schematic

theory has the benefit that its many predictions are consistent with the experimental data. But, since a rigorous solution of many-molecule dynamics does not exist at the present time, there is no need to apologize for the shortcomings of the CM. Although far short of solving the many-molecule dynamics problem, the CM is an expedient way or a shortcut to predict or explain the observed properties of τ_α. We have shown in Section III these properties are either governed by or correlated with the dispersion. Explanation of these properties and more [1,2] can be found in several publications [22,25,26,48,162,377].

The achievements of the CM using basically the same defining equation in explaining the relaxation behavior of several other classes of interacting systems are noteworthy [22,155,157,276]. The problems in some other systems actually are simpler than the dynamics of glass-forming liquids because there volume and entropy do not change with temperature and the relaxation times have Arrhenius temperature dependence. An example is the dynamics of ions in crystalline and glassy ionic conductors [276]. In some recent works, the activation energy of τ_0 deduced from the CM equations is the actual energy barrier that the ion has to surmount in migration, and the preexponential factor of τ_0 correspond to the ion vibrational frequency [378–380]. The simple relation between τ_α (or its equivalent for other interacting systems) and the primitive relaxation time τ_0 is the basis for all the CM explanations of the experimental data, particularly the anomalous properties which are more difficult to resolve. This feat of the CM is due to it having captured the many-molecule dynamics through the dispersion or the coupling parameter n, along with the fact that the properties of τ_0 are normal and usually known. On the other hand, conventional theories of glass transition usually have no application to the other coupled or interacting systems where volume and entropy do not change.

VII. CONCLUSION

One purpose of this chapter is to show by a variety of general experimental findings that the dispersion of the structural α-relaxation plays a fundamental role in governing the dynamic and kinetic properties of the α-relaxation. The most direct evidence comes from a recently discovered general experimental property of glass-formers: For a given material at a fixed value of τ_α, the dispersion of the structural relaxation is constant, independent of thermodynamic conditions (T and P); that is, the shape of the α-relaxation function depends only on the relaxation time. If the dispersion of the structural relaxation is derived independently of τ_α, it is an unlikely that it would be uniquely defined by τ_α. Most conventional theories and models of the glass transition either do not address the dispersion or derive it independently of τ_α; hence, they are in need of revision. We point out that the dispersion of the α-relaxation originates from the

dynamically heterogeneous many-molecule dynamics. Thus, a profitable way to revise conventional theories and models of glass transition is the incorporation of many-molecule dynamics, or at least the effects they have on the α-relaxation. The current trend of research in glass transition is in systems more complicated than bulk materials. Examples are nanoconfined glass-formers with the presence of surfaces or interfaces and miscible mixtures of two glass-formers. The tendency in these research communities is to take over the conventional theories of glass transition and apply them to these more complicated cases. Success in explaining the new phenomena is doubtful because of the conventional theories applied are already inadequate even for the simpler case of neat bulk materials.

Although glass transition is conventionally defined by the thermodynamics and kinetic properties of the structural α-relaxation, a fundamental role is played by its precursor, the Johari–Goldstein (JG) secondary relaxation. The JG relaxation time, τ_{JG}, like the dispersion of the α-relaxation, is invariant to changes in the temperature and pressure combinations while keeping τ_α constant in the equilibrium liquid state of a glass-former. For any fixed τ_α, the ratio, τ_{JG}/τ_α, is exclusively determined by the dispersion of the α-relaxation or by the fractional exponent, $1-n$, of the Kohlrausch function that fits the dispersion. There is remarkable similarity in properties between the JG relaxation time and the α-relaxation time. Conventional theories and models of glass transition do not account for these nontrivial connections between the JG relaxation and the α-relaxation. For completeness, these theories and models have to be extended to address the JG relaxation and its remarkable properties.

The Coupling Model (CM) is an exception. It recognizes the importance of many-molecule dynamics that give rise to as well as govern the α-relaxation and its dispersion. In addition, it recognizes the need to consider the faster primitive or independent relaxation from which the many-molecule dynamics are built. Although by no means a solution of the problem of many-molecule relaxation, it finds a physical principle that makes a quantitative relation between τ_α and the primitive relaxation time τ_0 given by $\tau_\alpha = [t_c^{-n}\tau_0]^{1/(1-n)}$. The relation involves the dispersion of the α-relaxation or its measure by the Kohlrausch exponent, $1-n$. An immediate consequences of this defining relation of the CM is that the dispersion of the α-relaxation does govern τ_α. As a tool, this relation has been used to explain many anomalous properties of τ_α from the normal properties of τ_0. This relation also implies that τ_0 has properties similar to that of τ_α, although the latter is more prominent because of the nonlinear exponent, $1/(1-n)$, in the relation. A further development of the CM is the recognition that the primitive relaxation time should correspond well to the JG relaxation time, *i.e.*, $\tau_0 \approx \tau_{JG}$. This expected correspondence has been verified for many different kinds of glass-formers, and the favorable results can be considered as a positive

reality check of the primitive relaxation. The observed similarity in properties of the JG relaxation to the α-relaxation is immediately explained by that of the primitive relaxation and the CM relation. We have emphasized in this chapter the importance of the recent general experimental findings that the dispersion of the α-relaxation is invariant to different combinations of T and P at constant τ_α. This property can be derived from the CM. In spite of the many accomplishments of the CM, it has not solved the many-molecule relaxation problem and should not be considered to be a solution of the glass transition problem. These problems are too complex to be solved rigorously for some time to come. Based on the CM, a pragmatic and schematic theory can be constructed to fill this void, providing a shortcut to reach the anomalous properties discussed in this chapter, which would otherwise remain unexplained. This schematic theory may be used as a stepping stone to reach a final solution of the problem.

Acknowledgments

The authors thanks all their collaborators in the works cited in this chapter. The work at the Naval Research Laboratory was supported by the Office of Naval Research, the work at the Università di Pisa was supported by I.N.F.M. and by MIUR (Cofin2002), and the work at Silesian University was supported by the Polish Committee for Scientific Research (KBN) (Project 2005–2007; No 1PO3B 075 28).

References

1. C. A. Angell, K. L. Ngai, G. B. McKenna, P. F. McMillan, and S. W. Martin, *J. Appl. Phys.* **88**, 3113 (2000).
2. K. L. Ngai, *J. Non-Cryst. Solids* **275**, 7 (2000).
3. H. Vogel, *Phys. Z*. **222**, 645 (1921).
4. G. S. Fulcher, *J. Am. Ceram. Soc.* **8**, 339 (1923).
5. V. G. Tammann and W. Hesse, *Z. Anorg. Allg. Chem.* **156**, 245 (1926).
6. J. D. Ferry, *Viscoelastic Properties of Polymers*, 3rd ed., John Wiley & Sons, New York, 1980.
7. A. K. Doolittle and D. B. Doolittle, *J. Appl. Phys.* **28**, 901 (1957).
8. G. Adam and J. H. Gibbs, *J. Chem. Phys.* **43**, 139 (1965).
9. G. Dlubek, J. Wawryszczuk, J. Pionteck, T. Gowrek, H. Kaspar, and K. H. Lochhass, *Macromolecules* **38**, 429 (2005).
10. R. Casalini, S. Capaccioli, M. Lucchesi, P. A. Rolla, and S. Corezzi, *Phys. Rev. E* **63**, 031207 (2001).
11. R. Casalini, S. Capaccioli, M. Lucchesi, P. A. Rolla, M. Paluch, S. Corezzi, and D. Fioretto, *Phys. Rev. E* **64**, 041504 (2001).
12. R. Casalini, M. Paluch, J. J. Fontanella, and C. M. Roland, *J. Chem. Phys.* **117**, 4901 (2002).
13. G. P. Johari, *J. Chem. Phys.* **119**, 635 (2003).
14. D. Prevosto, M. Lucchesi , S. Capaccioli, R. Casalini, P. A. Rolla , *Phys. Rev. B* **67**, 174202 (2003).

15. M. Goldstein, *Phys. Rev. B* **71**, 136201 (2005).
16. D. Prevosto, M. Lucchesi, S. Capaccioli, P. A. Rolla, and R. Casalini, *Phys. Rev. B* **71**, 136202 (2005).
17. G. P. Johari and M. Goldstein, *J. Chem. Phys.* **53**, 2372 (1970).
18. G. P. Johari, *J. Chem. Phys.* **58**, 1766 (1973).
19. G. P. Johari, *Ann. N.Y. Acad. Sci.* **279**, 117 (1976).
20. G. P. Johari, *J. Non-Cryst. Solids* **307–310**, 317 (2002).
21. K. L. Ngai, *Comments Solid State Phys.* **9**, 141 (1979).
22. K. L. Ngai, in *Disorder Effects on Relaxational Processes*, R. Richert and A. Blumen, eds., Springer-Verlag, Berlin, 1994, pp. 89–150.
23. K. L. Ngai and K. Y. Tsang, *Phys. Rev. E* **60**, 4511 (1999).
24. K. L. Ngai, and R. W. Rendell, in *Supercooled Liquids, Advances and Novel Applications*; J. T. Fourkas, D. Kivelson, U. Mohanty, and K. Nelson, eds., ACS Symposium Series Vol. 676, American Chemical Society, Washington, DC, 1997, Chapter 4, p. 45.
25. K. L. Ngai, D. J. Plazek, and R. W. Rendell, *Rheol. Acta* **36**, 307 (1997).
26. K. L. Ngai, *IEEE Trans. Dielectr. Electr. Insul.* **8**, 329 (2001).
27. K. Schmidt-Rohr and H. W. Spiess, *Phys. Rev. Lett.* **66**, 3020 (1991).
28. A. Heuer, M. Wilhelm, H. Zimmermann, and H. W. Spiess, *Phys. Rev. Lett.* **75**, 2851 (1997).
29. R. Böhmer, R. V. Chamberlin, G. Diezemann, B. Geil, A. Heuer, G. Hinze, S. C. Kuebler, R. Richert, B. Schiener, H. Sillescu, H. W. Spiess, U. Tracht, and M. Wilhelm, *J. Non-Cryst. Solids* **235–237**, 1 (1998).
30. R. Kohlrausch, *Pogg. Ann. Phys.* **12**(**3**), 393 (1847).
31. G. Williams, D. C. Watts, *Trans. Faraday Soc.* **66**, 80 (1970).
32. K. L. Ngai, *J. Chem. Phys.* **109**, 6982 (1998).
33. K. L. Ngai, *Macromolecules* **32**, 7140 (1999).
34. K. L. Ngai and S. Capaccioli, *Phys. Rev. E* **69** 031501(2004).
35. C. M. Roland, M. J. Schroeder, J. J. Fontanella, and K. L. Ngai, *Macromolecules* **37** 2630 (2004).
36. K. L. Ngai, *J. Phys.: Condens. Matter* **15**, S1107 (2003).
37. K. L. Ngai, in *AIP Conference Proceedings*, Vol. 708, American Institute of Physics, Melville, NY, 2004, p. 515.
38. K. L. Ngai and M. Paluch, *J. Chem. Phys.* **120**, 857(2004).
39. K. L. Ngai, P. Lunkenheimer, C. Leon, U. Schneider, R. Brand, and A. Loidl, *J. Chem. Phys.* **115**, 1405 (2001).
40. M. Paluch, K. L. Ngai, and S. Hensel-Bielowka, *J. Chem. Phys.* **114**, 10872 (2001).
41. K. L. Ngai and M. Beiner, *Macromolecules* **37**, 8123 (2004).
42. V. Y. Kramarenko, T. A. Ezquerra, and V. P. Privalko, *Phys. Rev. E* **64**, 051802 (2001).
43. A. Sanz, A. Nogales, and T. Ezquerra, paper presented at the 5th International Discussion Meeting on Relaxation in Complex Systems, July 7–13, 2005 and to be published.
44. S. Hensel-Bielówka, M. Paluch, and K. L. Ngai, *J. Chem. Phys.* **123**, 014502 (2005).
45. R. Böhmer, K. L. Ngai, C. A. Angell, and D. J. Plazek, *J. Chem. Phys.* **99**, 4201 (1993).
46. K. L. Ngai and C. M. Roland, *Macromolecules* **26**, 6824 (1993).
47. F. Stickel, E. W. Fischer, and R. Richert, *J. Chem. Phys.* **104**, 2043(1996).

48. R. Casalini, K. L. Ngai, and C. M. Roland, *Phys. Rev. B* **68**, 014201(2003).
49. K. L. Ngai and C. M. Roland, *Polymer* **43**, 567 (2002).
50. J. Colmenero, A. Alegria, P. G. Santangelo, K. L. Ngai, and C. M. Roland, *Macromolecules* **27**, 407 (1994).
51. G. Williams, *Trans. Faraday Soc.* **62**, 2091(1966).
52. G. Williams and D. A. Edwards, *Trans. Faraday Soc.* **62**, 1329 (1966).
53. G. Williams, *Trans. Faraday Soc.* **61**, 1564 (1965).
54. G. Williams, *Trans. Faraday Soc.* **60**, 1548 (1964).
55. H. Sasabe and S. Saito, *J. Polym. Sci. Polym. Phys. Ed.* **6**, 1401(1968).
56. H. Sasabe, S. Saito, M. Asahina, and H. Kakutani, *J. Polym. Sci., Polym. Phys. Ed.* **7**, 1405 (1969).
57. G. Williams and D. C. Watts, *Trans. Faraday Soc.* **67**, 2793 (1971).
58. G. P. Johari, E. Whalley, *Faraday Symp. Chem. Soc.* **6**, 23 (1972).
59. H. Sasabe and S. Saito, *Polym. J. (Tokyo)* **3**, 624 (1972).
60. G. Williams, *Adv. Polym. Sci.* **33**, 60 (1979).
61. G. Floudas, *Prog. Polym. Sci.* **29**, 1143 (2004).
62. C. M. Roland, R. Casalini, S. Hensel-Bielowka, and M. Paluch, *Rep. Prog. Phys.* **68**, 1405 (2005).
63. G. Floudas and T. Reisinger, *J. Chem. Phys.* **111**, 5201(1999).
64. S. P. Andersson and O. Andersson, *Macromolecules* **31**, 2999 (1998).
65. G. Floudas, C. Gravalides, T. Reisinger, and G. Wegner, *J. Chem. Phys.* **111**, 9847 (1999).
66. G. Floudas, G. Fytas, T. Reisinger, and G. Wegner, *J. Chem. Phys.* **111**, 9129 (1999).
67. J. Köplinger, G. Kasper, and S. Hunklinger, *J. Chem. Phys.* **113**, 4701 (2000).
68. A. Reiser, G. Kasper, and S. Hunklinger, *Phys. Rev. Lett.* **92**, 125701 (2004).
69. A. Alegría, D. Gómez, and J. Colmenero, *Macromolecules* **35**, 2030 (2002).
70. P. Papadopoulos, D. Peristeraki, G. Floudas, G. Koutalas, and N. Hadjichristidis, *Macromolecules* **37**, 8116 (2004).
71. R. Casalini, M. Paluch, and C. M. Roland, *J. Chem. Phys.* **118**, 5701 (2003).
72. S. Pawlus, R. Casalini, C. M. Roland, M. Paluch, S. J. Rzoska, and J. Ziolo, *Phys. Rev. E* **70**, 061501 (2004).
73. R. Casalini, M. Paluch, and C. M. Roland, *J. Phys. Chem. A* **107**, 2369 (2003).
74. R. Casalini, M. Paluch, and C. M. Roland, *Phys. Rev. E* **67**, 031505 (2003).
75. S. Hensel-Bielowka, J. Ziolo, M. Paluch, and C. M. Roland, *J. Chem. Phys.* **117**, 2317(2002).
76. S. Pawlus, M. Paluch, M. Sekula, K. L. Ngai, S. J. Rzoska, and J. Ziolo, *Phys. Rev. E*, **68**, 021503 (2003).
77. M. Sekula, S. Pawlus, S. Hensel-Bielowka, J. Ziolo, M. Paluch, and C. M. Roland, *J. Phys. Chem. B* **108**, 4997 (2004).
78. K. L. Ngai, E. Kaminska, M. Sekula, and M. Paluch, unpublished.
79. M. Paluch, S. Pawlus, S. Hensel-Bielowka, E. Kaminska, D. Prevosto, S. Capaccioli, P. A. Rolla, and K. L. Ngai, *J. Chem. Phys.* **122**, 234506 (2005).
80. S. Capaccioli, D. Prevosto, M. Lucchesi, P. A. Rolla, R. Casalini, and K. L. Ngai, *J. Non-Cryst. Solids* **351**, 2643 (2005).
81. S. Capaccioli, R. Casalini, D. Prevosto, and P. A. Rolla, unpublished.

82. S. Corezzi, P. A. Rolla, M. Paluch, J. Ziolo, and D. Fioretto, *Phys. Rev. E* **60**, 4444 (1999).
83. T. Psurek, J. Ziolo, and M. Paluch, *Physica A* **331**, 353 (2004).
84. R. Casalini, T. Psurek, M. Paluch, and C. M. Roland, *J. Mol. Liq.* **111**, 53 (2004).
85. T. Psurek, S. Hensel-Bielowka, J. Ziolo, and M. Paluch, *J. Chem. Phys.* **116**, 9882 (2002).
86. S. Hensel-Bielowka, T. Psurek, J. Ziolo, and M. Paluch, *Phys. Rev. E* **63**, 62301 (2001).
87. R. Casalini and C. M. Roland, *J. Chem. Phys.* **119**, 4052 (2003).
88. W. Heinrich and B. Stoll, *Colloid Polym. Sci.* **263**, 873 (1985).
89. S. H. Zhang, R. Casalini, J. Runt, and C. M. Roland, *Macromolecules* **36**, 9917 (2003).
90. M. Paluch, S. Pawlus, and C. M. Roland, *J. Chem. Phys.* **116**, 10932 (2002).
91. M. Paluch, S. Pawlus, and C. M. Roland, *Macromolecules* **35**, 7338 (2002).
92. C. M. Roland, R. Casalini, P. Santangelo, M. Sekula, J. Ziolo, and M. Paluch, *Macromolecules* **36**, 4954 (2003).
93. M. Paluch, S. Hensel-Bielowka, and J. Ziolo, *Phys. Rev. E* **61**, 526 (2000).
94. C. M. Roland, R.Casalini, and M. Paluch, *J. Polym. Sci. Polym. Phys. Ed.* **42**, 4313 (2004).
95. C. M. Roland, T. Psurek, S. Pawlus, and M. Paluch, *J. Polym. Sci.: Polym. Phys.* **41**, 3047 (2003).
96. R. Casalini and C. M. Roland, *Macromolecules* **38**, 1779 (2005).
97. C. M. Roland, R. Casalini, and M. Paluch, *Chem. Phys. Lett.* **367**, 259 (2003).
98. C. M. Roland, M. Paluch, and S. J. Rzoska, *J. Chem. Phys.* **119**, 12439 (2003).
99. K. L. Ngai, R. Casalini, S. Capaccioli, M. Paluch, and C. M. Roland, *J. Phys. Chem. B*, in press.
100. U. Schneider, R. Brand, P. Lunkenheimer, and A. Loidl, *Phys. Rev. Lett.* **84**, 5560 (2000).
101. R. Casalini and C. M. Roland, *Phys. Rev. Lett.* **91**, 15702 (2003).
102. R. Casalini and C. M. Roland, *Phys. Rev. B* **69**, 094202 (2004).
103. C. Svanberg, R. Bergman, and P. Jacobsson, *Europhys. Lett.* **64**, 358 (2003).
104. G. P. Johari and M. Goldstein *J. Chem. Phys.* **55**, 4245 (1971).
105. M. Naoki and M. Matsushita, *Bull. Chem. Soc. Jpn.* **56**, 2396 (1983).
106. M. Naoki, H. Endou, and K. Matsumoto, *J. Phys. Chem.* **91**, 4169 (1987).
107. M. Masuko, A. Suzuki, S. Hanai, and H. Okabe, *Jpn. J. Tribol.* **42**, 455 (1997).
108. A. Suzuki, M. Masuko, T. Nakayama, and H. Okabe, *Jpn. J. of Tribol.* **42**, 467 (1997).
109. A. Suzuki, M. Masuko, and T. Nikkuni, *Tribol. Int.* **33**, 107 (2000).
110. G. Williams in *Dielectric Spectroscopy of Polymeric Materials*, J. P. Runt and J. J. Fitzgerald, eds., American Chemical Society, Washington, DC, 1997.
111. K. Mpoukouvalas, G. Floudas, B. Verdonck, and F. E. Du Prez, *Phys. Rev. E* **72**, 011802 (2005).
112. P. K. Dixon, *Phys. Rev. B* **42**, 8179 (1990).
113. M. Paluch, R. Casalini, S. Hensel-Bielowka, and C. M. Roland, *J. Chem. Phys.* **116**, 9839 (2002).
114. R. Casalini and C. M. Roland, *Phys. Rev. E* **69**, 062501 (2004).
115. R. Casalini and C. M. Roland, *Coll. Polym. Sci.* **283**, 107 (2004).
116. G. Fytas, G. Meier, T. Dorfmuller, and A. Patkowski, *Macromolecules* **15**, 214 (1982).
117. G. Fytas, A. Patkowski, G. Meier, and T. Dorfmuller, *Macromolecules* **15**, 874 (1982).
118. G. Fytas, A. Patkowski, G. Meier, and T. Dorfmuller, *J. Chem. Phys.* **80**, 2214 (1980).
119. G. D. Patterson, J. R. Stevens, and P. J. Carroll, *J. Chem. Phys.* **77**, 622 (1980).

120. S. W. Smith, B. D. Freeman, and C. K. Hall, *Macromolecules* **30**, 2052 (1997).
121. G. Fytas, T. Dorfmuller, and C. H. Wang, *J. Phys. Chem.* **87**, 5041 (1983).
122. Y.-H. Hwang and G. Q Shen, *J. Phys.: Condens. Matter* **11**, 1453 (1999).
123. H. Leyser, A. Schulte, W. Doster, and W. Petry, *Phys. Rev. E* **51**, 5899 (1995).
124. A. Tölle, *Rep. Prog. Phys.* **64**, 1473 (2001).
125. L. Comez, D. Fioretto, H. Kriegs, and W. Steffen, *Phys. Rev. E* **66**, 032501 (2002).
126. L. Comez, S. Corezzi, D. Fioretto, H. Kiegs, A. Best, and W. Steffen, *Phys. Rev. E* **70**, 011504 (2004).
127. D. L. Sidebottom and C. M. Sorensen, *Phys. Rev. B* **40**, 461 (1988).
128. T. Berger, Ph.D. thesis, Max Planck Institute for Polymer Research, Mainz, Germany, 1996.
129. M. Paluch, C. M. Roland, J. Gapinski, and A. Patkowski, *J. Chem. Phys.* **118**, 3177 (2003).
130. M. Paluch, A. Patkowski, and E.W. Fischer, *Phys. Rev. Lett.* **85**, 2140 (2000).
131. M. Paluch, J. Gapinski, A. Patkowski, and E. W. Fischer, *J. Chem. Phys.* **114**, 8048 (2001).
132. A. Patkowski, M. Paluch, and H. Kriegs, *J. Chem. Phys.* **117**, 2192 (2002).
133. M. Paluch, R. Casalini, A. Best, and A. Patkowski, *J. Chem. Phys.* **117**, 7624 (2002).
134. A. Patkowski, J. Gapinski, and G. Meier, *Colloid Polym. Sci.* **282**, 874 (2004).
135. J. Gapinski, M. Paluch, and A. Patkowski, *Phys. Rev. E* **66**, 011501 (2002).
136. K. L. Ngai and S. Capaccioli, *J. Phys. Chem. B* **108**, 11118 (2004).
137. D. J. Plazek and K. L. Ngai, *Macromolecules* **24**, 1222 (1991).
138. C. M. Roland and K. L. Ngai, *Macromolecules* **24**, 5315 (1991); **25**, 1844 (1992).
139. C. M. Roland, *Macromolecules* **25**, 7031 (1992).
140. K. L. Ngai and O. Yamamuro, *J. Chem. Phys.* **111**, 10403 (1999).
141. R. Casalini and C. M. Roland, *Phys. Rev. B*, **71**, 014210 (2005).
142. K. L. Ngai, J. Colmenero, A. Arbe, and A. Alegria, *Macromolecules* **25**, 6727 (1992).
143. R. Zorn, A. Arbe, J. Colmenero, B. Frick, D. Richter, and U. Buchenau, *Phys. Rev. E* **52**, 781 (1995).
144. D. Richter, A. Arbe, J. Colmenero, M. Monkenbusch, B. Farago, and R. Faust, *Macromolecules* **31**, 1133 (1998).
145. B. Farago, A. Arbe, J. Colmenero, R. Faust, U. Buchenau, and D. Richter, *Phys. Rev. E* **65**, 051803 (2002).
146. J. Colmenero, F. Alvarez, and A. Arbe, *Phys. Rev. E* **65**, 041804 (2002).
147. A. Arbe, D. Richter, J. Colmenero, and B. Farago, *Phys. Rev. E* **54**, 3853 (1996).
148. A. Arbe, D. Richter, J. Colmenero, and B. Farago, *Physica B* **234–236**, 437 (1997).
149. B. Frick, G. Dosseh, A. Cailliaux, C. Alba-Simionesco, *Chem. Phys.* **292**, 311 (2003).
150. A. Neelakantan and J. K. Maranas, *J. Chem. Phys.* **120**, 465 (2004).
151. J. Colmenero, F. Alvarez, and A. Arbe, *Phys. Rev. E* **65**, 041804 (2002).
152. P. N. Segre and P. N. Pusey, *Phys. Rev. Lett. 77*, 771 (1996).
153. S. Z. Ren, W. F. Shi, W. B. Zhang, and C. M. Sorensen, *Phys. Rev. A* **45**, 2416 (1992).
154. G. D. J. Phillies, C. Richardson, C. A. Quinlan, and S. Z. Ren, *Macromolecules* **26**, 6849 (1993).
155. K. L. Ngai and G. D. J. Phillies, *J. Chem. Phys.* **105**, 8385 (1996).
156. B. Nyström, H. Walderhaug, and F. N. Hansen, *J. Phys. Chem.* **97**, 7743 (1993).
157. K. L. Ngai, *Adv. Colloid Interface Sci.* **64**, 1 (1996).

158. M. Adam, M. Delasanti, J. P. Munch, and D. Durand, *Phys. Rev. Lett.* **61**, 706 (1988).
159. F. Stickel, E.W. Fischer, and R. Richert, *J. Chem. Phys.* **102**, 6251 (1995).
160. K. L. Ngai, J. H. Magill, and D. J. Plazek, *J. Chem. Phys.* **112**, 1887 (2000).
161. C. Leon and K. L. Ngai, *J. Phys. Chem. B*, **103**, 4045 (1999),
162. K. L. Ngai, *J. Phys. Chem. B*, **103**, 5895 (1999).
163. K. L. Ngai, *J. Chem. Phys.* **111**, 3639 (1999).
164. K. L. Ngai, L-R Bao, A. F. Yee, and C. L. Soles, *Phys. Rev. Lett.* **87**, 215901 (2001).
165. R. Casalini, M. Paluch, and C. M. Roland *J. Chem. Phys.* **118**, 5701 (2003).
166. R. Casalini, M. Paluch, and C. M. Roland *J. Phys. Cond. Matter* **15**, S859 (2003).
167. F. Fujara, B. Geil, H. Sillescu, and G. Fleischer, *Z. Phys. B* **88**, 195 (1992).
168. M. T. Cicerone, F. R. Blackburn, and M. D. Ediger, *J. Chem. Phys.* **102**, 471 (1995).
169. M. T. Cicerone and M. D. Ediger, *J. Chem. Phys.* **104**, 7210 (1996).
170. F. R. Blackburn, C.-Y. Wang, and M. D. Ediger, *J. Phys. Chem.* **100**, 18249 (1996).
171. M. D. Ediger, *J. Non-Cryst. Solids*, **235–237**, 10 (1998).
172. K. L. Ngai, *J. Phys. Chem.* **103**, 10684 (1999).
173. J. H. Magill and H.-M. Li, *J. Cryst. Growth* **20**, 135 (1973).
174. J. H. Magill and D. J. Plazek, *J. Chem. Phys.* **46**, 3757 (1967).
175. D. J. Plazek and J. H. Magill, *J. Chem. Phys.* **45**, 3038 (1966).
176. J. H. Magill and D. J. Plazek, *Nature* **209**, 70 (1966).
177. D. J. Plazek and J. H. Magill, J. Chem. Phys. **49**, 3678 (1968).
178. S. F. Swallen, P. A. Bonvallet, R. J. McMahon, and M. D. Ediger, *Phys. Rev. Lett.* **90**, 015901 (2003).
179. M. D. Ediger, *Annu. Rev. Phys. Chem.* **51**, 99 (2000).
180. R. Richert, K. Duvvuri, and L.-T. Duong, *J. Chem. Phys.* **118**, 1828 (2003).
181. G. B. McKenna, K. L. Ngai, and D. J. Plazek, *Polymer* **26**, 1651 (1985).
182. K. L. Ngai, S. Mashimo and G. Fytas, *Macromolecules* **21**, 3030 (1988).
183. I. Chang and H. Sillescu, *J. Phys. Chem.* **101**, 8794 (1997).
184. L. Comez, D. Fioretto, L. Palmieri, L. Verdini, P. A. Rolla, J. Gapinski, A. Patkowski, W. Steffen, and E. W. Fischer *Phys. Rev. E* **60**, 3086 (1999).
185. R. J. Roe, *J. Chem. Phys.* **94**, 7446 (1992).
186. R. J. Roe, *J. Chem. Phys.* **100** 1610 (1994).
187. K. L. Ngai, *Philos. Mag. B* **79**, 1793 (1999).
188. S. A. Reinsberg, A. Heuer, B. Doliwa, H. Zimmermann, and H. W. Spiess, *J. Non-Cryst. Solids*, **307–310**, 208 (2002).
189. K. L. Ngai and D. J. Plazek, *Rubber Chem. Tech. Rubber Revs.* **68**, 376 (1995).
190. D. J. Plazek, X. D. Zheng, and K. L. Ngai, *Macromolecules* **25**, 4920 (1992).
191. K. L. Ngai, D. J. Plazek, and C. Bero, *Macromolecules* **26**, 1065 (1993).
192. K. L. Ngai, D. J. Plazek, and A. K. Rizos, *J. Polym. Sci. Part B Polym. Phys.* **35**, 599 (1997).
193. D. J. Plazek, *J. Rheol.* **40**(**6**), 987 (1996).
194. J. Y. Cavaille, C. Jordan, J. Perez, L. Monnerie, and G. P. Johari, *J. Polym. Sci.: Part B, Polym. Phys.* **25**, 1235 (1987).
195. R. Zorn, G. B. McKenna, L. Wilner, and D. Richter, *Macromolecules* **28**, 8552 (1995).

196. L. I. Palade, V. Verney, and P. Attené, *Macromolecules* **28**, 7051 (1995).
197. R. W. Gray, G. Harrison, and J. Lamb, *Proc. R. Soc. London Ser. A* **356**, 77 (1977).
198. J. Cochrane, G. Harrison, J. Lamb, and D. W. Phillips, *Polymer* **21**, 837 (1980).
199. D. J. Plazek, C. Bero, S. Neumeister, G. Floudas, and G. Fytas, *Colloid Polym. Sci.* **272**, 1430 (1994).
200. G. Fytas and K. L. Ngai, *Macromolecules* **21**, 804 (1988).
201. G. Fytas, G. Floudas, and K. L. Ngai, *Macromolecules* **23**, 1104 (1990).
202. K. L. Ngai, A. Schönhals, and E. Schlosser, *Macromolecules* **25**, 4915 (1992).
203. D. J. Plazek, A. Schönhals, E. Schlosser, and K. L. Ngai, *J. Chem. Phys.* **98**, 6488 (1993).
204. K. L. Ngai and D. J. Plazek, *Macromolecules* **35**, 9136 (2002).
205. C. M. Roland, K. L. Ngai, and D. J. Plazek, *Macromolecules* **37**, 7051 (2004).
206. C. M. Roland, K. L. Ngai, P. G. Santangelo, X. H. Qiu, M. D. Ediger, and D. J. Plazek, *Macromolecules* **34**, 6159 (2001).
207. K. L. Ngai, R. Casalini, and C. M. Roland, *Macromolecules* **38**, 4363 (2005).
208. K. L. Ngai, Chapter in *Physical Properties of Polymers*, Cambridge University Press, Cambridge, England, 2004.
209. C. G. Robertson and C. M. Rademacher, *Macromolecules* **37**, 10009 (2004).
210. C. P. Linsay and G. D. Patterson *J. Chem. Phys.* **73**, 3348 (1980).
211. A. K. Rizos, T. Jian, and K. L. Ngai, *Macromolecules* **28**, 517 (1995).
212. K. L. Ngai and J. Habasaki, to be published. For ionic relaxation, see J. Habasaki, K. L. Ngai and Y. Hiwatari, *Phys. Rev. E* **66**, 021205 (2002); *J. Chem. Phys.* **122**, 054507 (2005).
213. E. R. Weeks, J. C. Crocker, A. Levitt, A. Schofield, and D. A. Weitz, *Science* **287**, 627 (2000).
214. N. G. McCrum, B. E. Read, and G. Williams, *Anelastic and Dielectric Effects in Polymeric Solids*, John Wiley & Sons, London, 1967 and Dover Publications, New York, 1991.
215. K. Pathmanathan and G. P. Johari, *J. Phys. C* **18**, 6535 (1985).
216. R. Brand, P. Lunkenheimer, and A. Loidl, *J. Chem. Phys.* **116**, 10386 (2002).
217. C. Mai, S. Etienne, J. Perez, and G. P. Johari, *J. Non-Cryst. Solids* **74**, 119 (1985).
218. C. Mai, S. Etienne, J. Perez, and G. P. Johari, *Philos. Mag. B* **50**, 657 (1985).
219. H. S. Chen and N. Morito, *J. Non-Cryst. Sol.* **72**, 287 (1985).
220. H. Okumura, H. S. Chen, A. Inoue, and T. Masumoto, *J. Non-Cryst. Sol.* **130**, 401 (1991).
221. H. Okumura, H. S. Chen, A. Inoue, and T. Masumoto, *J. Non-Cryst. Sol.* **150**, 401 (1992).
222. J. M. Pelletier, B. Van de Moortele, and I. R. Lu, *Mater. Sci. Eng.* **A336**, 190 (2002).
223. P. Rösner, K. Samwer, and P. Lunkenheimer, *Europhys. Lett.* **68**, 226 (2004).
224. K. Schmidt-Rohr and H. W. Spiess, *Phys. Rev. Lett.* **66**, 3020 (1991).
225. A. Heuer, M. Wilhelm, H. Zimmermann, and H.W. Spiess, *Phys. Rev. Lett.* **75**, 2851 (1997).
226. H. Sillescu, R. Böhmer, G. Diezemann, G. Hinze, *J. Non-Cryst. Solids* **307–310**, 16 (2002).
227. M. Vogel, C. Tschirwitz, G. Schneider, C. Koplin, and P. Medick, *J. Non-Cryst. Solids* **307–310**, 326 (2002).
228. S. Maślanka, M. Paluch, W. W. Sulkowski, and C. M. Roland, *J. Chem. Phys.* **122**, 084511 (2005).
229. K. L. Ngai, E. Kamińska, M. Sekula, and M. Paluch, submitted to *J. Chem. Phys.*
230. G. Meier, B. Gerharz, D. Boese, and E. W. Fischer, *J. Chem. Phys.* **94**, 3050 (1991).

231. D. Morineau, C. Alba-Simionesco, M. C. Bellisent-Funel, and M. F. Lauthie, *Europhys. Lett.*, **43**, 195 (1998).
232. D. Morineau and C. Alba-Simionesco, *J. Chem. Phys.* **109**, 8494 (1998).
233. H. Wagner and R. Richert, *J. Phys. Chem. B* **103**, 4071 (1999).
234. T. Fujima, H. Frusawa, and K. Ito, *Phys. Rev. E* **66**, 031503 (2002).
235. R. Nozaki, H. Zenitani, A. Minoguchi, and K. Kitai, *J. Non-Cryst. Solids* **307–310**, 349 (2002).
236. T. Fujima, H. Fruzawa, and K. Ito, *Phys. Rev. E* **66**, 031503 (2002).
237. A. Arbe, J. Colmenero, D. Richter, J. Gomez, and B. Farago, *Phys. Rev. Lett.* **60**, 1103 (1999).
238. G. Williams, *Adv. Polym. Sci.* **33**, 59 (1979).
239. M. Paluch, C. M. Roland, S. Pawlus, J. Ziolo, and K. L. Ngai, *Phys. Rev. Lett.* **91**, 115701 (2003).
240. D. Prevosto, S. Capaccioli, M. Lucchesi, P. A. Rolla, and K. L. Ngai, *J. Chem. Phys.*, **120**, 4808 (2004).
241. T. Blochowicz and E. A. Rössler, *Phys. Rev. Lett.* **92**, 225701 (2004).
242. T. Blochowicz, *Broadband Dielectric Spectroscopy in Neat and Binary Molecular Glass Formers*, ISBN 3-8325-0320-X, Logos Verlag, Berlin, 2003.
243. G. P. Johari, *J. Chem. Phys.* **77**, 4619 (1982).
244. P. Lunkenheimer, R. Wren, U. Schneider, and A. Loidl, *Phys. Rev. Lett.* **95**, 055702 (2005).
245. N. B. Olsen, *J. Non-Cryst. Solids* **235–237**, 99 (1998).
246. P. Lunkenheimer, R. Wehn, T. Riegger, and A. Loidl *J. Non-Cryst. Solids* **307**, 336 (2002).
247. B. Olsen, private communication.
248. J. C. Dyre and B. N. Olsen, *Phys. Rev. Lett.* **91**, 155703 (2003).
249. M. Paluch, unpublished.
250. G. P. Johari, G. Power, and J. K. Vij, *J. Chem. Phys.* **116**, 5908 (2002).
251. G. P. Johari, G. Power, and J. K. Vij, *J. Chem. Phys.* **117**, 1714 (2002).
252. G. Power, G. P. Johari, and J. K. Vij, *J. Chem. Phys.* **119**, 435 (2003).
253. R. Casalini, D. Fioretto, A. Livi, M. Lucchesi, and P. A. Rolla, *Phys. Rev. B* **56**, 3016 (1997).
254. A. L. Lichtenberg and M. A. Lieberman, *Regular and Chaotic Dynamics*, Springer, New York, 1992.
255. See, for example, the review by P.G. Debenedetti and F. H. Stillinger, *Nature*, **410**, 259 (2001). P. G. Debenedetti, *Metastable Liquids, Concepts and Principles*, Princeton University Press, Princeton, NJ, 1996.
256. K. L. Ngai, *Comment Solid State Phys.*, **9**, 127 (1979).
257. K. L. Ngai, *Comment Solid State Phys.*, **9**, 141 (1979).
258. K. L. Ngai and C. T. White, *Phys. Rev. B* **20**, 2475 (1979).
259. K. L. Ngai, A. K. Jonscher, and C. T. White, *Nature* **277**, 185 (1979).
260. K. Y. Tsang and K. L. Ngai, *Phys. Rev. E*, **54**, R3067 (1997).
261. K. Y. Tsang and K. L. Ngai, *Phys. Rev. E*, **56**, R17 (1997).
262. K. L. Ngai and K. Y. Tsang, *Phys. Rev. E*, **60**, 4511 (1999).
263. M. Pettini and M. Landolfi, *Phys. Rev. A*, **41**, 768 (1990).
264. R. Mannella and L. Fronzoni, *Phys. Rev. A*, **43**, 5261 (1990).
265. S. H. Strogatz, R. Mirollo, and P. C. Matthews, *Phys. Rev. Lett.* **68**, 2730 (1992).
266. A. Bikaki, N. K. Voulgarakis, S. Aubry, and G. P. Tsironis, *Phys. Rev. E* **59**, 1234 (1999).

267. F. Gobet, S. Ciliberto, and T. Dauxois, *Eur. Phys. J. B*, **34**, 193 (2003).
268. F. Piazza, S. Lepri, and R. Livi, *Chaos*, **13**, 637 (2003).
269. C. K. Hall and E. Helfand, *J. Chem. Phys.*, **77**, 3275 (1982).
270. K. L. Ngai and R. W. Rendell, *J. Non-Cryst. Solids* **131–133**, 942 (1991).
271. J. Colmenero, A. Arbe, G. Coddens, B. Frick, C. Mijangos, and H. Reinecke, *Phys. Rev. Lett.*, **78**, 1928(1997).
272. G. D. Smith, D. Y. Yoon, A. Zirkel, J. Hendricks, D. Richter, and H. Schober, *J. Chem. Phys.* **107**, 4751(1997).
273. J. Colmenero, F. Alvarez, and A. Arbe, *Phys. Rev. E*, **65**, 041804 (2002).
274. L. J. Lewis and G. Wahnström, *Phys. Rev. E*, **50**, 3865 (1994).
275. C. M. Roland, K. L. Ngai, and L. Lewis, *J. Chem. Phys.* **103**, 4632 (1995).
276. K. L. Ngai, J. Habasaki, C. León, and A. Rivera, *Z. Phys. Chem.* **219**, 47 (2005).
277. P. Bordat, F. Affouard, M. Descamps, and K. L. Ngai, *Phys. Rev. Lett.* **93**, 105502 (2004).
278. C. León, K. L. Ngai, and C. M. Roland, *J. Chem. Phys.* **110**, 11585 (1999).
279. R. Casalini, K. L. Ngai, C. G. Robertson, and C. M. Roland, *J. Polym. Sci. Polym. Phys. Ed.* **38**, 1841 (2000).
280. R. Böhmer, G. Diezemann, G. Hinze, and E. Rössler, *Prog. Nucl. Magn. Reson. Spectrosc.* **39**, 191 (2001).
281. M. Vogel and E. Rössler, *J. Chem. Phys.* **114**, 5802 (2000).
282. J. Y. Cavaille, J. Perez, and G. P. Johari, *Phys. Rev. B* **39**, 2411 (1989).
283. R. Richert, *Europhys. Lett.* **54**, 767 (2001).
284. R. Böhmer, G. Hinze, T. Jörg, F. Qui, and H. Sillescu, *J. Phys.: Condens. Matter* **12**, A383 (2000).
285. G. P. Johari, *J. Non-Cryst. Solids* **307–310**, 317 (2002).
286. K. Abbes, G. Vigier , J. Y. Cavaille, L. David, A. Faivre, and J. Perez, *J. Non-Cryst. Solids* **235–237**, 286 (1998).
287. A. Faivre, G. Niquet, M. Maglione, J. Fornazero, J. F. Jal, and L. David, *Eur. Phys. J. B* **10** 277 (1999).
288. B. Sixou, A. Faivre, L. David, and G. Vigier, *Mol. Phys.* **99**, 1845 (2001).
289. M. L. Cerrada and G.B. McKenna, *Macromolecules*, **33**, 3065 (2000).
290. S. Corezzi, M. Beiner, H. Huth, K. Schröter, S. Capaccioli, R. Casalini, D. Fioretto, and E. Donth, *J. Chem. Phys.* **117**, 2435 (2002).
291. D. Pisignano, S. Capaccioli, R. Casalini, M. Lucchesi, P. A. Rolla, A. Justl, and E. Rössler, *J. Phys.: Condens. Matter* **13**, 4405 (2001).
292. S.P. Bravard and R. Boyd, *Macromolecules* **36**, 741(2003).
293. G. N. Lewis and M. Randall, *Thermodynamics*, 2nd ed., McGraw-Hill, NewYork, 1961.
294. A. Alegria, L. Goitiandia, I. Telleria, and J. Colmenero, *Macromolecules* **30**, 3881 (1997).
295. K. L. Ngai and D. J. Plazek, *J. Polym. Sci. Part B: Polym. Phys. Ed.* **24**, 619 (1986).
296. T. Ruths, Ph.D. Thesis, Johannes Gutenberg University, Mainz, 1997.
297. A. Patkowski, T. Ruths, and E. W. Fischer, *Phys. Rev. E* **67**, 021501 (2003).
298. K. L. Ngai, *J. Phys: Condens. Matter* **11**, A119 (1999).
299. M. Arndt, R. Stannarius, H. Groothues, E. Hempel, and F. Kremer, *Phys. Rev. Lett.* **79**, 2077 (1997).

300. A. Schönhals, H. Goering, C. Schick, B. Frick, and R. Zorn, *Eur. J. Phys. E Soft Matter* **12**, 173 (2003).
301. A. Schönhals, H. Goering, C. Schick, B. Frick, and R. Zorn, *Colloid Polym. Sci.* **282**, 882 (2004).
302. K. L. Ngai, *Philos. Mag. B* **82**, 291 (2002).
303. K. L. Ngai, *Eur. Phys. J. E* **8**, 225 (2002).
304. H. Fujimori, M. Mizukami, and M. Oguni, *J. Non-Cryst. Solids* **204**, 38(1996).
305. S. H. Anastasiadis, K. Karatasos, G. Vlachos, E. Manias, and E. P. Giannelis, *Phys. Rev. Lett.* **84**, 915 (2000).
306. Z. Fakhraai and J. A. Forrest, *Phys. Rev. Lett.* **95**, 025701 (2005).
307. K. L. Ngai, G. Floudas, A. K. Rizos, and D. J. Plazek, Amorphous polymers, in *Encyclopedia of Polymer Properties*, John Wiley & Sons, New York, 2002.
308. D. J. Plazek, I.-C. Chay, K. L. Ngai, and C. M. Roland, *Macromolecules*, **28**, 6432 (1995).
309. A. Schönhals, *Macromolecules* **26**, 1309 (1993).
310. K. L. Ngai, *Eur. Phys. J. E* **12**, 93 (2003).
311. C. L. Jackson and G. B. McKenna, *J. Non-Cryst. Solids* **131**, 221–224 (1991).
312. G. Reiter, *Europhys. Lett.* **23**, 579–584 (1993).
313. J. L. Keddie, R. A. L. Jones, and R. A. Cory, *Europhys. Lett.* **27**, 59–64 (1994).
314. J. A. Forrest, *Eur. Phys. J. E* **8**, 261(2002).
315. K. L. Ngai, *Eur. Phys. J. E* **8**, 225 (2002).
316. G. B. McKenna, *Eur. Phys. J. E* **12**, 191(2003).
317. (a) M. Alcoutlabi, and G. B. McKenna, *J. Phys.: Condens. Matter* **17**, R461 (2005). (b) K. L. Ngai, *J. Polym. Sci. Polym. Phys.* in press (2006).
318. C. M. Roland and K. L. Ngai, *Macromolecules* **24**, 2261 (1991).
319. C. M. Roland and K. L. Ngai, *J. Rheol.* **36**, 1691 (1992).
320. C. M. Roland and K. L. Ngai, *Macromolecules* **25**, 363 (1992).
321. C. M. Roland and K. L. Ngai, *Macromolecules* **33**, 3184 (2000).
322. A. Alegria, J. Colmenero, K. L. Ngai, and C. M. Roland, *Macromolecules* **27**, 4486 (1994).
323. K. L. Ngai and C. M. Roland, *Macromolecules* **28**, 4033 (1995).
324. C. M. Roland, K. L. Ngai, J. M. O'Reilly, and J. S. Sedita, *Macromolecules* **25**, 3906 (1992).
325. A. K. Rajagopal, K. L. Ngai, and S. Teitler, *Nucl. Phys. B (Proc. Suppl.)* **5A**, 97; **5A**, 102 (1988).
326. K.L. Ngai, A. K. Rajagopal, and T. P. Lodge, *J. Polym. Sci. Polym. Phys.* **28**, 1367 (1990).
327. P. Scheidler, W. Kob, and K. Binder, *Europhys. Lett.* **52**, 277 (2000).
328. A. Zetsche, W. Jung, F. Kremer, and H. Schulze, *Polymer* **31**, 1883 (1990).
329. K. L. Ngai and C. M. Roland, *Rubber Chem. Tech.* **77**, 579 (2004)
330. A. Zetsche and E. W. Fischer, *Acta Polym.* **45**, 168 (1994).
331. G. Katana, E. W. Fischer, T. Hack, V. Abetz, and F. Kremer, *Macromolecules* **28**, 2714 (1995).
332. S. K. Kumar, R. H. Colby, S. H. Anastasiadis, and G. Fytas, *J. Chem. Phys.* **105**, 3777 (1996).
333. S. Kamath, R. H. Colby, and S. K. Kumar *Phys. Rev. E* **67**, 010801 (2003).
334. T. Lodge and T. C. B. McLeish, *Macromolecules* **33**, 5278 (2000).
335. J. C. Haley, T. P. Lodge, Y. He, M. D. Ediger, E. D. von Meerwall, and J. Mijovic, *Macromolecules* **36**, 6142 (2003).

336. T. R. Lutz, Y. He, M. D. Ediger, H. Cao, G. Lin, and A. A. Jones, *Macromolecules* **36**, 1724 (2003).
337. K. L. Ngai and C. M. Roland, *Macromolecules* **37**, 2817 (2004).
338. S. Kahle, J. Korus, E. Hempel, R. Unger, S. Höring, K. Schröter, and E. Donth, *Macromolecules* **30**, 7214 (1997).
339. K. L. Ngai, *Macromolecules* **32**, 7140 (1999).
340. C. Lorthioir, A. Alegria, and J. Colmenero, *Phys. Rev. E* **68**, 031805 (2003).
341. O. Urakawa, Y. Fuse, H. Hori, Q. Tran-Cong, and K. Adachi, *Polymer* **42**, 765 (2001).
342. S. Capaccioli and K. L. Ngai, *J. Phys. Chem. B* **109**, 9727 (2005).
343. K. Kessairi, S. Capaccioli, D. Prevosto, M. Lucchesi, and P. Rolla, to be published.
344. K. Duvvuri and R. Richert, *J. Phys. Chem. B* **108**, 10451 (2004).
345. T. Psurek, S. Maslanka, M. Paluch, R. Nozaki, and K. L. Ngai, *Phys. Rev. E* **70**, 011503 (2004).
346. J. Mattsson, R. Bergmann, P. Jacobsen, and L. Börjesson, *Phys. Rev. Lett.* **94**, 165701 (2005).
347. S. E. B. Petrie, *J. Macromol. Sci. Phys. B* **12**, 225 (1976).
348. M. B. M. Mangion, G. P. Johari, *J. Polym. Sci., Part B: Polym. Phys.* **28**, 71(1990); **28**, 1621 (1990); **29**, 437 (1991).
349. G. P. Johari, Dynamics of irreversibly forming macromolecules, in *Disorder Effects in Relaxational Processes*, R. Richert and A. Blumen, eds., Springer-Verlag, Berlin, 1994, p. 627.
350. A. Lee and G. B. McKenna, *Polymer* **31**, 423 (1990).
351. A. Lee and G. B. McKenna, *Polymer* **29**, 1812 (1988).
352. D. J. Plazek and I.-C. Chay, *Polym. Sci., Part B: Polym. Phys. Ed.* **29**, 17 (1991).
353. I. Alig, G. P. Johari, *J. Polym. Sci., Part B: Polym. Phys.* **31**, 299 (1993).
354. I. Alig, D. Lellinger, G. P. Johari, *J. Polym. Sci., Part B: Polym. Phys. Ed.* **30**, 791 (1992).
355. M. G. Parthun and G. P. Johari, *Macromolecules* **29**, 3254 (1992).
356. M. G. Parthun and G.P. Johari, *J. Chem. Phys.* **102**, 6301 (1995).
357. M. G. Parthun and G. P. Johari, *J. Chem. Phys.* **103**, 7611 (1995).
358. M. G. Parthun and G. P. Johari, *J. Chem. Phys.* **103**, 440 (1995).
359. S. Monserrat, J. L. Gomez-Ribelles, and J. M. Meseguer, *Polymer* **39**, 3801 (1998).
360. J. M. Hutchinson, D. McCarthy, S. Monserrat, and P. Cortes, *J. Polym. Sci., Part B: Polym. Phys. Ed.* **34**, 229 (1996).
361. D. A. Wasylyshyn and G. P. Johari, *J. Chem. Phys.* **104**, 5683 (1996).
362. D. A. Wasylyshyn, M. G. Parthun, and G. P. Johari, *J. Mol. Liq.* **69**, 283 (1996).
363. D. A. Wasylyshyn and G. P. Johari, *J. Polym. Sci., Part B: Polym. Phys.* **35**, 437 (1997).
364. E. Tombari, C. Ferrari, G. Salvetti, and G. P. Johari, *J. Phys.: Condens. Matter.* **9**, 7017 (1997).
365. C. Ferrari, E. Tombari, G. Salvetti, and G. P. Johari, *J. Chem. Phys.* **110**, 10599 (1999).
366. E. Tombari, C. Ferrari, G. Salvetti, and G. P. Johari, *J. Phys. Chem. Phys.* **1**, 1965 (1999).
367. E. Tombari, G. Salvetti, and G. P. Johari, *J. Chem. Phys*, **113**, 6957 (2000).
368. D. Lairez, J. R. Emery, D. Durand, and R. A. Pethrick, *Macromolecules* **25**, 7208 (1992).
369. R. Casalini, A. Livi, P.A. Rolla, G. Levita, and D. Fioretto, *Phys. Rev. B* **53**, 564 (1996).
370. G. Levita, A. Livi, P. A. Rolla, and C. Culicchi, *J. Polym. Sci. Part B: Polym. Phys.* **34**, 2731 (1996).
371. G. Gallone, S. Capaccioli, G. Levita, P. A. Rolla, and S. Corezzi, *Polym. Int.*, **50**, 545 (2001).

372. B. Fitz, S. Andjelic, and J. Mijovic, *Macromolecules* **30**, 5227 (1997).

373. S. Monserrat, F. Roman, and P. Colomer, *Polymer* **44**, 101 (2003).

374. S. Corezzi, D. Fioretto, and P. A. Rolla, *Nature*, **420**, 653 (2003) but see comments by G. P. Johari, *Chem. Phys.* **305**, 231(2004).

375. S. Corezzi, D. Fioretto, D. Puglia, and J. M. Kenny, *Macromolecules*, **36**, 5271 (2003).

376. This procedure should not be applied when there are other factors affecting the dispersion, such as concentration fluctuations in mixtures of two glass-formers, spatial heterogeneity, and so on.

377. K. L. Ngai, *J. Phys. Chem. B* **103**, 10694 (1999).

378. K. L. Ngai, G. N. Greaves, and C. T. Moynihan, *Phys. Rev. Lett.* **80**, 1018 (1998).

379. K. L. Ngai, *Philos. Mag. B* **77**, 187 (1998).

380. K. J. Moreno, G. Mendoza-Suarez, A. F. Fuentes, J. García-Barriocanal, C. León, and J. Santamaria, *Phys. Rev. B* **71**, 132301 (2005).